To the Graduate Council:

We are submitting herewith a thesis written by Thomas D. Radcliff entitled "Visualization and Control of Vortical Flow in the Lower Plenum of the Westinghouse AP600 Reactor." We have examined the final copy of this thesis for form and content and recommend that it be accepted in partial fulfillment of the requirements for the degree of Master of Science with a major in Nuclear Engineering.

J.R. Parsons, Major Professor

W.S. Johnson, Major Professor

We have read this thesis
and recommend its acceptance:

Belle R Upadhyaya

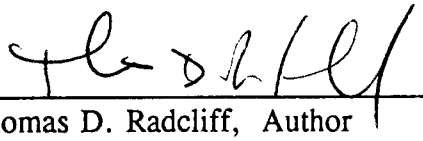
Accepted for the Council:

Associate Vice Chancellor
and Dean of the Graduate School

STATEMENT OF PERMISSION TO USE

In presenting this thesis in partial fulfillment of the requirements for a M.S. degree at the University of Tennessee, Knoxville, I agree that the library shall make it available to borrowers under the rules of the library. Brief quotations from this thesis are allowable without special permission, provided that accurate acknowledgement of the source is made.

Permission for extensive quotation from or reproduction of this thesis may be granted by my major professors, or in their absence, by the Head of Interlibrary Services when, in the opinion of either, the proposed use is for scholarly purposes. Any copying or use of the material in this thesis for financial gain shall not be allowed without my written permission.



Thomas D. Radcliff, Author

10 April 1992

Date

VISUALIZATION AND CONTROL OF VORTICAL FLOW IN THE LOWER PLENUM OF THE WESTINGHOUSE AP600 REACTOR

A Thesis

Presented for the

Master of Science

Degree

The University of Tennessee, Knoxville

Thomas D. Radcliff

May, 1992

ACKNOWLEDGEMENTS

The author would like to express his appreciation to Westinghouse Electric Corporation and the U.S. Department of Energy for providing the opportunity to perform this research. Also greatly appreciated was the advice given by Drs. W.S. Johnson and J.R. Parsons who served as co-advisors, Dr. B.R. Upadhyaya who served on the thesis committee, and Dr. T.W. Kerlin who initiated the whole project. Dick Bailey and Gary Graves provided invaluable assistance in building and operating the experiments, while Ms. Ann Lacava was instrumental in formatting the thesis. Finally, the author would like to thank Ms. Elizabeth Brackett, for giving him the opportunity to follow his dreams.

ABSTRACT

The initial design for the Westinghouse AP600 reactor called for a reactor vessel lower plenum relatively free from obstructions. There was some concern that this design could result in vortical flow in the plenum. To research this hypothesis, a 1:9 scale model of the reactor vessel was built from clear acrylic plastic, with accurate geometric reproduction of the cold legs, downcomer, lower plenum, and core support plate.

Because of the difficulties of reproducing actual reactor flow conditions, air was used as the working fluid, with fluid velocity maintained as the similarity parameter. The flow field in the lower plenum was visualized using a horizontally positioned tuft grid. Schlieren optical techniques were also used to locally visualize injected helium.

With no obstructions present in the lower plenum, two strong counterrotating vertical-axis vortices were observed. These vortices were positioned around a circle of constant radius and extended from the core support plate to the plenum surface. The vortices moved azimuthally about this circle, sometimes joining but seldom dissipating.

To prevent vortical flow, a vortex suppression device designed by Westinghouse was placed in the plenum perpendicular to the vortex axis. Repetition of the tests showed that all signs of organized vortical flow had disappeared. This result held under all flow conditions studied, including cases of gross flow imbalance between cold legs.

From these results it was concluded that vortical flow could develop in the AP600 lower plenum if the plenum were free from obstruction, but that vortex formation could be effectively controlled by placing an appropriate suppression device in the plenum.

TABLE OF CONTENTS

1.0 BACKGROUND 1

1.1 Problem Description 1
1.2 Vortex Theory 1
1.3 Previous Research 7

2.0 EXPERIMENTAL DESIGN 12

2.1 Scale Model Design 12
2.2 Instrumentation and Calibration 20
2.3 Flow Visualization 28

2.3.1 Tuft Methods 29
2.3.2 Schlieren Optical Method 31

2.4 Vortex Suppression Devices 35

3.0 EXPERIMENTAL RESULTS 38

3.1 Characterization of the Unobstructed Flow Field 38

3.1.1 Observed Flow Fields with Radial Keys Offset from the Cold Legs . . . 39
3.1.2 Observed Flow Fields with Radial Keys Aligned Below the Cold Legs . . 46

3.2 Characterization of the Suppressed Flow Field 47

3.2.1 Observed Flow Fields with Offset Radial Keys 50
3.2.2 Observed Flow Fields with Aligned Radial Keys 56

3.3 Sensitivity of Flow Fields to Loop Flow Imbalance 63

3.3.1 Single Loop Imbalance 63
3.3.2 Adjacent Loop Imbalances 69
3.3.3 Opposing Loop Imbalances 71

3.4 Downcomer Azimuthal Velocity Profiles 75

4.0 CONCLUSIONS AND RECOMMENDATIONS 84

4.1 Conclusions 84
4.2 Recommendations for Future Research 86

LIST OF REFERENCES 88

APPENDIX: Dimensioned Drawings 91

VITA 100

LIST OF FIGURES

FIGURE **PAGE**

1: Superimposed Sink and Irrotational Vortex Potential Flows 6
2: Velocity Vector Map from Siemens Experiment 8
3: Core Inlet Velocity Map from Siemens Experiment 9
4: Reactor Vessel Model Side View 14
5: Reactor Vessel Model Top View 15
6: Front View of the AP600 Model 16
7: Top Oblique View of the AP600 Model 16
8: View of the Lower Plenum Region 19
9: View of the Blower and Gate Valve 20
10: Meriam Laminar Flowmeter and Diffuser 22
11: Flow Instrumentation Display 22
12: Cold Leg Radial Velocity Profiles 24
13: Flange Tap Orifice Assembly 25
14: Loop 1 Flow Rate vs. Orifice Pressure Drop 26
15: Loop 2 Flow Rate vs. Orifice Pressure Drop 26
16: Loop 3 Flow Rate vs. Orifice Pressure Drop 27
17: Loop 4 Flow Rate vs. Orifice Pressure Drop 27
18: Fine and Coarse Mesh Tuft Grids 30
19: Schlieren Optical System 33
20: Helium Injection Probes 33
21: Bottom View of the Vortex Suppression Device 37
22: Side View of the VSD and Tuft Grid 37
23: 120% Flow; Keys Offset; 100/340° 40
24: 120% Flow; Keys Offset; 30/120° 40
25: 100% Flow; Keys Offset; 100/340° 42
26: 100% Flow; Keys Offset; 30/120° 42
27: 100% Flow; Keys Offset; Single Vortex 43
28: 100% Flow; Keys Offset; Grid Lowered 1" 43
29: 100% Flow; Keys Offset; Grid Lowered 2" 44
30: 100% Flow; Keys Offset; Grid Lowered 3" 44

FIGURE **PAGE**

31: 80% Flow; Keys Offset 45
32: 50% Flow; Keys Offset 45
33: 120% Flow; Keys Aligned; 100/180° 48
34: 120% Flow; Keys Aligned; 20/100° 48
35: 80% Flow; Keys Aligned 49
36: 50% Flow; Keys Aligned 49
37: 120% Flow; Keys Offset; No VSD 52
38: 120% Flow; Keys Offset; VSD Nominal 52
39: 120% Flow; Keys Offset; VSD Lowered 1" 53
40: 60% Flow; Keys Offset; VSD Lowered 1" 53
41: 120% Flow; Keys Offset; VSD Raised 1" 54
42: 100% Flow; Keys Offset; VSD Raised 1" 54
43: 80% Flow; Keys Offset; VSD Raised 1" 55
44: 60% Flow; Keys Offset; VSD Raised 1" 55
45: 120% Flow; Keys Aligned; No VSD 58
46: 120% Flow; Keys Aligned; VSD Nominal; No Curl 58
47: 120% Flow; Keys Aligned; VSD Nominal; Curl 59
48: 60% Flow; Keys Aligned; VSD Nominal 59
49: 120% Flow; Keys Aligned; VSD Lowered 1" 60
50: 60% Flow; Keys Aligned; VSD Lowered 1" 60
51: 120% Flow; Keys Aligned; VSD Raised 1" 61
52: 100% Flow; Keys Aligned; VSD Raised 1" 61
53: 80% Flow; Keys Aligned; VSD Raised 1" 62
54: 60% Flow; Keys Aligned; VSD Raised 1" 62
55: Keys Offset; No VSD; 15% Single Loop Imbalance 65
56: Keys Offset; No VSD; 35% Single Loop Imbalance 65
57: Keys Offset; VSD; 15% Single Loop Imbalance 67
58: Keys Offset; VSD; 35% Single Loop Imbalance 67
59: Keys Aligned; No VSD; 15% Single Loop Imbalance 68
60: Keys Aligned; No VSD; 35% Single Loop Imbalance 68
61: Keys Aligned; VSD; 35% Single Loop Imbalance 70
62: Keys Aligned; VSD; 100% Single Loop Imbalance 70
63: Keys Offset; VSD; 15% Adjacent Loop Imbalance 72

FIGURE **PAGE**

64: Keys Offset; VSD; 100% Adjacent Loop Imbalance 72
65: Keys Aligned; VSD; 15% Adjacent Loop Imbalance 73
66: Keys Aligned; VSD; 100% Adjacent Loop Imbalance 73
67: Keys Offset; VSD; 15% Opposing Loop Imbalance 74
68: Keys Aligned; VSD; 15% Opposing Loop Imbalance 74
69: Downcomer Radial Velocity Profile 76
70: Downcomer Azimuthal Velocity Profile
Keys Offset; No VSD; Single Loop Imbalance @ 45° 77
71: Downcomer Azimuthal Velocity Profile
Keys Aligned; No VSD; Single Loop Imbalance 79
72: Downcomer Azimuthal Velocity Profile
Keys Offset; VSD; Single Loop Imbalance 79
73: Downcomer Azimuthal Velocity Profile
Keys Aligned; VSD; Single Loop Imbalance 80
74: Downcomer Azimuthal Velocity Profile
Keys Offset; VSD; Adjacent Loop Imbalance 80
75: Downcomer Azimuthal Velocity Profile
Keys Offset; VSD; Opposing Loop Imbalance 81
76: Downcomer Azimuthal Velocity Profile
Comparison: VSD Placement 81
77: Downcomer Azimuthal Velocity Profile
Comparison: Radial Key Alignment 82
78: Downcomer Azimuthal Velocity Profile
Comparison: Imbalance Configuration 82
A1: AP600 Reactor Vessel Model Side View 92
A2: AP600 Model As-Built Dimensions 93
A3: AP600 Model Top View 94
A4: Core Support Plate 95
A5: Radial Support Key and Outlet Nozzle 96
A6: Orifice Plates and Flanges 97
A7: Schlieren Optical System 98
A8: Vortex Suppression Device 99

1.0 BACKGROUND

1.1 Problem Description

The original design of the Westinghouse AP600 advanced reactor featured a reactor vessel lower plenum uncluttered by mechanical structures (Westinghouse, 1989). This was accomplished by using radial support keys to serve as secondary core support and using novel incore instruments which entered through the downcomer. Previous testing and operating plant experience have indicated that a lack of significant flow obstruction could allow vortices to form in the plenum (Cadek et al., 1988). The objective of this research was to determine if vortical flow would be present in the plenum under expected operating conditions, and if so, to find and test methods of suppressing these vortices.

1.2 Vortex Theory

A vortex has been defined as rotational motion of a multitude of material particles about a common center (Lugt, 1983). Vortices can be divided into two broad groups; rotational and irrotational. Rotational vortices occur when the individual elements of matter which are circulating about a common center also rotate about their own center of mass. Fluid rotating at steady-state in a centrifuge is an example of rotational flow.

If the elements of matter do not rotate about their own center, the flow is considered irrotational. A classic example of irrotational flow occurs external to a solid rotating rod immersed within a fluid. Most vortices observed in nature consist of a combination of both vortex types, where a rotational vortex core is surrounded by irrotational flow. This type of vortex is called a Rankine vortex.

Since rotational vortices move as a solid about a center, it is clear that the radial velocity component must be zero and that the tangential velocity component is directly related to the radius (Olsen, 1973).

$$V_\theta = -\omega r \qquad (1)$$

where V_θ is the tangential velocity,

r is the radius, and

ω is the angular velocity, defined as positive when rotating counterclockwise.

From this relation, it can be seen that the tangential velocities in a rotational vortex are highest at the outer radius. Since centrifugal force increases as the velocity increases, the pressure in this type of vortex will also be maximized at the outer radius. Within a rotational vortex there is no shear, so this type of vortex requires no energy to maintain rotation. For example, the fluid centrifuge mentioned earlier would spin eternally if there were no friction between the fluid and its surroundings.

Irrotational vortices behave quite differently from rotational vortices. From the previous example of a spinning rod (which in itself can be considered a rotational vortex)

immersed in a fluid, intuition suggests that the highest tangential velocities will occur at the interface between the rod and fluid. As the rod diameter approaches zero, the peak velocity occurs nearer the center, with velocity decreasing to a minimum at the outer radius. The tangential velocity is in fact related to the radius by (Olsen, 1973):

$$V_\theta = \frac{C}{r} \qquad (2)$$

where C is a constant which varies with vortex strength.

This equation becomes singular as the radius approaches zero, indicating that irrotational flow theory cannot account for behavior at this limit. As the singularity is approached, the asymptotically increasing velocity will result in a sharp decrease in pressure near the center. This type of vortex must be maintained by a continual input of energy since energy is constantly dissipated by shear between adjacent radial layers. The example of an irrotational vortex created by a rod spinning in a fluid demonstrates this effect, since this vortex will dissipate if the rod is withdrawn even if there is no friction between the fluid and its surroundings.

The Rankine vortex combines the behavior of both vortex types. The velocity and pressure at the center are non-singular, since the core, however small, behaves as a solid. In this combined vortex, the energy to drive the irrotational outer vortex is derived from the rotational core, which behaves as the rod in the example.

A more realistic scenario results if friction losses are considered. In this case, a constant supply of energy is needed to maintain a vortex. One common source of energy for vortices is pressure differential created by pumping fluid. A sink in a body

of fluid can result in a vortex if the fluid has any angular component. As fluid is pulled toward the sink, conservation of angular momentum requires that the tangential velocity increase as the radius decreases. This behavior corresponds to an irrotational vortex, with the exception that fluid particles have a radial velocity component inward toward the sink. This is the type of sustainable vortex most likely to occur in the reactor vessel lower plenum, where the sink effect results from removal of fluid along the axis of the vortex.

The theory of potential flow is useful in predicting the flow fields that can be expected in the reactor vessel. These predictions can be compared to visualization of the actual flow field to achieve better understanding of the cause of any vortices.

Both rotational and irrotational flow are governed by the principles of conservation of mass, momentum, and energy. For an incompressible, newtonian, inviscid fluid, the continuity equation can be written in vector form:

$$\nabla \cdot V = 0 \qquad (3)$$

where **V** is the velocity vector.

A solution to this equation, known as the stream function ψ, is defined in two dimensional flow by:

$$u = -\frac{\partial \psi}{\partial y}; \quad v = \frac{\partial \psi}{\partial x} \qquad (4)$$

where u is the x component of the velocity, and

v is the y component of the velocity.

Plotting the stream function gives the streamlines, which represent the tangent of the velocity vector at all points at any time. This should not be confused with pathlines, which are the time dependent traces of the position of a single particle, or streaklines, which are the time dependent traces of different particles at the same spatial position. Streamlines, streaklines and pathlines only coincide in steady-state flow. Most flow visualization techniques show streaklines or pathlines.

Conservation of momentum in an inviscid fluid, ignoring body forces, can be described by the Euler equation:

$$\frac{D\boldsymbol{V}}{Dt} = -\frac{1}{\rho}\nabla p \qquad (5)$$

where ρ is the fluid density, and

p is the pressure.

For irrotational flow, the curl of the velocity is zero and there is no velocity component across the outer surface of the vortex. Given these conditions and considering steady-state two dimensional flow, the Euler equation can be simplified to:

$$\frac{\partial v}{\partial x} - \frac{\partial u}{\partial y} = 0 \qquad (6)$$

The velocity may be written as the gradient of the scalar potential ϕ:

$$u = -\frac{\partial \phi}{\partial x}; \quad v = -\frac{\partial \phi}{\partial y} \qquad (7)$$

Substituting the definition of potential into the continuity equation and the definition of the stream function into the simplified Euler equation gives:

$$\nabla^2\phi = 0; \quad \nabla^2\psi = 0 \tag{8}$$

So streamlines and equipotential lines are orthogonal and together form a mesh which graphically illustrates potential flow. These functions can be derived for many conditions and may be superimposed to represent complex flow. Figure 1 shows a map of streamlines and isotachs for a combined sink and irrotational vortex (Kirchoff, 1985). This superposition of potential flow solutions are expected to most reasonably describe the vortices which may form in the reactor vessel lower plenum.

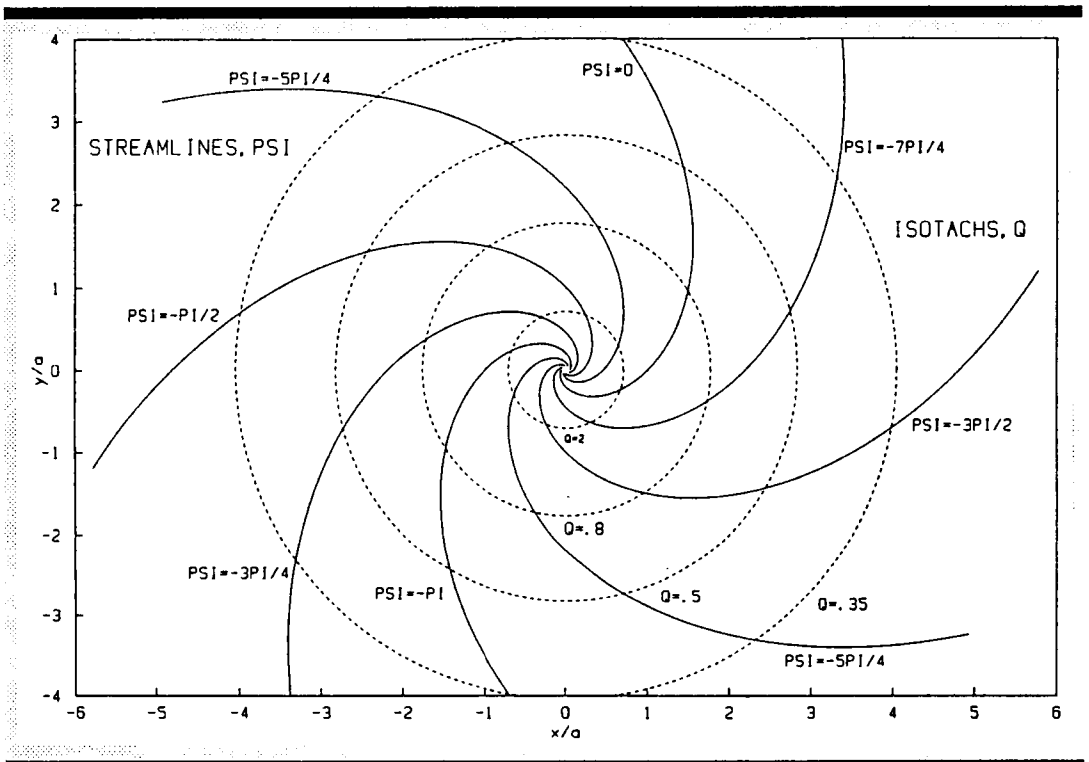


Figure 1: Superimposed Sink and Irrotational Vortex Potential Flows

1.3 Previous Research

The first clear evidence of vortical flow in modern pressurized water reactors (PWRs) was noted during experiments performed by Siemens Corporation in 1972. The results of these experiments were translated and published by the Nuclear Regulatory Commission in 1977 (Weber and Dittrich, 1973). The object of this research was to determine which secondary core support design led to the best core inlet flow distribution. Siemens assembled a 1:10 scale model of an unspecified 4-loop PWR which appears similar to Westinghouse 4-loop PWR design. The lower plenum was formed from a block of clear acrylic and air was used as the working fluid. Initially, three point pitot tubes were used to measure the fluid velocity at 290 points within the plenum. This was ultimately determined to be too time consuming, and subsequent tests measured the core inlet flow rate.

A wide variety of core support designs were tested, during which the experimenters noted that vortical activity was occasionally present, stating " a blade inserted into the flow begins to rotate under certain circumstances, however, it was apparent in the test that no definite rotation is present (Weber and Dittrich, 1973)." They also noted that the presence of rotation was affected by the flow balance in the four cold legs.

Because the experimenters were not specifically studying vortical flow, no visualization to illustrate the flow field was attempted, however, the data collected shows clear evidence of vertical-axis vortices. A map of velocity vectors in a horizontal cross-

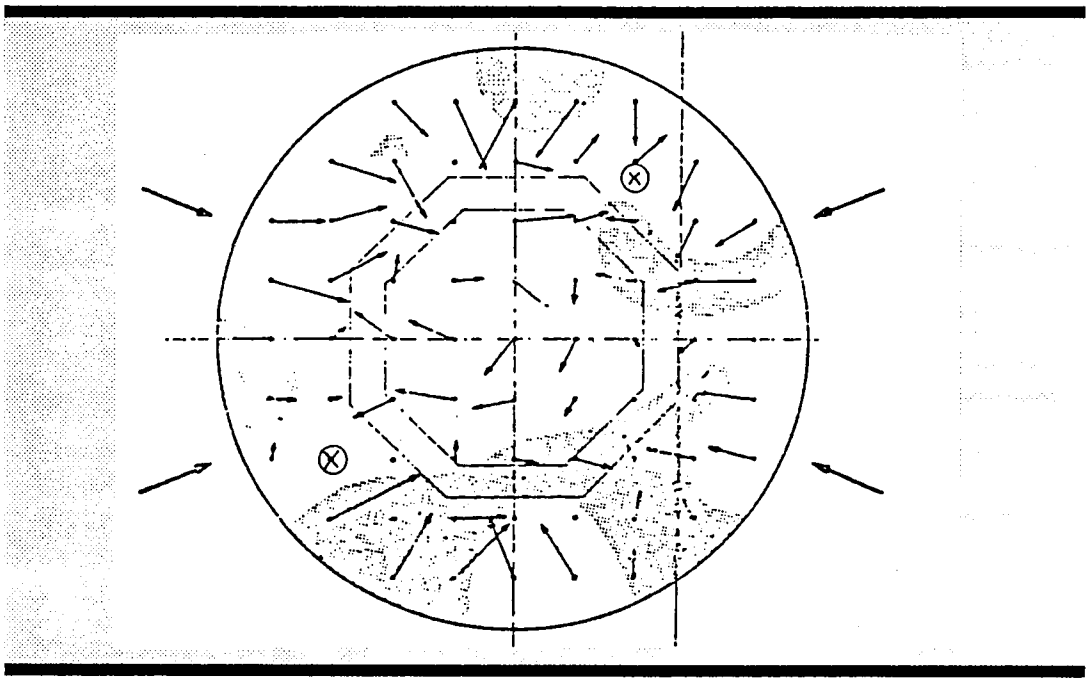


Figure 2: Velocity Vector Map from Siemens Experiment

section of the model lower plenum, shown in Figure 2, suggests two counterrotating vortices centered on the added "X"s, while Figure 3 shows a map of core inlet velocity which clearly shows concentric isotachs characteristic of twin vortices (Weber and Dittrich, 1973). Since the vortical flow could be controlled by an appropriate choice of core support design, the Siemens engineers did not recommend further study.

The possibility of vortices in reactor vessel lower plenums surfaced again in the late 1980s. The 4-loop Westinghouse Callaway plant in Missouri developed an unusual flow anomaly. The symptoms of this anomaly included simultaneous small aperiodic changes in several parameters within one radial quadrant of the plant. The changes noted were a decrease in the power reading at both the incore and excore detectors, an increase in the temperature at some core-exit thermocouples, a reduction in the Reactor Vessel Level Indicator System (RVLIS) pressure drop, and a decrease in the overall (not

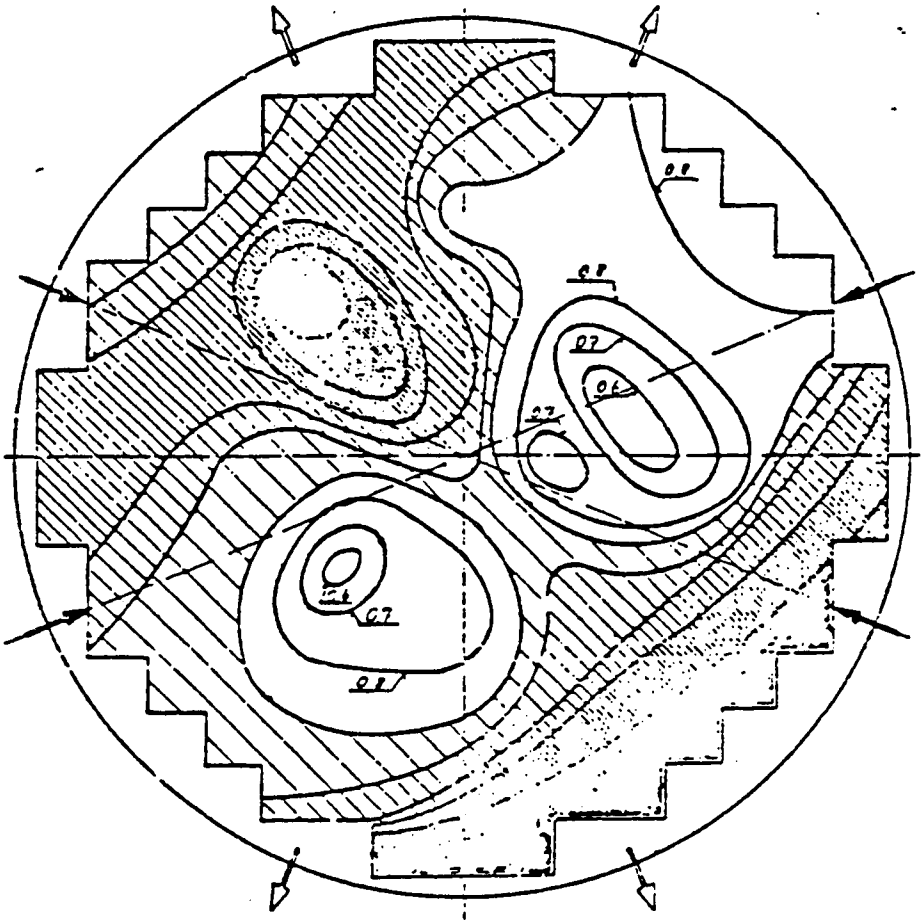


Figure 3: Core Inlet Velocity Map from Siemens Experiment

quadrant) reactor flow (Cadek et al., 1988).

Westinghouse engineers determined that vertical-axis vortices were the most probable explanation of the observed symptoms. Examination of other operating Westinghouse plants showed that some plants experienced the flow anomaly with varying periodicity while other plants did not. Correlating the data showed that the anomaly only occurred in 4-loop plants and was exacerbated by vessel inlet nozzle pairing, radial support key locations which caused lower downcomer flow resistance, non-symmetric tie plate design, reduced structural density in the lower plenum, and loop flow imbalances. Overall, the anomaly was of little concern with the exception of the reduced flow rate, which was accounted for in the reactor safety analysis.

While Westinghouse was studying this problem, a foreign reactor vendor tested a Westinghouse-based plant design to determine if similar flow anomalies could be expected (Garner, 1991). The vendor assembled a 1:7 scale model of the downcomer and lower plenum region. The model was operated upside-down and used cold water as the working fluid. Pressure at the lower plenum surface and differential pressure at the core support plate (CSP) were monitored continuously. Flow visualization using dye injection was also attempted.

These experiments were able to duplicate some of the symptoms present in the Westinghouse plants and could relate these symptoms to the formation or movement of vortices in the lower plenum. The vendor engineers noted that the flow field was sensitive to tie plate thickness as Westinghouse had noted, but further experimentation showed that the gap between the tie plate and the inner surface of the lower plenum was

the most significant parameter. This sensitivity was also seen in the testing performed by Siemens.

Other sensitivities noted by the vendor included the radial support key azimuthal position and loop flow imbalance. Also, some sensitivity to the experimental configuration was seen. In particular, the experiment repeatability was affected by the gate valves used to control loop flow, while the vortex activity was reduced by the presence of pressure taps in the surface of the lower plenum. The attempt at dye visualization was at least partially successful, briefly showing circulation if not vortices at the surface of the plenum as dye was injected.

From this collection of experiments, it appears clear that vortices form in certain reactor designs. The formation of vortices is affected by many factors, most of which seem to be related to the transition of flow from the downcomer into the lower plenum. The observed vortices appear to be of the combined sink-irrotational type expected from theory. These experiments show which parameters need to be studied in the test series for the AP600 reactor design.

2.0 EXPERIMENTAL DESIGN

2.1 Scale Model Design

To study vortical flow in the Westinghouse AP600 reactor design, it was necessary to build a model of the reactor. Ideally, an exact reproduction of the reactor could be used, but this was not practical. The main objective of this test program was to study vortical flow in the reactor vessel lower plenum. Reactor features upstream of or within the lower plenum had to be modeled carefully to ensure that the model represented the reactor, however, features downstream of the core support plate, with its large pressure drop, were not considered to be as important.

Visualization of the flow field in the lower plenum (and possibly the downcomer and cold legs) was also an objective, so optically clear material had to be used in at least part of the model. Commercial availability of clear acrylic hemispheres and tubing is somewhat limited, so the model was based on a standard 18 inch outside diameter. Compared to the design dimensions from the reactor drawings (Westinghouse Drawings RXS, PLOI and M101, 1990), this gives a model scale of 1:8.95, which is in a range often used for vessel model flow testing.

The AP600 reactor has average design coolant parameters of 567.9°F and 2250 psia, with a best estimate total flow of 206,000 gpm (Westinghouse, 1989). These parameters give a Reynolds number of 5.8×10^7 in the 22 inch diameter cold legs, with

a cold leg velocity of 43.5 ft/s. Maintaining dynamic similarity in a 1:9 scale model with water at atmospheric conditions as the working fluid would require a cold leg velocity of over 2500 ft/s, which is clearly not practical. In fact, given the strength of the acrylic structural material, even the static weight of water would be difficult to support.

Since it appeared impractical to achieve true dynamic similarity in the scale model, water was replaced by air as the working fluid. This is not an uncommon technique for large scale flow experiments, as evidenced by the Siemens test described in Section 1.3, and it allows much simplification of the pumping system. The theory presented in Section 1.2 describing the formation of combined sink-irrotational flow vortices indicates that the overall velocity should have little effect on vortex formation. With no obvious constraints, flow velocities were chosen to match the design coolant velocities for the actual reactor.

Given the model requirements, the detailed design of the model firmed up. The cold legs from the steam generator flange, the downcomer (including vestigial hot leg nozzles), the lower plenum, and the core support plate (CSP) were modeled as accurately as possible, while the core and upper plenum regions were not modeled in detail. A partially dimensioned cross-sectional drawing of the reactor vessel is presented in Figure 4, while a top view of the complete model including cold legs is shown in Figure 5. A front-view photograph of the assembled model is shown in Figure 6, while a top-oblique photograph is shown in Figure 7.

The cold legs were formed from cast heavy-wall clear acrylic with an inside

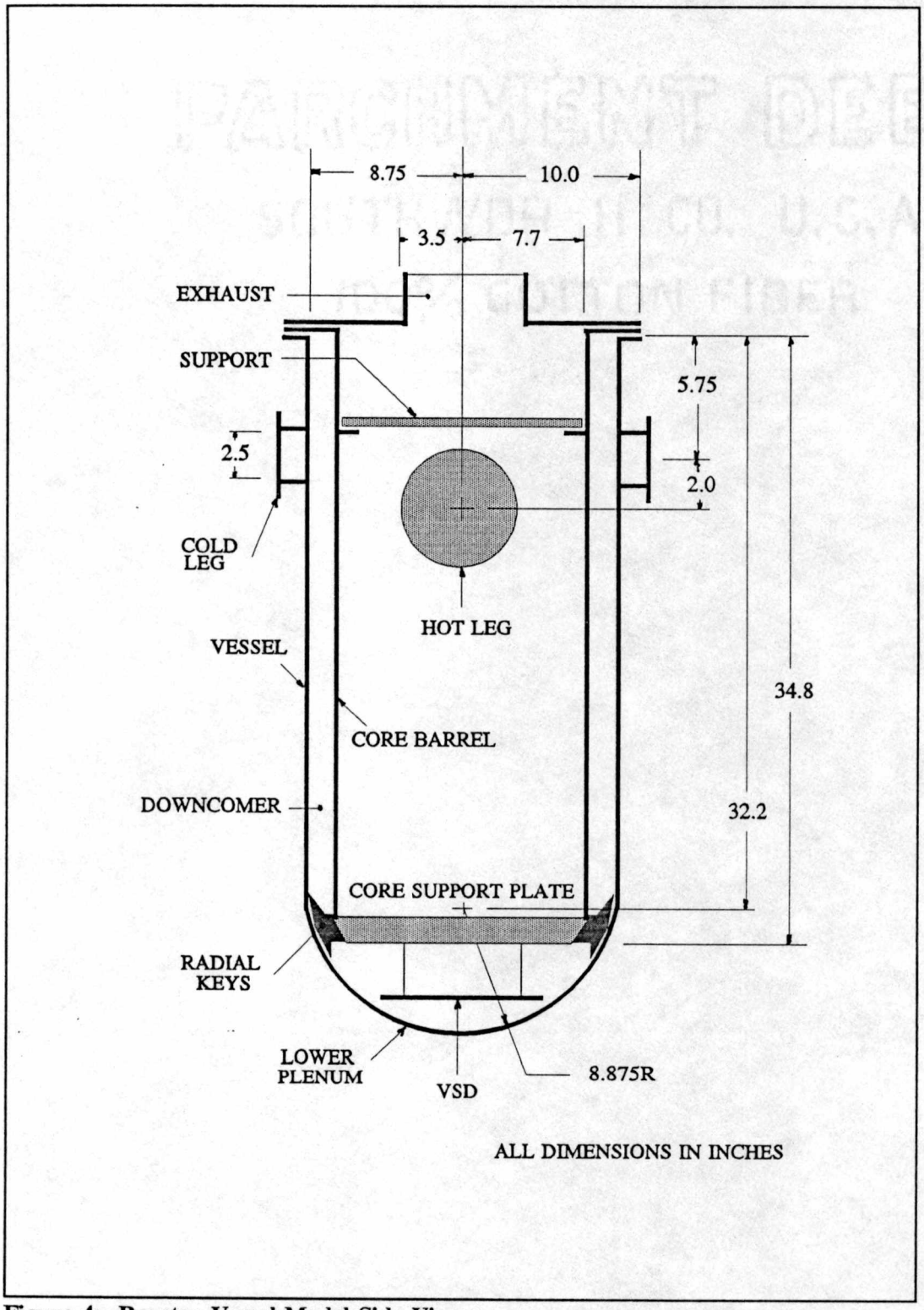


Figure 4: Reactor Vessel Model Side View

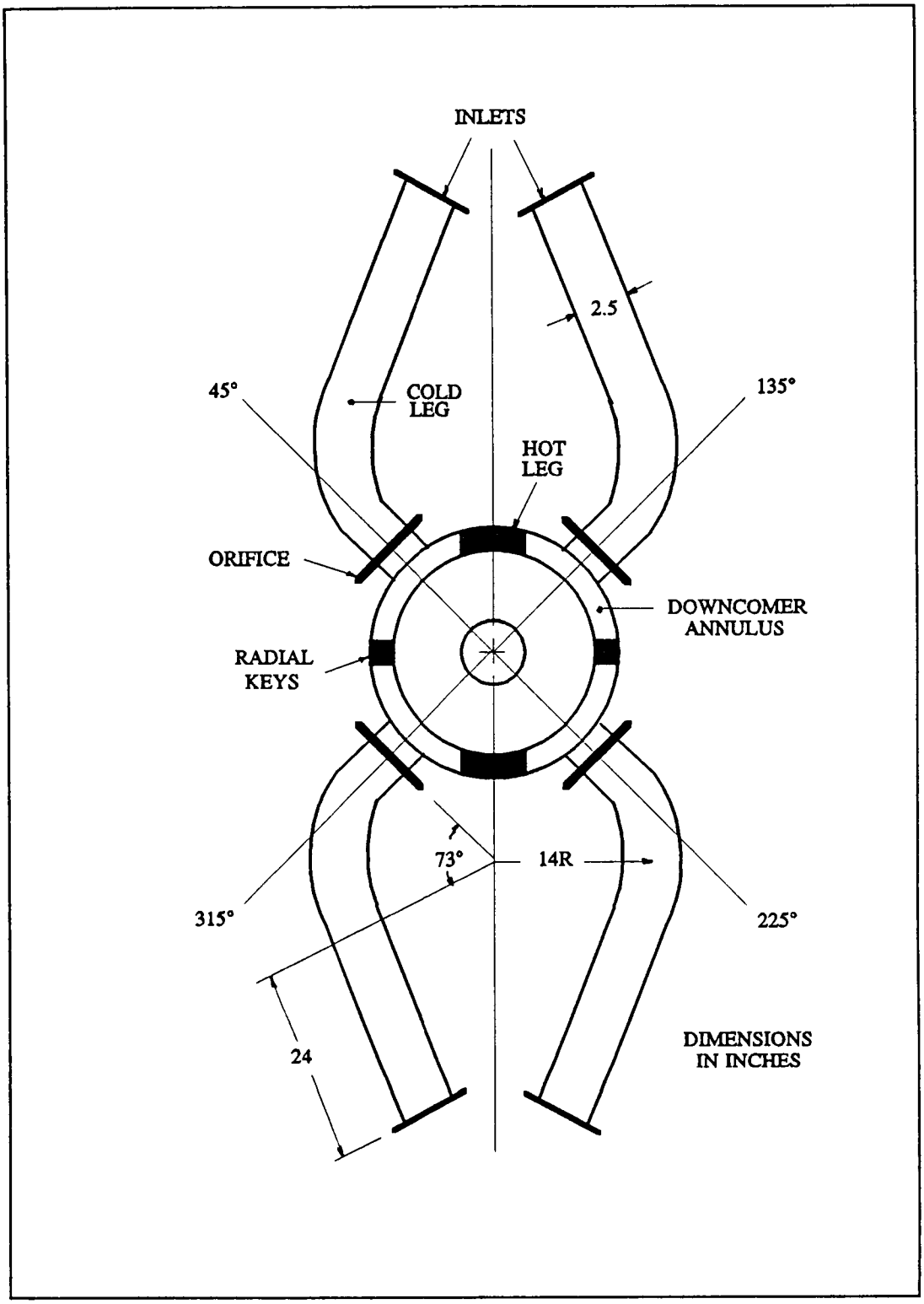


Figure 5: Reactor Vessel Model Top View

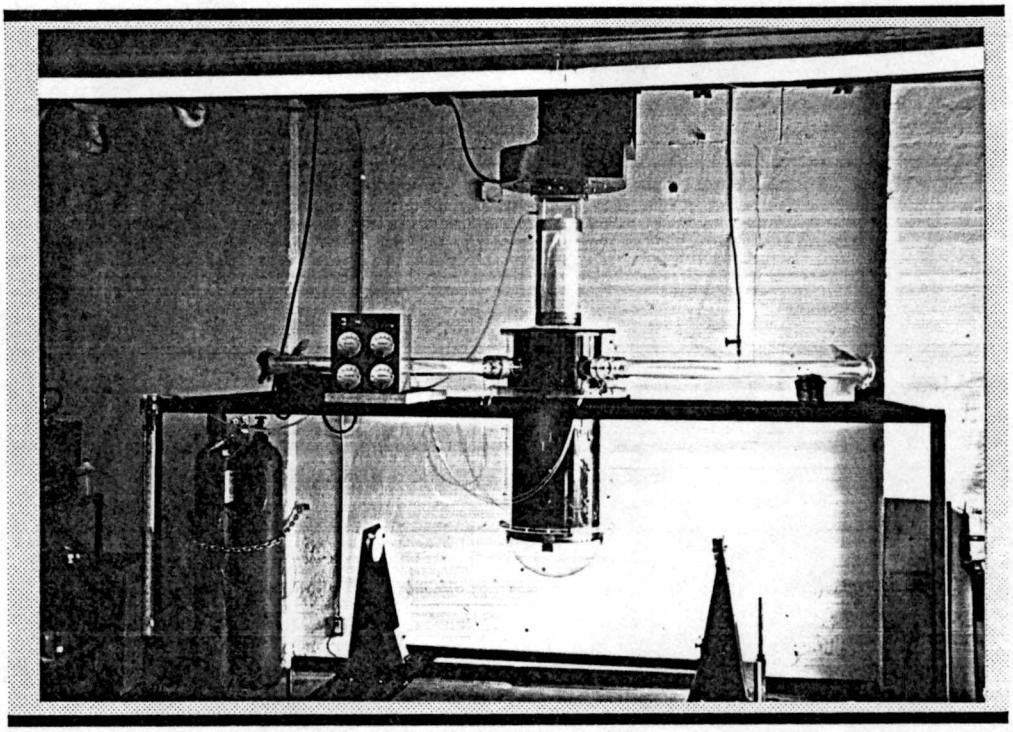


Figure 6: Front View of the AP600 Model

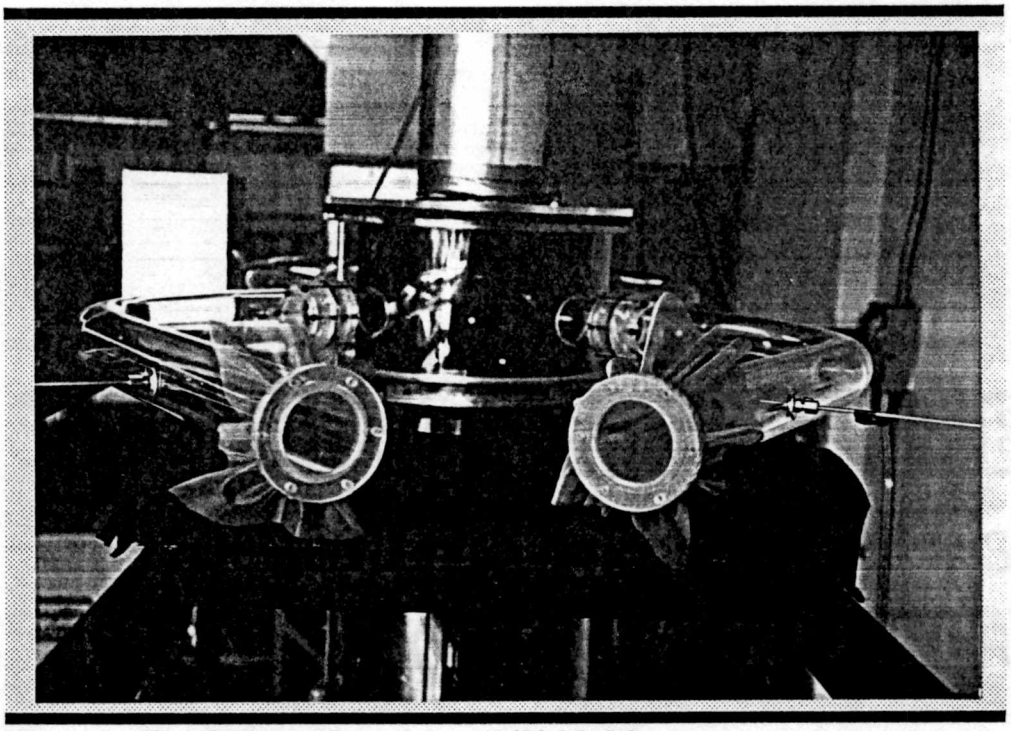


Figure 7: Top Oblique View of the AP600 Model

diameter of 2.49 inches. The scale dimensions were maintained accurately from the downcomer upstream through the bend. The bend was achieved by sealing the ends of the tubing and heating the acrylic in a water bath. The heat increased the air pressure in the sealed tube, preventing the tube from collapsing while being bent. An additional foot of length was added to the inlet end of the legs where the steam generators would be located to provide extra flow straightening. The legs were flanged at the inlet and downcomer for ease of assembly. The inlets are covered by fine mesh plastic screen to smooth the inlet flow. The cold legs and screens are pictured in Figure 7.

The downcomer was formed from cast acrylic tubing with an inside diameter of 17.5 inches and a 0.25 inch wall thickness. This tubing was drilled for the cold leg nozzles and flanged at the top and bottom. The bottom end was carefully machined to a knife-edge with a radiused taper to mate with the lower plenum. This was necessary because the reactor lower plenum is not a complete hemisphere. The straight wall of the downcomer extends 1.1 inches into the hemisphere used for the lower plenum to achieve the plenum curvature specified for the reactor. This area is detailed in Figure A1 of the Appendix. The downcomer region is pictured in Figure 6.

One necessary exception in scaling the model was the use of a constant downcomer annular dimension. The reactor design calls for a small reduction in the downcomer annulus in the upper plenum region. Machining of the model walls without reducing the optical clarity would have been difficult, so after discussion with Westinghouse engineers, the annulus was held constant at the larger diameter. This variation is located well away from the critical downcomer/lower plenum transition

region, and it was not expected to affect the results.

The lower plenum is modeled with a cast acrylic hemisphere with a 9 inch outer radius and a 0.125 inch wall thickness. Because most of the visualization was performed in this region, optical clarity was vital. An inexpensive blow-molded hemisphere was also acquired, but was optically unacceptable. This hemisphere was prepared for non-optical instrumentation.

The core support plate was fabricated from a 1.5 inch thick sheet of cast acrylic. The sheet was fly-cut to fit the bottom of the core barrel. The outer diameter was given a straight taper of 4° as called for in the drawings. About 600 holes of 0.193 inch diameter were drilled on a 0.435 inch pitch to match the design pattern (Westinghouse Drawing M101, 1990). Additional threaded holes were drilled to accommodate the vortex suppression device.

The radial support keys were modeled from dense closed-cell foam. This material allowed easy fabrication of the complex radii required, as well as conforming to the lower plenum hemisphere contours. Both sides of the keys were formed as one piece and attached to the core support plate, allowing the azimuthal position of the keys to be readily changed. A closeup photograph of the lower plenum region, including the tapered joint, CSP, and radial keys, is shown in Figure 8.

The core barrel was fabricated from 15.3 inch outside diameter PVC pipe, painted flat black. This pipe was flanged at the top to mate with the downcomer tube and supports the CSP at the bottom. Tubing sections to model the hot legs were attached to the side of this pipe. A sheet drilled similarly to the CSP was located near the top of the

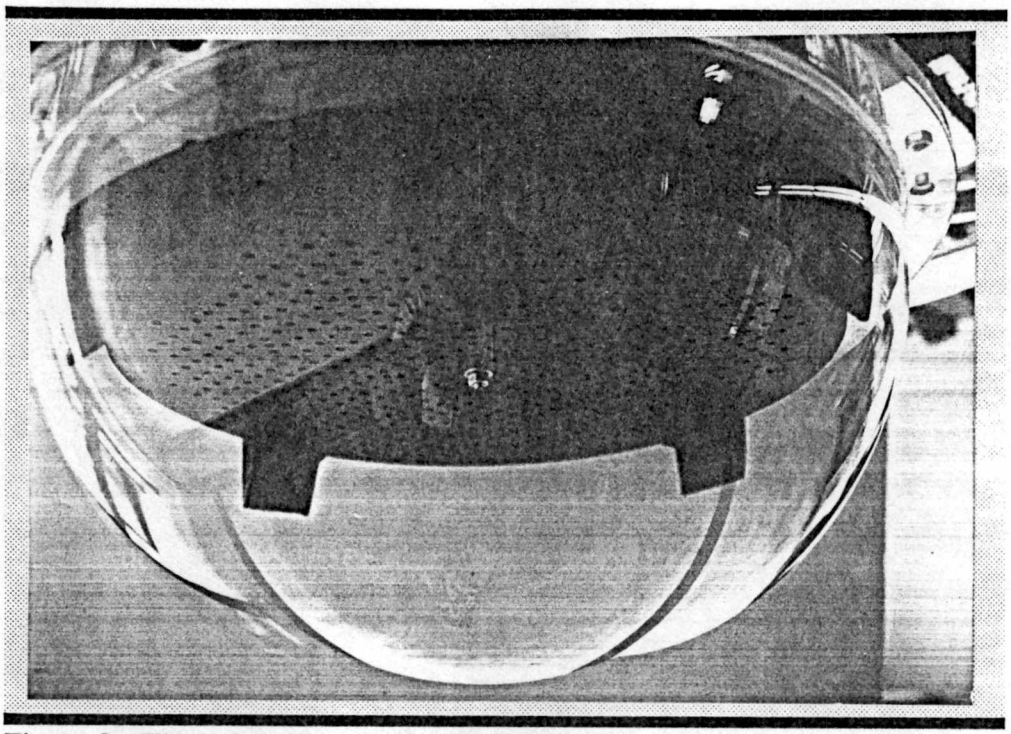


Figure 8: View of the Lower Plenum Region

core barrel to give additional pressure drop and smooth flow, as well as providing accurate location for test equipment.

A centrifugal fan, pictured in Figure 9, was used to exhaust air from the upper plenum region, minimizing turbulence at the cold leg inlets. The fan was sized to allow a minimum velocity of at least 120% of the reactor design velocity by performing a detailed calculation of the pressure drop expected in the model, including calibration devices. The fan is suspended from the ceiling and connected to the reactor vessel with a slip-joint to minimize transmission of vibrations to the model. Total model flow is controlled by an 8 inch diameter gate valve attached to the fan inlet. Adding or removing extra layers of fine mesh screen at the cold leg inlets allows coarse control of the loop flow with virtually no perturbation of the cold leg radial velocity profile.

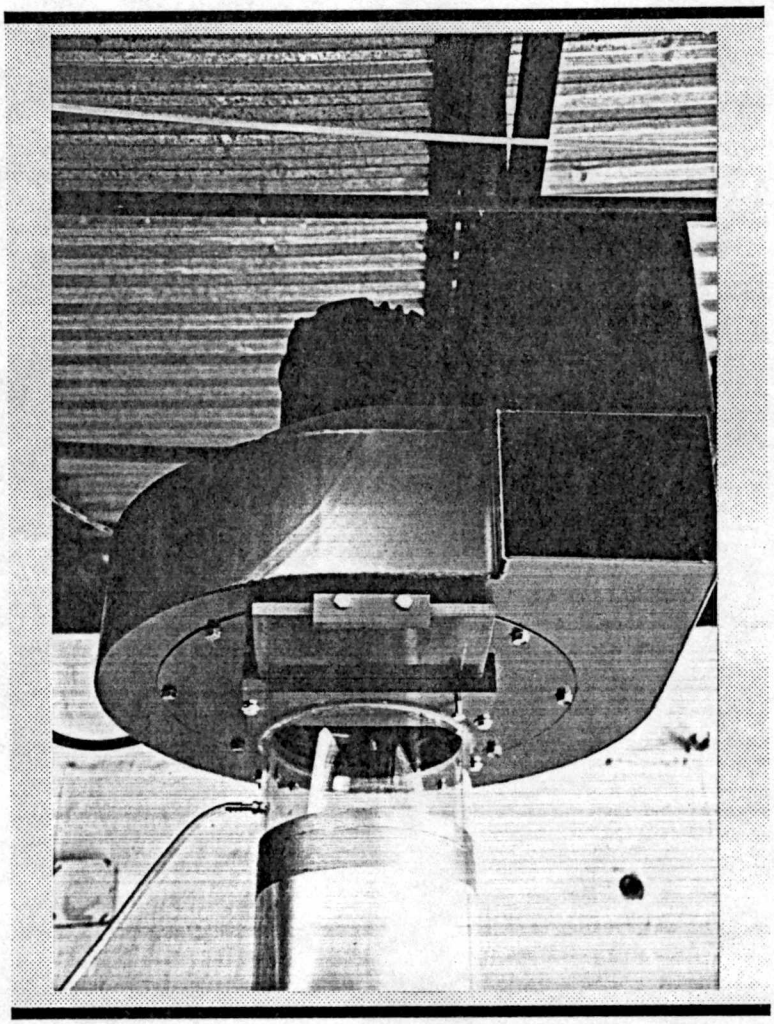


Figure 9: View of the Blower and Gate Valve

A set of completely dimensioned drawings of the reactor model, one including the reactor vessel as-built dimensions, are presented in Appendix A.

2.2 Instrumentation and Calibration

Ideally, flow instrumentation for this model would include four NIST traceable flowmeters, one in each cold leg, for continuous use. Instruments considered for this

purpose included venturis, orifices, and laminar flowmeters (LFMs). Orifices and LFMs have prohibitively large pressure drops for air systems operating in suction mode while LFMs and venturis are quite expensive, so it was determined that a single instrument would be used to calibrate the operational nonlinear flowmeters one leg at a time.

A Meriam laminar flowmeter, with calibration traceable to NIST (Meriam, 1991), was procured for this purpose. This device develops a pressure drop of 8 inches of water with 103.21 cfm of flow at standard conditions. Calibration of one loop to 120% of the reactor nominal design cold leg velocity (subsequently referred to as 120% of the design flow rate or just 120% flow rate) was achieved without exceeding the capacity of the centrifugal blower by blocking the other three loops. The pressure drop across the LFM was measured using a Meriam inclined manometer. The LFM and a diffuser to connect the flow element to the cold leg inlet flanges are pictured in Figure 10.

Pitot tubes were initially used as the operational flow instrumentation. These devices develop a pressure drop related to local flow velocity. The pressure drop was normally presented by Magnehelic pressure gauges (MHGs), although pressure transducers were also available to convert the pressure drop into a current signal which could be displayed digitally. The MHGs were primarily used for visual readings because they have a relatively slow response which steadies fluctuations in the pitot tube pressure difference. A photograph of the instrumentation readouts is shown in Figure 11.

With the LFM and its associated inclined manometer connected to the inlet of one cold leg, local velocities were measured every 0.25 inch across the cold leg diameter with a pitot traverse. These local velocities were then integrated over the flow area to

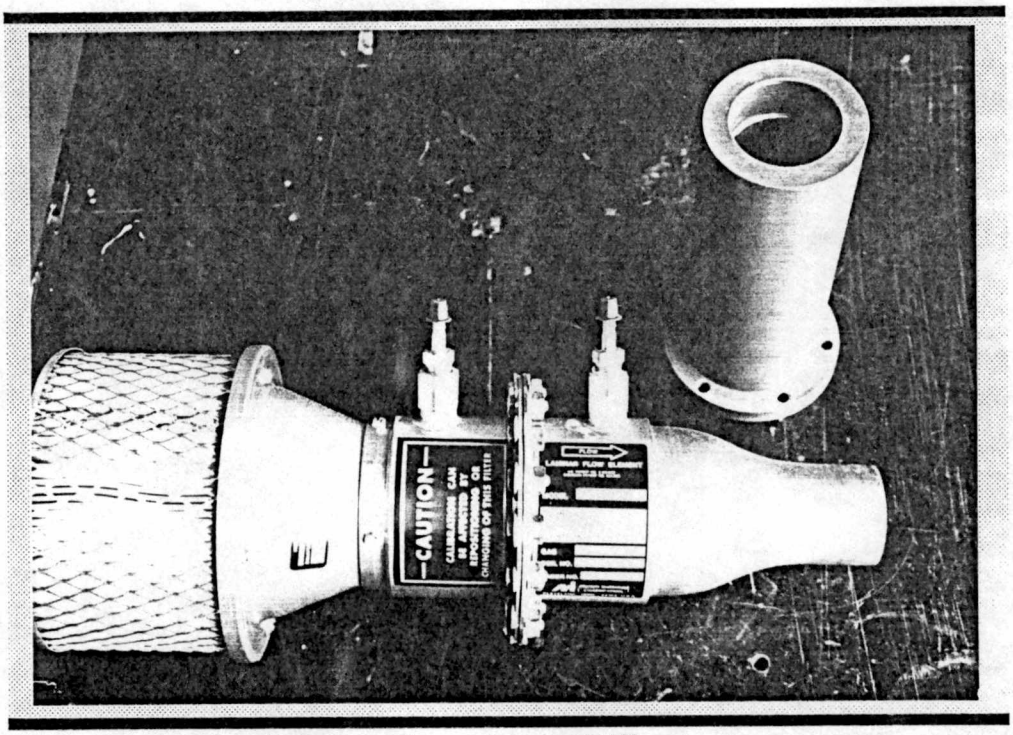


Figure 10: Meriam Laminar Flowmeter and Diffuser

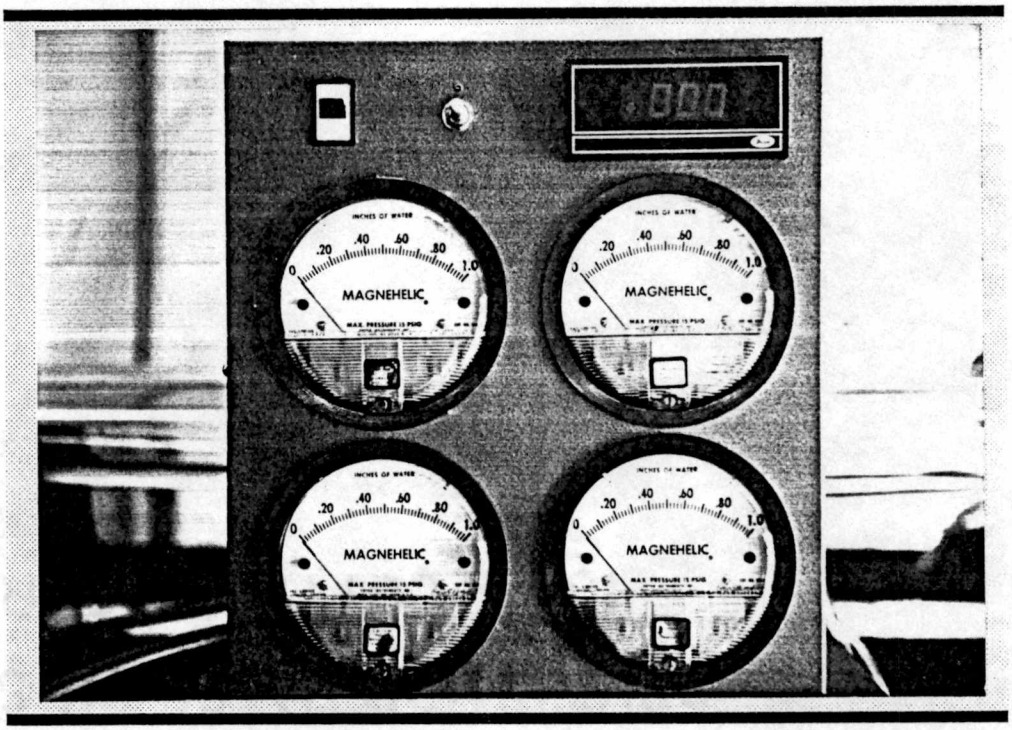


Figure 11: Flow Instrumentation Display

find the total flow in the leg for comparison to the LFM reading. The intent of this calibration was to determine the error between the LFM reading and the traverse integration, and also the difference between peak and average local velocities, so that the peak local velocity could be related to the calibrated total flow. The point of this procedure was to allow routine loop flow measurement with a single pitot tube reading of the peak local velocity in each leg.

For this relationship to be valid, the shape of the velocity profile in the cold leg must not change between calibration and normal operation. To verify this, two velocity profiles were obtained. The first profile was measured by pitot traverse while the LFM indicated 107.2 cfm, which is 121% of the design flow. A peak velocity of 60.1 ft/s was indicated by the pitot traverse, with an averaged velocity of 57.9 ft/s. This integrated to a flow rate of 118.5 cfm and an error of 11% compared to the LFM reading.

After removing the LFM, the peak velocity indicated by the pitot tube was again set to 60.1 ft/s by adjusting the gate valve to account for the change in system pressure drop, and the second profile was measured. In this, the normal system operating configuration, the profile was more peaked and the average velocity dropped to 54.4 ft/s for a flow of 111.4 cfm. The two radial velocity profiles are shown in Figure 12.

Although the difference between these total flow measurements differ by only 7%, the difference in the shape of the profiles invalidates the relationship between peak local velocity and the total flow. Using the pitot tubes for flow measurement would require a full traverse and integration in each cold leg, resulting in 44 different measurements for each change in the flow setting.

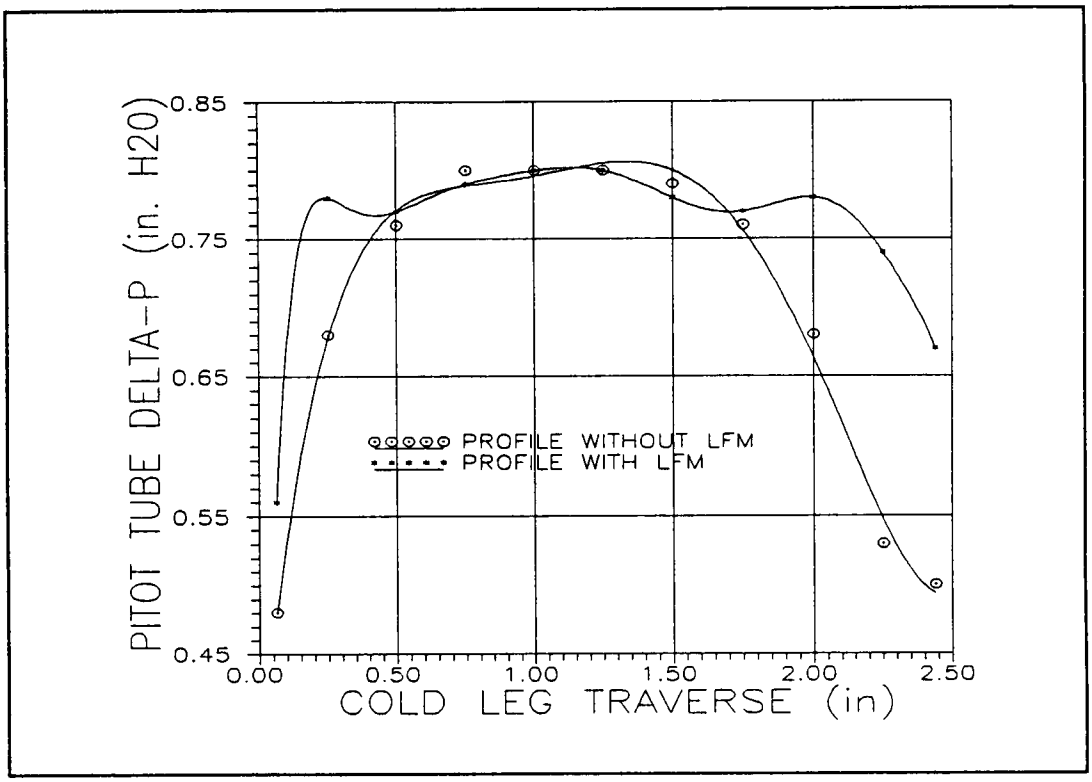


Figure 12: Cold Leg Radial Velocity Profiles

Because the calibration flowmeter affected the local velocity, it appeared necessary to either increase the cold leg length between the LFM and the pitot tube to allow more flow recovery or to use instrumentation less sensitive to local velocity. The current model allows little room to extend the cold legs, so new instruments were considered. Originally, orifice plates calibrated by construction to ASME specifications had been discounted because of the relatively high pressure drops which occur when a reasonable d/D ratio is used. Since another calibration instrument had been procured, it became feasible to construct an uncalibrated orifice with a high d/D (and therefore low pressure drop) which could be calibrated in-situ with the LFM.

Experimentation with the orifice design resulted in a 0.25 inch thick orifice with

a d/D of 0.88 installed at the cold leg nozzles. Flange taps were located at three positions, 120° apart, 0.5 inches on either side of the orifice. This arrangement, pictured in Figure 13, provided a pressure drop of approximately 0.9 inch of water at 120% flow, which allowed use of the MHGs originally procured for use with the pitot tubes. Comparison of orifice pressure drops with the LFM connected and removed showed that the readings were consistent within 4%, which is comparable to the precision of the MHG readings.

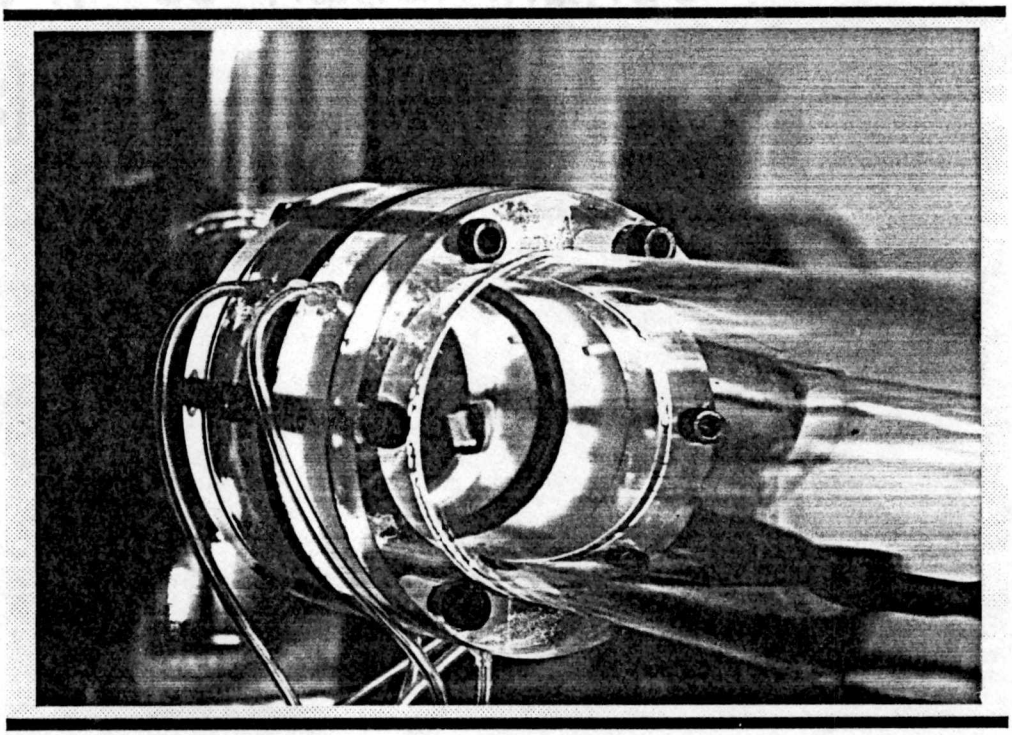


Figure 13: Flange Tap Orifice Assembly

Each orifice was marked for repeatability in assembly and assigned a dedicated MHG. They were then calibrated in-situ with the LFM. These calibrations resulted in four orifice pressure drop vs. SCFM curves, which are shown in Figures 14 through 17 for loops 1 through 4 respectively. The calibrations were corrected for temperature

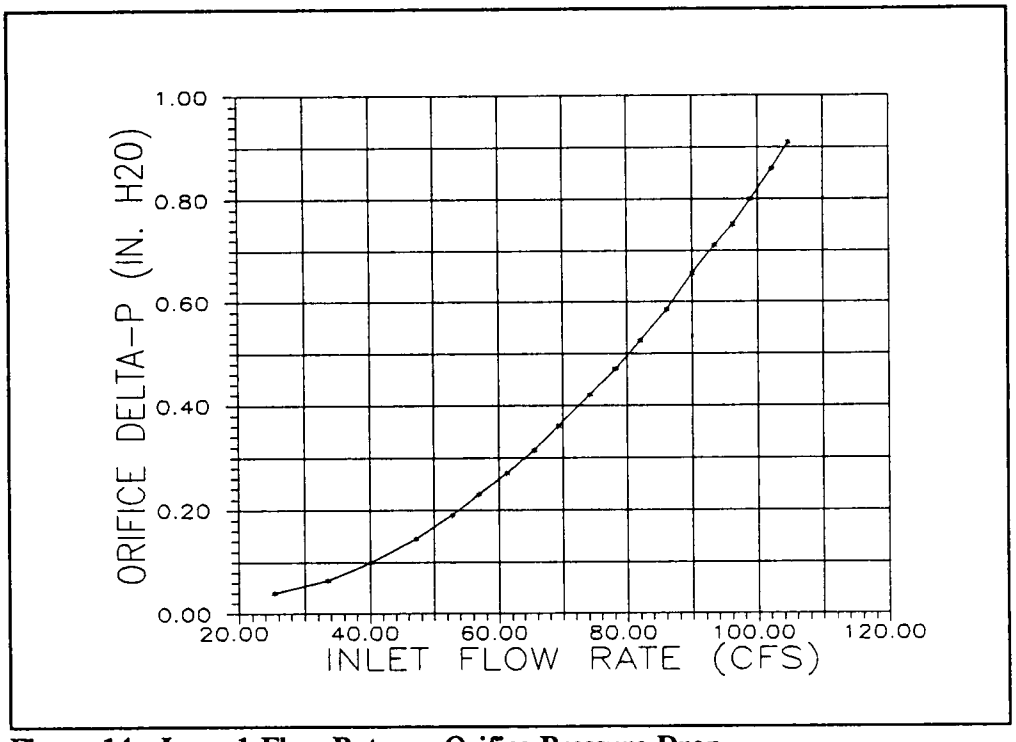


Figure 14: Loop 1 Flow Rate vs. Orifice Pressure Drop

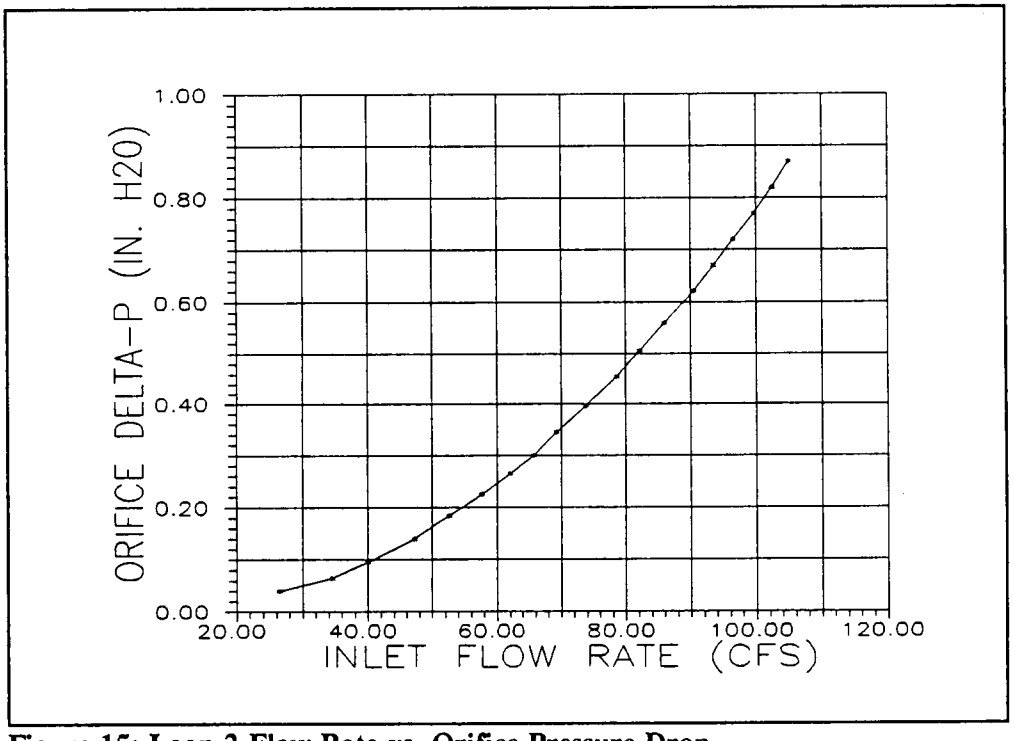


Figure 15: Loop 2 Flow Rate vs. Orifice Pressure Drop

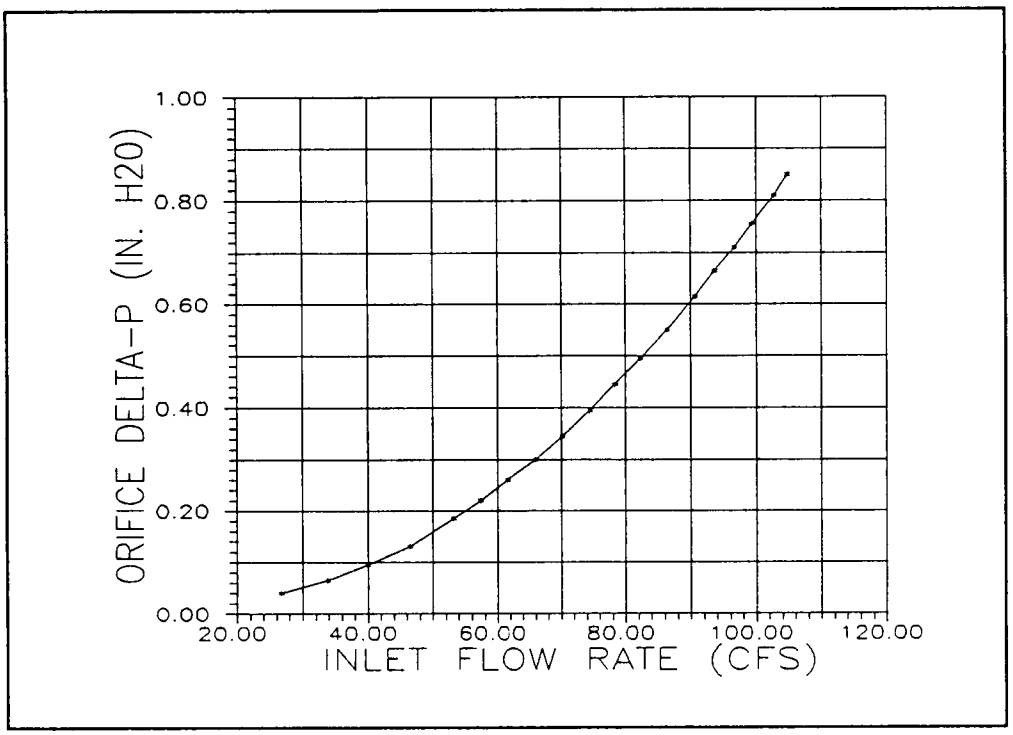


Figure 16: Loop 3 Flow Rate vs. Orifice Pressure Drop

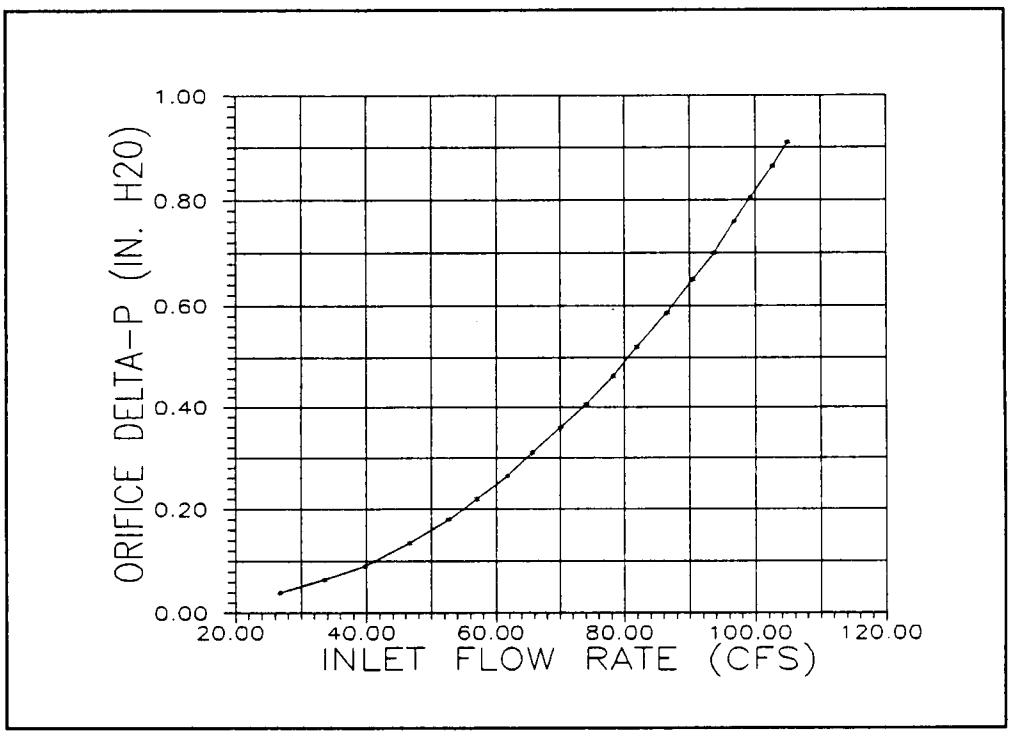


Figure 17: Loop 4 Flow Rate vs. Orifice Pressure Drop

related density and viscosity effects, as well as barometric pressure effects. It should be noted that the maximum flow achieved in each individual loop during calibration (with the LFM in place and the other three loops blocked) agreed within 0.2%, indicating excellent overall model flow balance.

2.3 Flow Visualization

To determine if vortical flow existed in the reactor model, it was necessary to either measure or visualize the flow field. Measurement of the velocity vectors in a large three-dimensional space is very difficult. Siemens engineers attempted to accomplish this by using 3-hole pitot tubes in a 1:10 scale air flow reactor model and eventually abandoned the task (Weber and Dittrich, 1973). Since the objective of these experiments was to confirm the absence or presence of vortices rather than measure their strength, visualization of the flow appeared to be a good choice.

Many techniques of flow visualization are available to the researcher. Most fall into three categories; intrusive interaction, injection, and non-intrusive optical techniques (Yang, 1984). In intrusive techniques, objects are placed in the flow field and are deflected to indicate the local flow direction. Such devices can perturb the flow field significantly. Wind vanes or tufts are examples of this technique. Injection techniques introduce a foreign material into the flow field. This material travels with the flow and can show full pathlines. This method is less intrusive than the last category but the injected material tends to disperse quickly if the Reynolds number is too large. Smoke

or neutral buoyancy bubble injection are examples of this technique. Optical techniques can be completely non-intrusive, but require distortion-free view paths and can be prohibitively expensive. Laser doppler anemometery, interferometry, and schlieren imaging fall into this category.

For the experiment at hand, it was clear that the visualization had to be relatively non-intrusive, since previous tests had shown that vortical flow in the lower plenum was sensitive to structures present in the plenum. On the other hand, laser-based optical methods were not clearly suitable and too expensive. Given these restrictions, tuft probe methods and schlieren visualization of helium injected into the flow field were chosen.

2.3.1 Tuft Methods

Tufts were used in several different ways. For general visualization of the surface flow field in the downcomer and the lower plenum, tufts were fixed to the surfaces with clear tape. Only the optically imperfect lower plenum hemisphere was prepared in this manner. Also, penetrations were provided in the cold legs, downcomer and the aforementioned lower plenum hemisphere for the insertion of probes with tufts attached to visualize local flow away from the surface.

Further development of these point visualization methods indicated that they were unacceptable for flow fields that changed rapidly. Since vertical-axis vortices were the most likely form of vortical flow expected, a method of visualizing a complete horizontal plane appeared necessary. Grids of tufts have been used extensively for this type of

visualization (Bradshaw, 1970), so this method was selected.

A tuft grid was constructed by forming a 12 inch diameter circle of heavy gauge steel wire and welding a grid of 36 gauge wires to it in a 0.5 inch crosshatch pattern. Tufts of polyester thread were epoxied at each wire junction, which also strengthened the grid structure. The optimum length of these tufts was determined experimentally. Longer tufts are more sensitive to low flow velocities, but tend to tangle with the crosswires and other tufts. A second, sturdier grid was also constructed with 30 gauge nichrome wires on 1 inch centers. This grid allowed longer tufts, giving greater sensitivity but less resolution. Both tuft grids are shown in Figure 18.

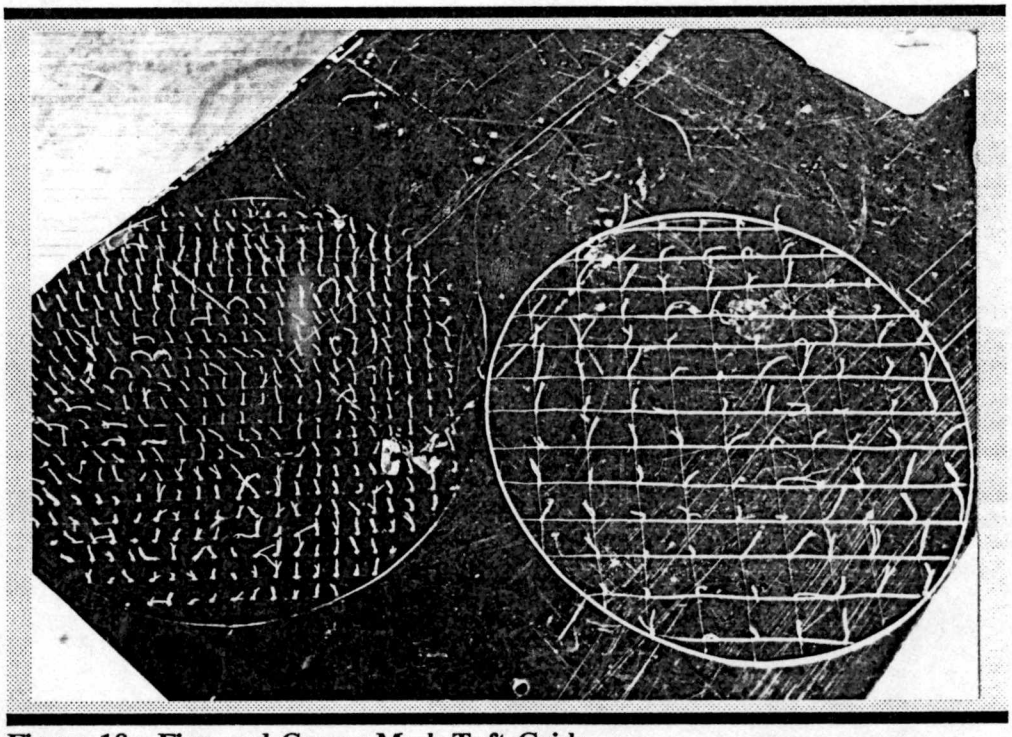


Figure 18: Fine and Coarse Mesh Tuft Grids

In operation, the tuft grid works very well. Since the complete horizontal plane can be seen at once, a cross-section of any vortex perpendicular to its axis of rotation can

easily be visualized. The grid was suspended with 30 gauge wires, giving about a 5 inch range of vertical motion which covers the upper two-thirds of the plenum. This travel allows visualization of much of the vertical axis of the vortices, although grid motion is limited by the overall diameter of the grid.

This method of visualization is clearly superior to any point visualization techniques because it can show multiple vortices and is not impaired by their movement. A good picture of the width of the vortices can also be easily obtained. On the other hand, the tuft grid is more intrusive than the schlieren technique and therefore more likely to perturb the flow field.

2.3.2 Schlieren Optical Method

Schlieren optical systems are used to visualize gradients in index of refraction. This is accomplished by collimating light from a point or slit source, directing the collimated light through the test region, and then focusing the light to a point which is partially blocked by a knife edge. Light which passes uniformly through the region causes a uniformly gray image on a screen beyond the knife edge. Refracted light will either be diverted into the knife edge causing a dark area on the image or away from the edge forming a bright spot. The resulting image depicts the first derivative of the index of refraction in the test image. If the knife edge is removed, the second derivative is visualized. The resulting image is called a shadowgraph (Holder and North, 1963).

To visualize the flow field in the reactor model with this technique, it was

necessary to create some local gradient in the index of refraction. This was accomplished by using a thin probe to inject helium gas. Helium was chosen because it has an index of refraction substantially different from air, it is not toxic or flammable, and it would not contaminate the model. This last problem is common with other injection methods such as smoke or bubble injection. Attempts to use neutral bubble injection in these experiments resulted in rapid fouling of the transparent model surfaces.

The schlieren optical system provides resolution in a vertical y-z plane, with x being the horizontal axis of the light beam. This allows visualization of a cross-section of a vertical vortex parallel to the axis of rotation. To allow visualization of some length of vortex, multiple hole helium injectors were devised. These probes consist of thin steel tubing with small holes drilled along both sides at one inch intervals. The holes are staggered so that the initial direction of the helium stream can be determined even if the opposing streams are parallel to the schlieren imaging. If this probe were to be placed in the center of a vortex with the initial injection path parallel to the schlieren axis, the staggered streams of helium should be deflected across the schlieren image in opposite directions by the rotational flow, making the vortex easily recognizable. Away from the vortex center, the helium streams would all be deflected to one side. The schlieren system is pictured in Figure 19, while two probes are shown in Figure 20.

Several techniques were attempted to improve the resolution and contrast of the schlieren image. The first acrylic hemisphere procured for the reactor model was formed essentially by blowing a bubble in an extruded sheet of acrylic plastic. Viewed with the schlieren system, a pattern of variations in the index of refraction of this material became

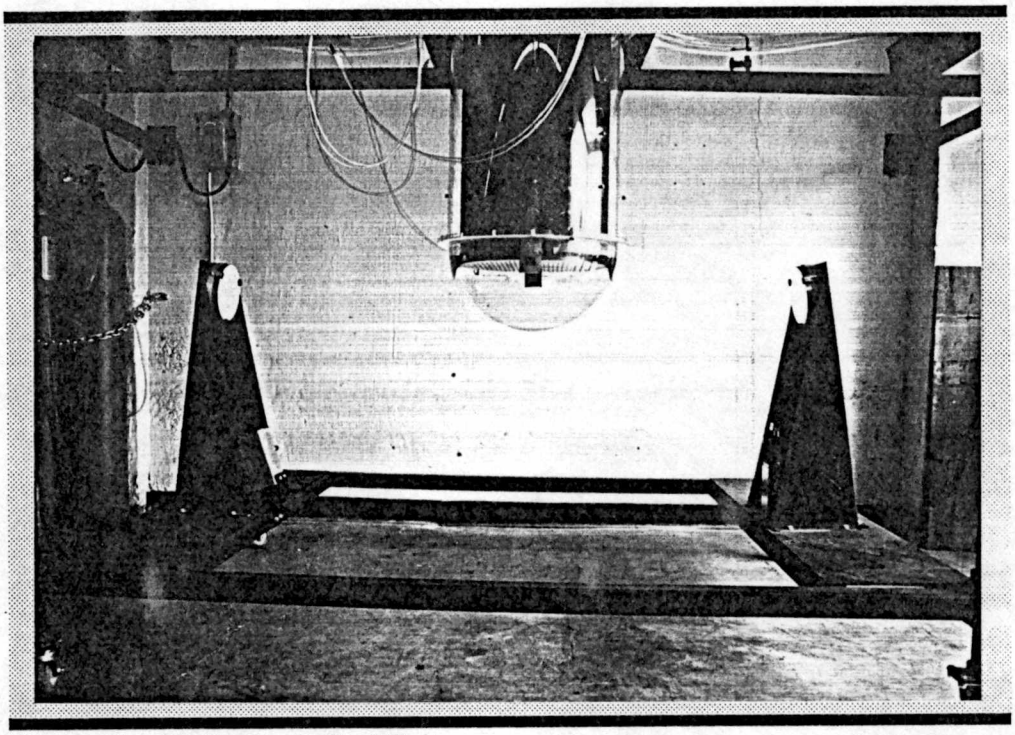


Figure 19: Schlieren Optical System

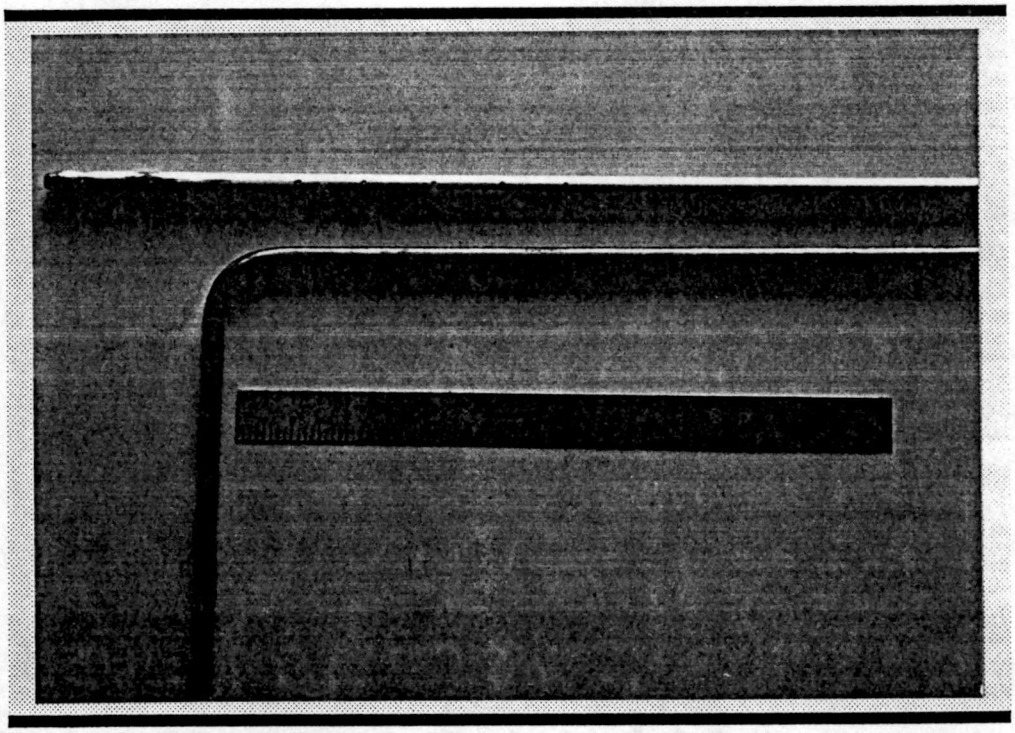


Figure 20: Helium Injection Probes

very noticeable. Hypothesizing that a cast acrylic material may perform better, a vacuum molded cast acrylic dome sample was obtained and tested. This material was free of any patterning, however, passing the light beam through what are effectively two thin lenses prevented focusing the light to a symmetric focal point on the knife edge, the heart of the schlieren optics. By removing the knife edge, a shadowgraph image of the injected helium was clearly observed.

Further improvements to the optics of the system did not appear to be economical, so variations on the use of the knife edge were attempted. Since the focal point was asymmetric, opaque filters in the shape of rods, circles, and the shape of the focal point itself were applied to block the direct image. Colored gels were also applied in the place of the opaque filters to try to obtain a multicolor image. The use of a wire through the long axis of the focal point did provide some small improvement in contrast, but not sufficient to justify its use. No significant improvement over the basic shadowgraph image was obtained.

Using the improved optical system and injection probes proved somewhat disappointing. The helium stream was clearly visible as it left the injector, but dissipated quickly in the model air flow. Although the stream deflection expected within a vortex was observed occasionally, it did not appear constant and did not always occur in the same areas. It became apparent that the vortices either moved or dissipated quickly. This made it difficult to be certain that a vortex existed as opposed to some transient shear flow conditions.

These tests demonstrated that although the schlieren technique was workable, no

point visualization method was going to provide the conclusive evidence of vortical motion that was desired. For this reason, the tuft grid was used for virtually all of the flow field visualization.

2.4 Vortex Suppression Devices

The main objective of this research was to prevent the excitation of vortical flow in the lower plenum. Vortex suppression has been studied extensively for a variety of reasons. In particular, suppression of vortices caused by flow separation from a surface has applications in reducing drag or minimizing flow induced vibration. Most of these methods involve forcing the flow to adhere to the surface or diverting flow to fill the area following separation to smooth the separated flow (Wong, 1982).

In the reactor model, vortical flow is thought to be driven by a sink. In this case, there is no physical flow separation, nor can the sink be filled. To suppress this type of vortex, it is necessary to remove the initial source of angular momentum or prevent the vortex from organizing. The hypothesized source for angular momentum in the lower plenum is azimuthal velocity shear in the flow exiting the downcomer. It may be possible to equalize the velocity in this flow by creating a large pressure drop, such as would be caused by a restriction at the bottom of the downcomer annulus.

Disorganizing the vortex is a more straightforward approach. Previous research has shown that a dome-shaped core support plate suppresses vortices in some of the operating Westinghouse plants (Cadek et al., 1988). This is probably the result of an

inability of the vortex to seal against the CSP, allowing fluid to flow radially into the low pressure vortex core. Surface roughness on either the CSP or the plenum hemisphere should have the same effect.

Previous experiments have also shown that structural material in the plenum can break up vortices. In this vein, Westinghouse engineers have designed a vortex suppression device (Westinghouse Drawing M101, 1990). This device is essentially two concentric rings positioned perpendicular to the axis of the expected vortices. It is located in the lower plenum below and parallel to the core support plate, supported by twelve columns. This method of vortex suppression was chosen for the experiment.

A 1:9 scale model of the vortex suppression device (VSD) was fabricated from clear acrylic. Rather than duplicate the twelve support columns, the device was supported by four thin threaded steel rods which allow a full range of elevation adjustment. The intent of this change was to minimize the effect of the columns, thereby isolating the effect of the VSD. The tuft grid used to visualize the flow field was supported by small brass wires about one inch above the VSD. This rigid mounting was designed to prevent damage to the grid from the support rods. Figures 21 and 22 show the vortex suppression device from below and from the side, respectively, while installed in the lower plenum of the model.

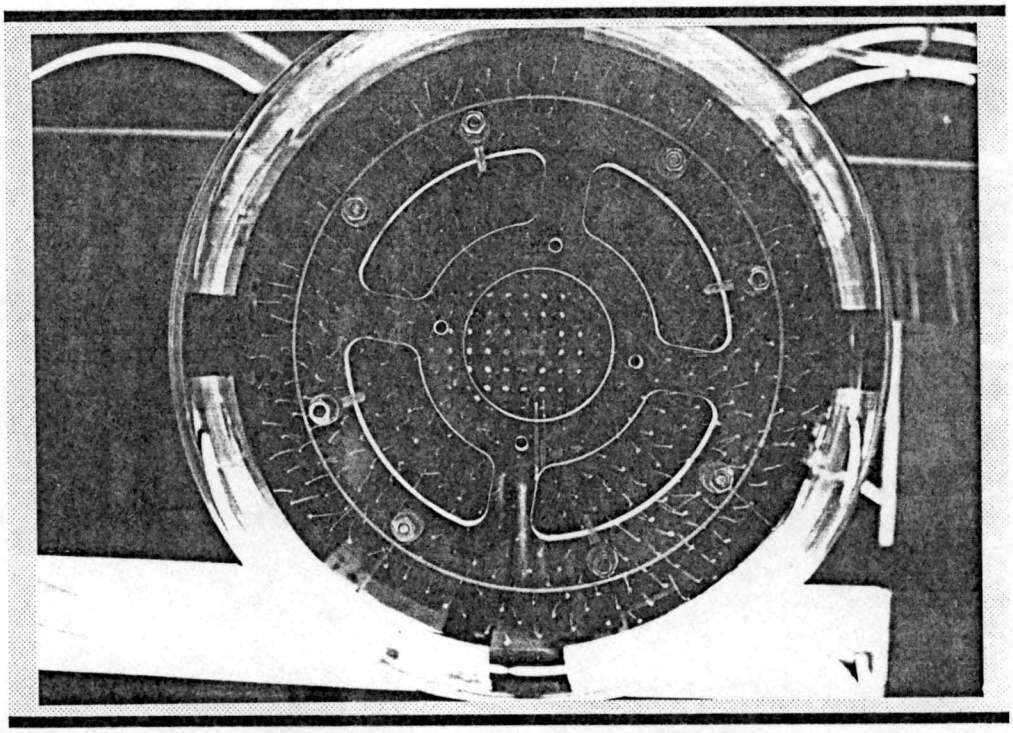


Figure 21: Bottom View of the Vortex Suppression Device

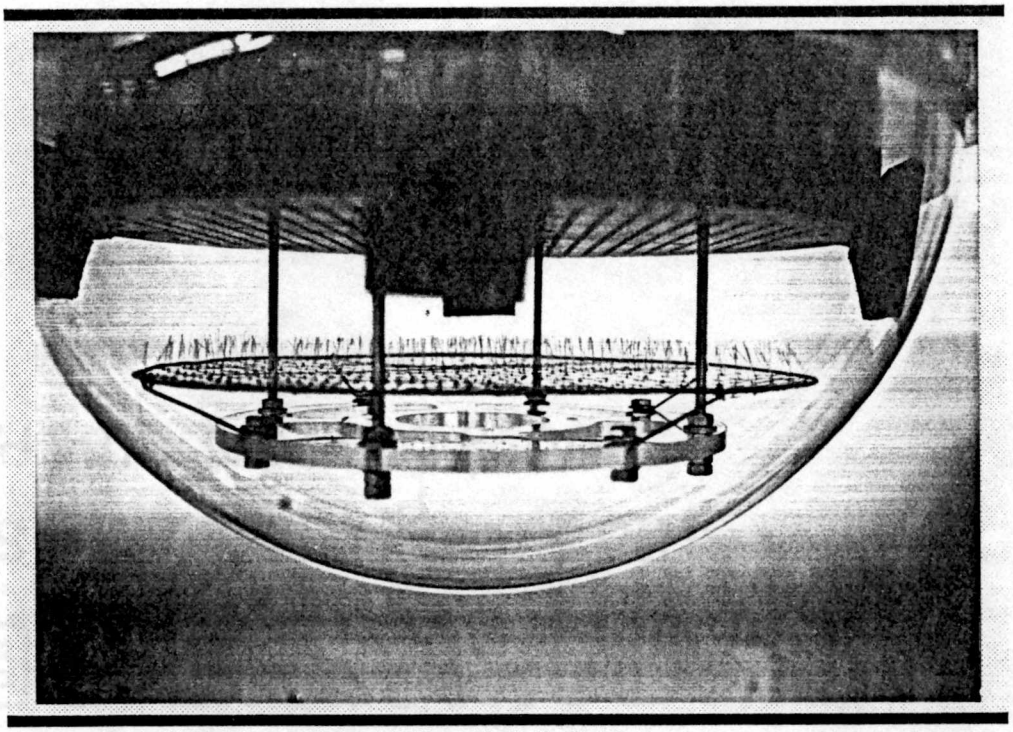


Figure 22: Side View of the VSD and Tuft Grid

3.0 EXPERIMENTAL RESULTS

3.1 Characterization of the Unobstructed Flow Field

The first set of experiments was designed to characterize the flow field in the lower plenum when no structures were located below the core support plate. The vortex suppression device and its associated hardware were not installed. The flow field visualization was accomplished with the fine mesh tuft grid, which provided much better resolution than the coarse mesh grid. The tuft grid was supported by wires passing through holes in the vessel wall, allowing positional changes without disassembling the model. It should be noted that the presence of the tuft grid had some effect on the flow field, however minor. More sophisticated visualization techniques would be necessary to quantify this effect, but it is thought to be small, since this technique has been used to visualize a variety of flow fields (Bradshaw, 1970).

Still photographs were taken as necessary to record the flow field whenever a parameter was changed. Photographs were taken with a Canon A-1 SLR camera using Kodak Ektar 1000 ISO print film. Experimentation with the exposure showed that an aperture of f2.8 and a shutter speed of 1/125 s provided the best combination of brightness and resolution. The tuft grid was preferentially lighted using a slit light source.

3.1.1 Observed Flow Fields With Radial Keys Offset From the Cold Legs

Two parameters were varied in the set of tests designed to characterize the flow field with an unobstructed plenum; the flow rate and the position of the radial support keys. For the first series of tests performed, the radial support keys were aligned at 0°, 90°, 180° and 270° referenced to the inlet legs which are located at 45°, 135°, 225°, and 315° in agreement with Figure 5. This geometry is hereafter referred to as having "offset radial keys", and is based on the Westinghouse design (Westinghouse Drawing M101, 1990). Using this model geometry, the total model flow rate was set to eight specific values ranging from 50% to 120% of the nominal design flow rate in 10% increments. This flow adjustment was accomplished using the system gate valve.

The test series was initiated at 120% flow with the tuft grid located 1 inch below the core support plate, about one-sixth of the distance to the bottom of the plenum and just below the bottom of the radial keys. Fluctuating vortical flow was immediately apparent. The predominant flow field consisted of two counter-rotating vortices positioned around a horizontal circle of constant radius about halfway between the center of the CSP and the plenum wall. The vortices tended to fluctuate between two specific azimuthal positions with vortices centered at about 100° and 340° or at 30° and 120°. Other flow fields were also observed, including instances when the vortex centered near 100° dissipated completely, but these configurations were less predominant. The two most common flow fields are shown in Figures 23 and 24.

The flow fields observed at 120% flow were little changed as flow rate was

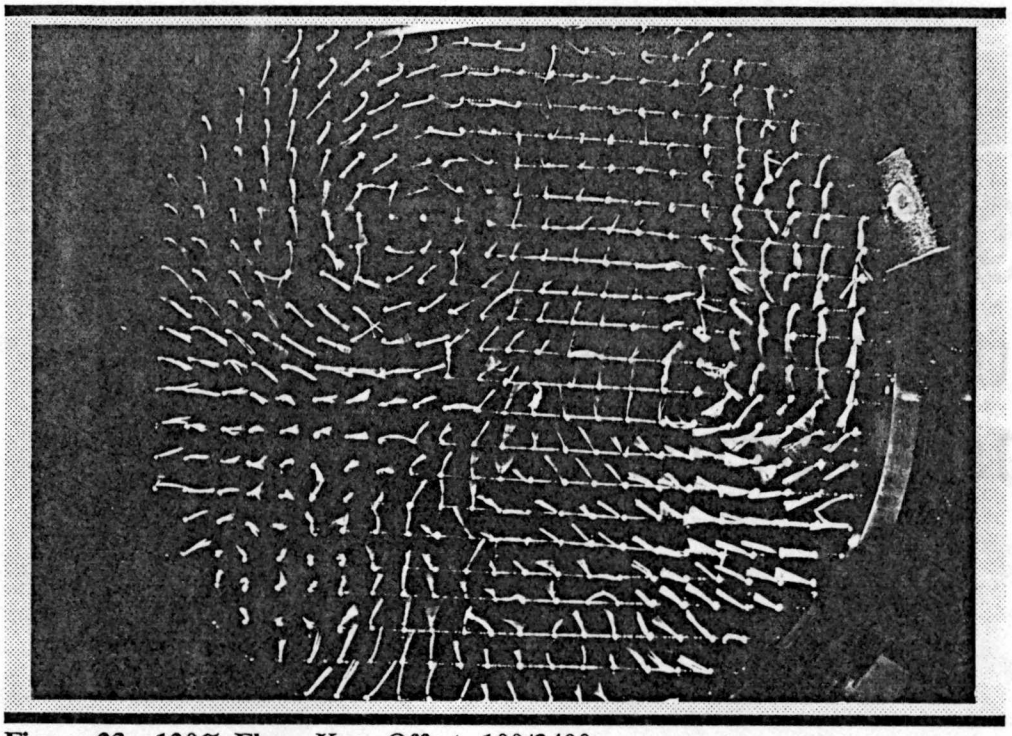


Figure 23: 120% Flow; Keys Offset; 100/340°

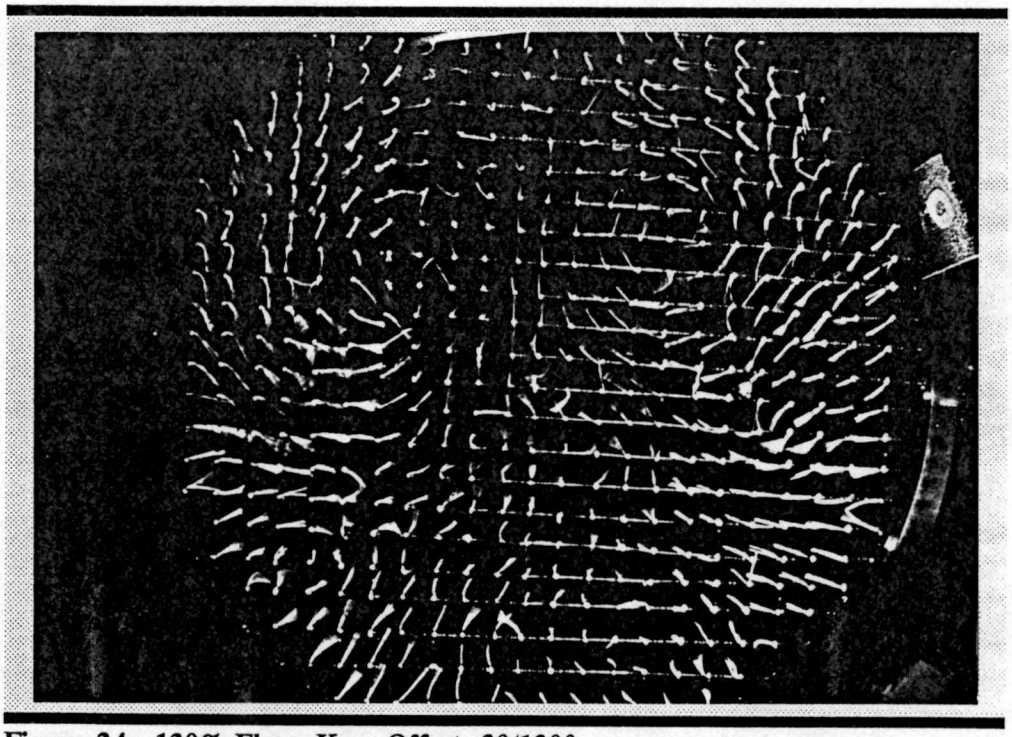


Figure 24: 120% Flow; Keys Offset; 30/120°

reduced to 110%, and then 100%. Visualizations at 100% flow rate which are almost identical to those at 120% flow are shown in Figures 25 and 26. In addition, Figure 27 shows a good visualization of the case where one of the vortices has mostly dissipated.

In an attempt to visualize the length of the vortices, the tuft grid was moved downward in three one inch increments until the grid rested against the plenum wall. This range of tuft grid elevations cover the upper two-thirds of the plenum, similar to the range of motion of the VSD shown in Figure 4. Figure 28 shows a flow field similar to that in Figure 26 but with the tuft grid lowered one inch. This series is continued with the tuft grid lowered two and three inches in Figures 29 and 30, respectively.

From this series of photographs, it would appear that the size, strength and location of the vortices change very little over this three inch elevation range. The center of each vortex has moved slightly outward by about 0.5 inch. Subjectively, the azimuthal position of the vortices appeared less stable lower in the plenum. The movement of a tornado, with a fixed top and a roving bottom, was suggested.

As the flow rate was reduced further, the positions and behavior of the vortices remained the same while the overall strength dropped. Photographs with 80% and 50% flow rates are shown in Figures 31 and 32, respectively. At 50% flow rate, the vortices were weak but clear to the eye, and barely visible in the photograph. This is almost certainly caused by lack of sensitivity in the tuft grid. Experimentation with the coarse mesh grid did not improve the observed results. Although the sensitivity was increased slightly, the coarse grid has lower resolution which prevented good visualization.

All indications from the visualizations performed while flow was reduced are that

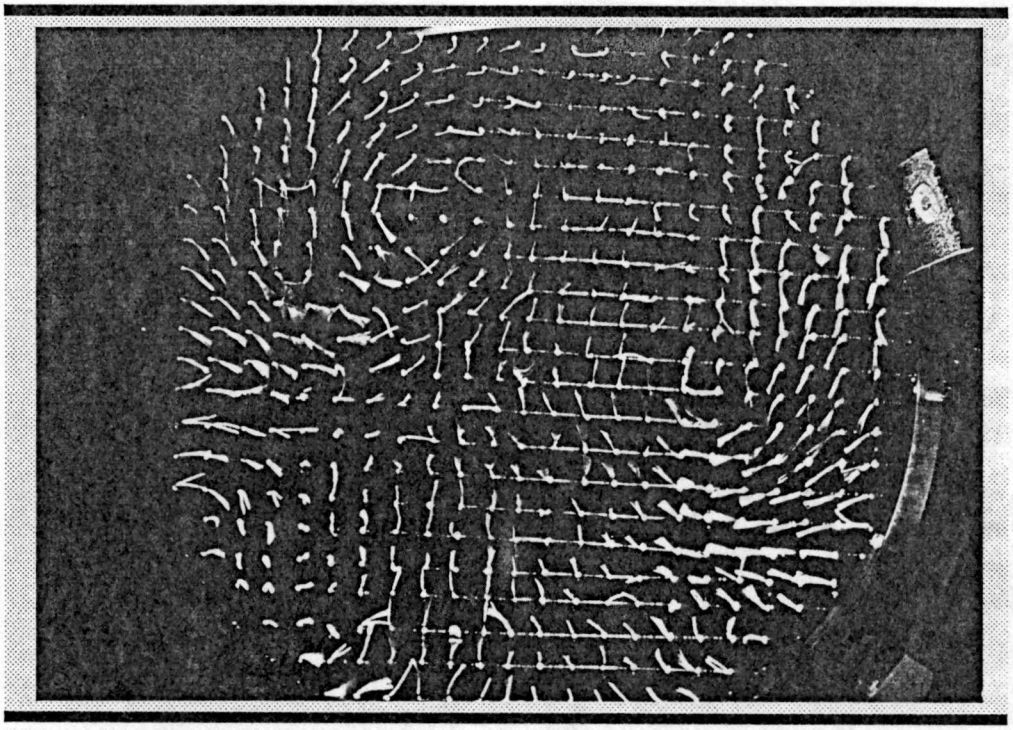


Figure 25: 100% Flow; Keys Offset; 100/340°

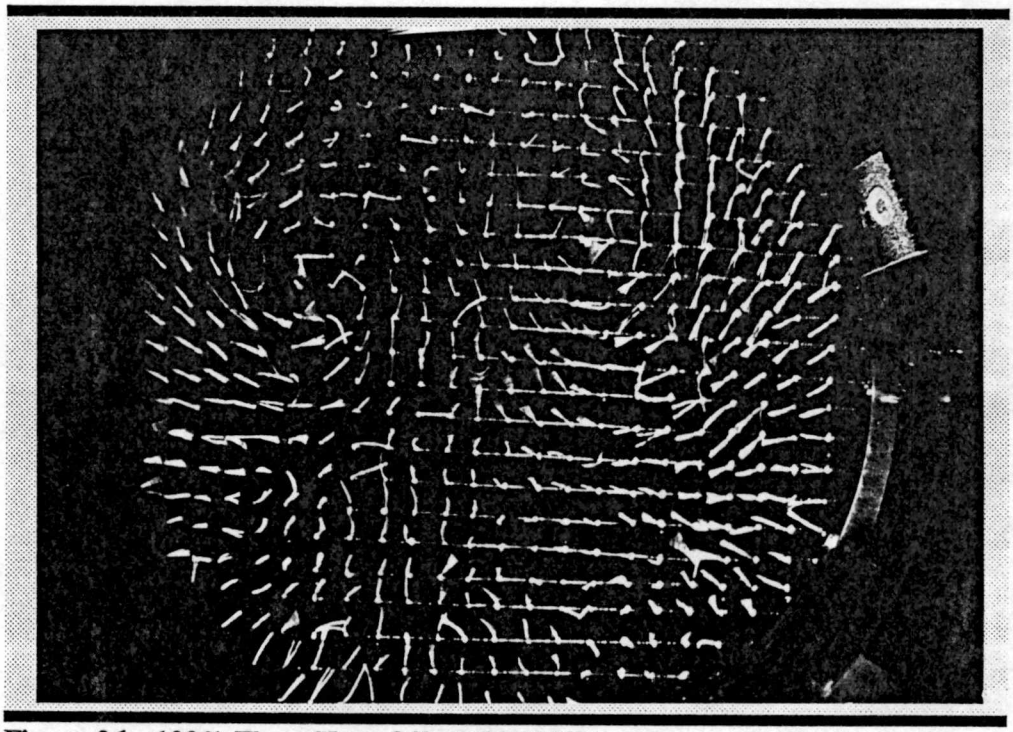


Figure 26: 100% Flow; Keys Offset; 30/120°

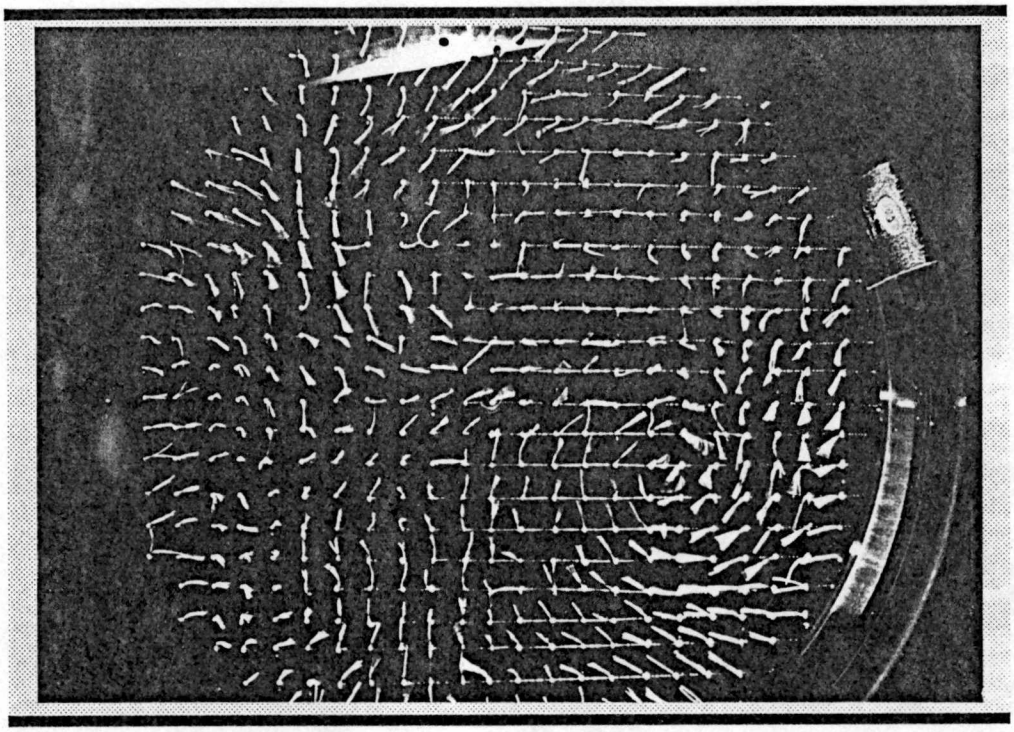


Figure 27: 100% Flow; Keys Offset; Single Vortex

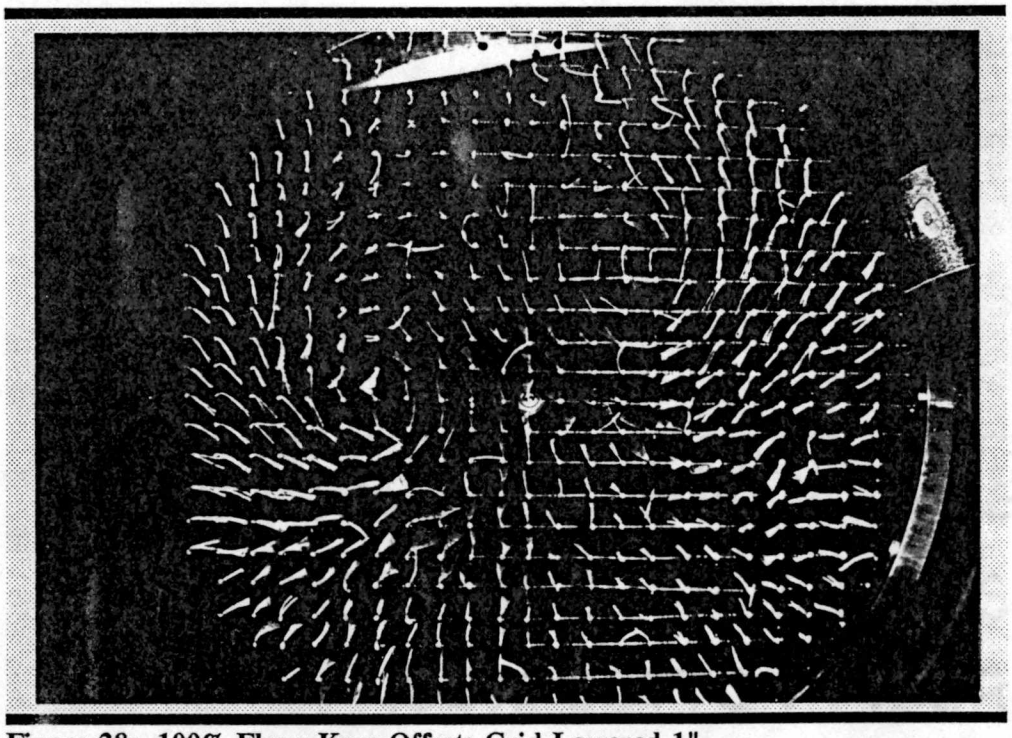


Figure 28: 100% Flow; Keys Offset; Grid Lowered 1"

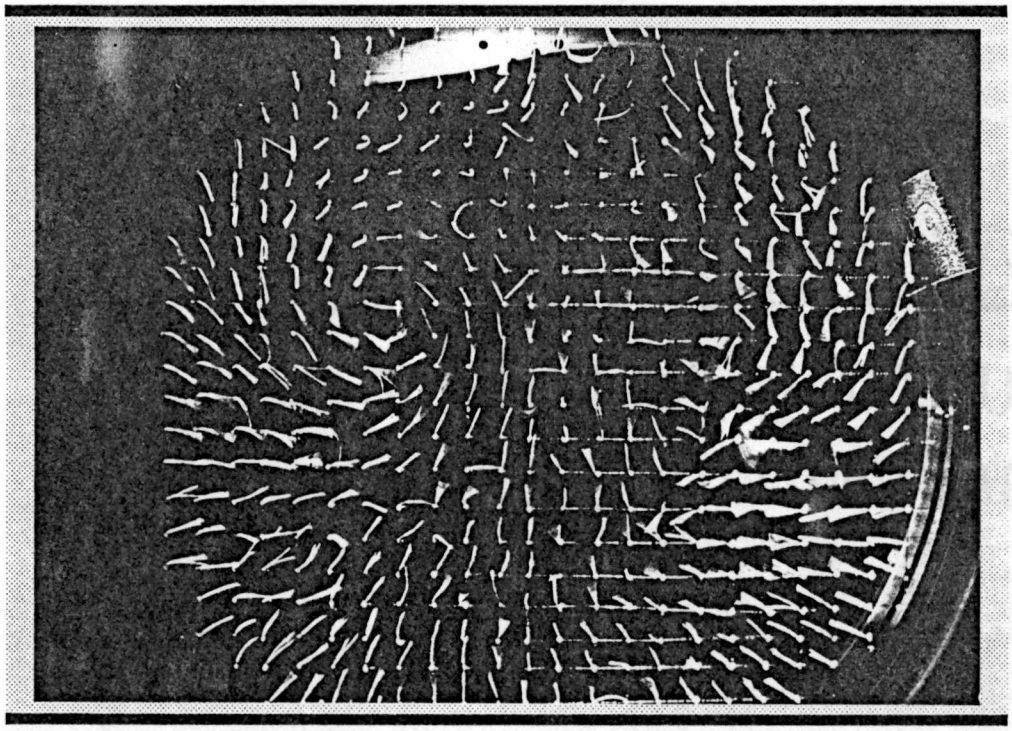


Figure 29: 100% Flow; Keys Offset; Grid Lowered 2"

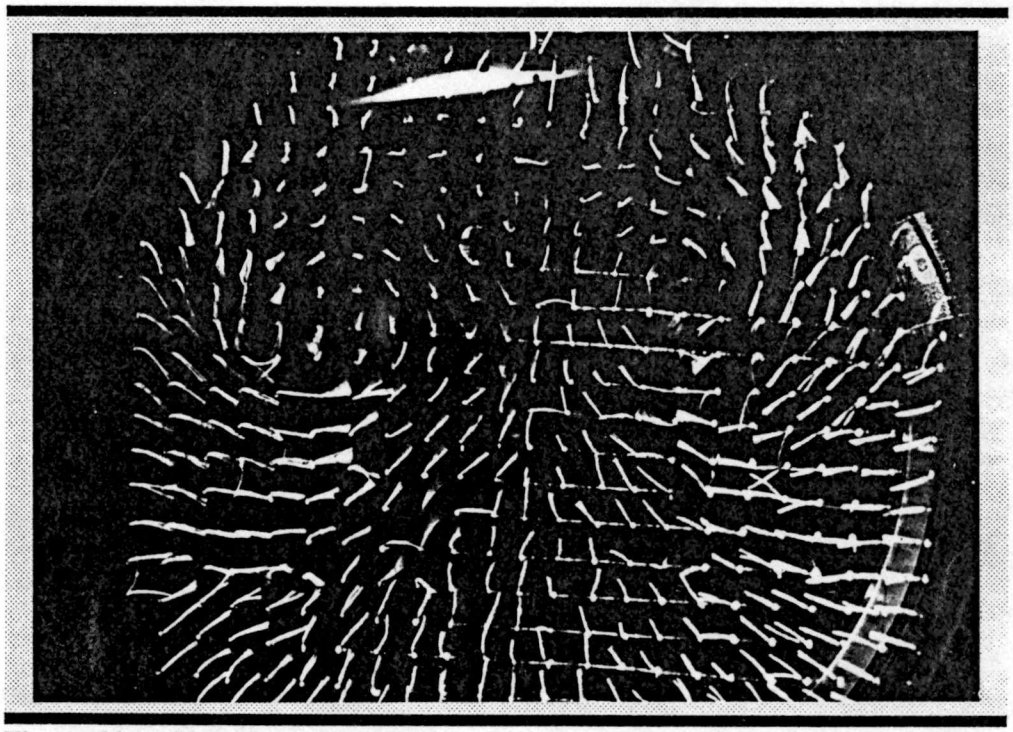


Figure 30: 100% Flow; Keys Offset; Grid Lowered 3"

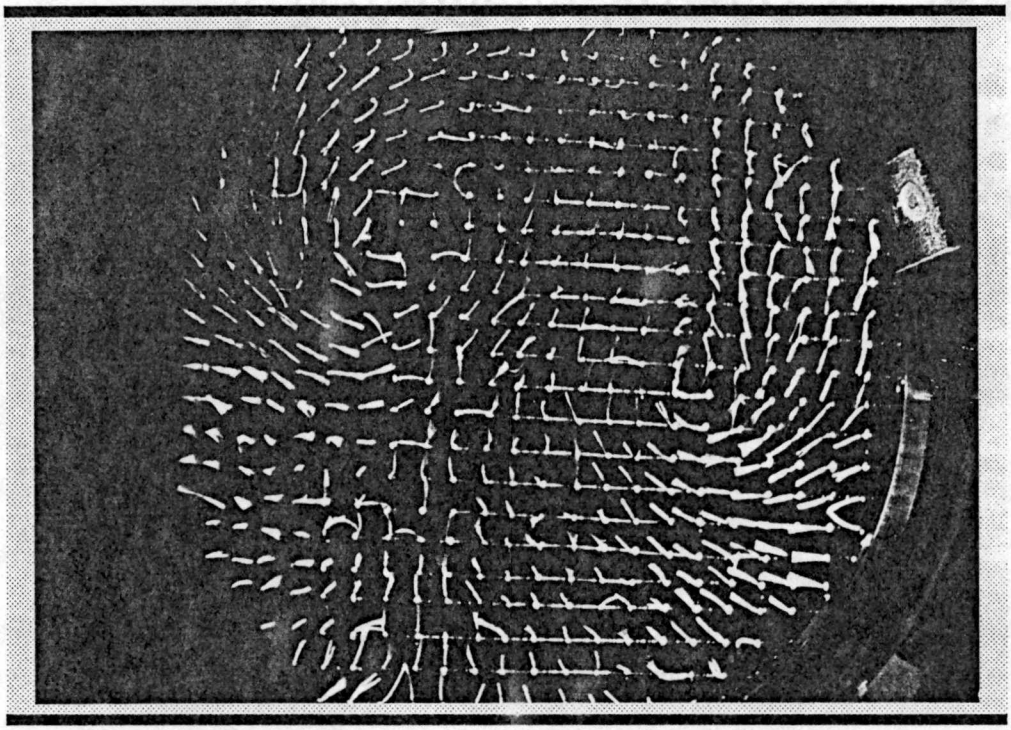


Figure 31: 80% Flow; Keys Offset

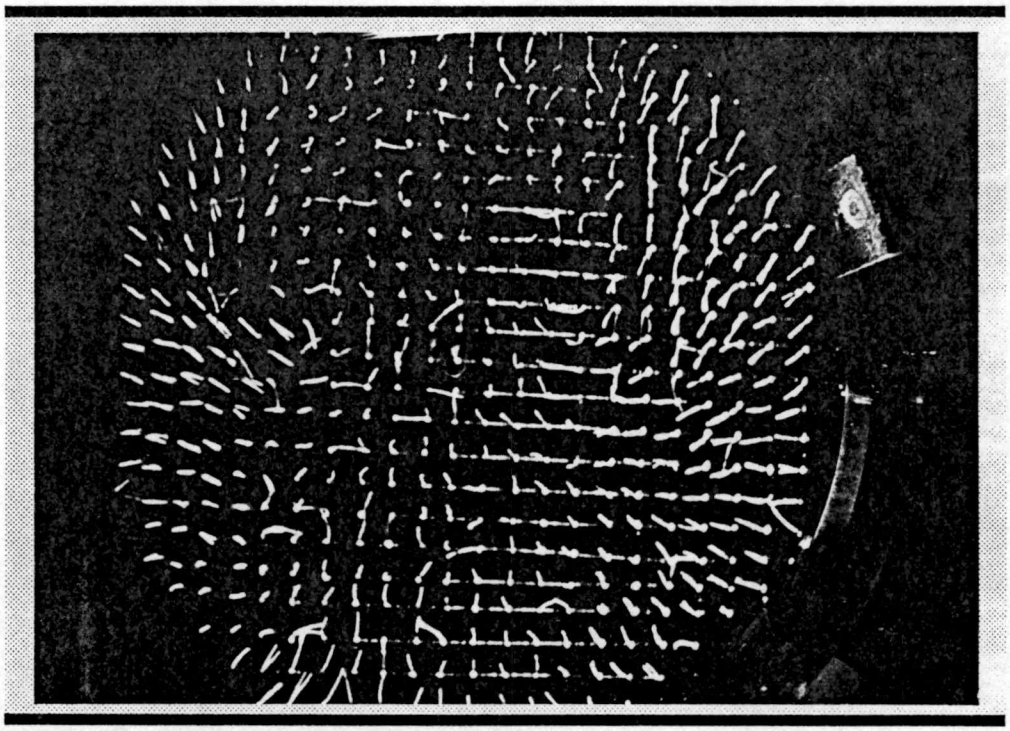


Figure 32: 50% Flow; Keys Offset

the vortices do not dissipate at lower flow rates. This result is consistent with the theory of combination sink-irrotational vortices as discussed in Section 1.2. Flow fields observed with flow rates besides those pictured exhibit an appearance virtually identical to the figures presented, so they are not reproduced here.

3.1.2 Observed Flow Fields With Radial Keys Aligned Below the Cold Legs

For the next series of tests, the CSP, with radial keys attached, was rotated 45°, so that the keys were at 45°, 135°, 225°, and 315°, aligned directly under the cold leg nozzles. This configuration is referred to as having "aligned radial keys." As before, eight flow rates were studied, ranging from 50% to 120% of the design flow rate in 10% increments.

The flow fields observed at 120% flow rate were quite similar to those seen in the last series of tests, with two counter-rotating vortices forming along a horizontal circle of constant radius. In general, the vortices observed in this configuration were less robust than those observed with the radial keys offset, and the azimuthal positions of the vortices are significantly different. The flow field was much less stable, with vortices forming and dissipating. Much of the time, no organized vortices existed at all, a condition which was seldom observed in the offset radial key configuration.

When the vortices were organized, two flow fields predominated as before, with vortices centered around 100° and 180° in one case and 20°and 100° in the other. In the first case, the vortices appear fairly strong, although not as well defined as those in

the last test series. The second case shows weaker vortices, perhaps not even complete vortices but upward spiraling flow which does not complete a full rotation. These two flow fields are pictured in Figures 33 and 34, respectively.

The vortices were observed to weaken but not dissipate as the flow rate was reduced to 80%, with the 100°/180° vortex pattern most commonly seen. This flow field at 80% flow rate is shown in Figure 35. At 70% flow rate and below, the partial vortex pattern centered about 20°/100° predominated, with even less indication that a full circle was being completed. The flow field at 50% flow rate, pictured in Figure 36, shows "J" shaped flow patterns which would appear to indicate flow spiraling steeply upward. This observation may result from a lack of sensitivity in the tuft grid, but it appears to be the true flow pattern. Moving the tuft grid vertically might provide a better picture of the overall flow field.

3.2 Characterization of the Suppressed Flow Field

The next set of tests was performed to evaluate the effect of the vortex suppression device on the flow field under conditions similar to those which excited vortices in Section 3.1. The suppression device described in Section 2.4 was placed in the lower plenum, supported from the core support plate by four adjustable threaded rods. The nominal elevation for the VSD was scaled to 3.66 inches below the CSP based on the reactor design drawing (Westinghouse Drawing M101, 1990). The tuft grid was supported by thin rods one inch above the VSD, so the two pieces were adjusted

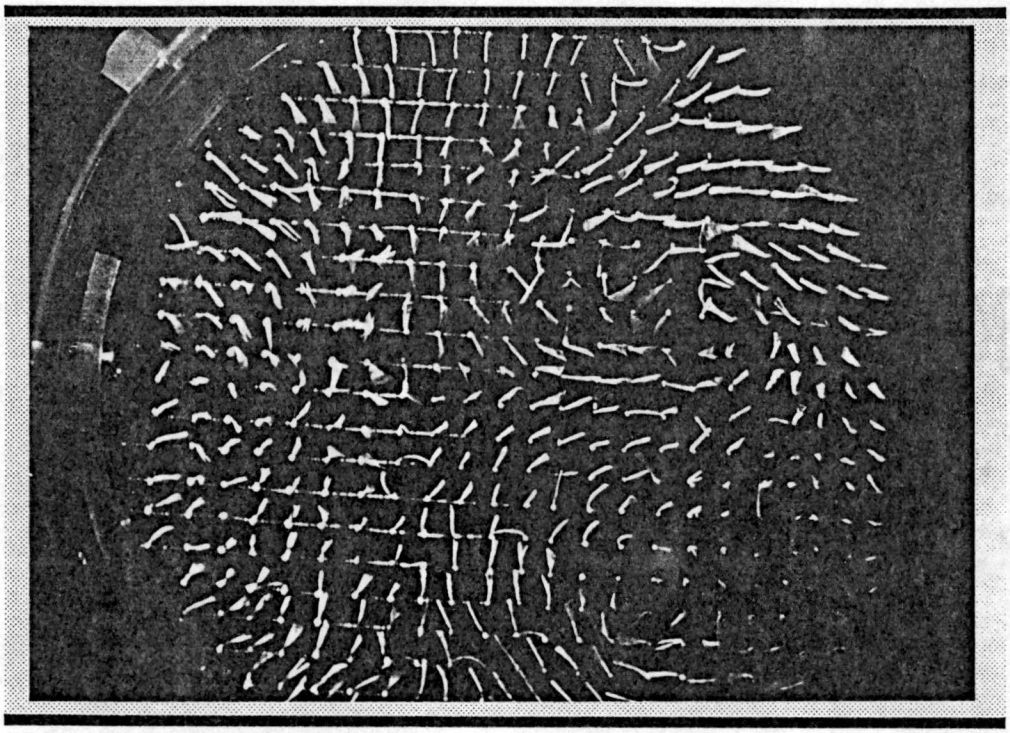


Figure 33: 120% Flow; Keys Aligned; 100/180°

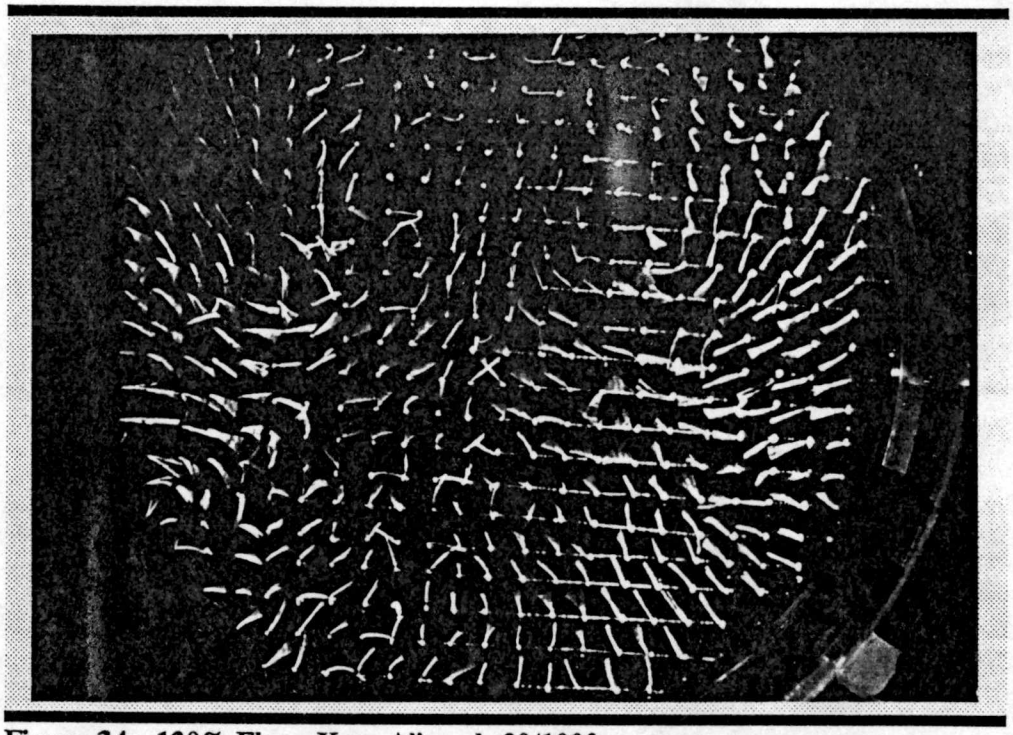


Figure 34: 120% Flow; Keys Aligned; 20/100°

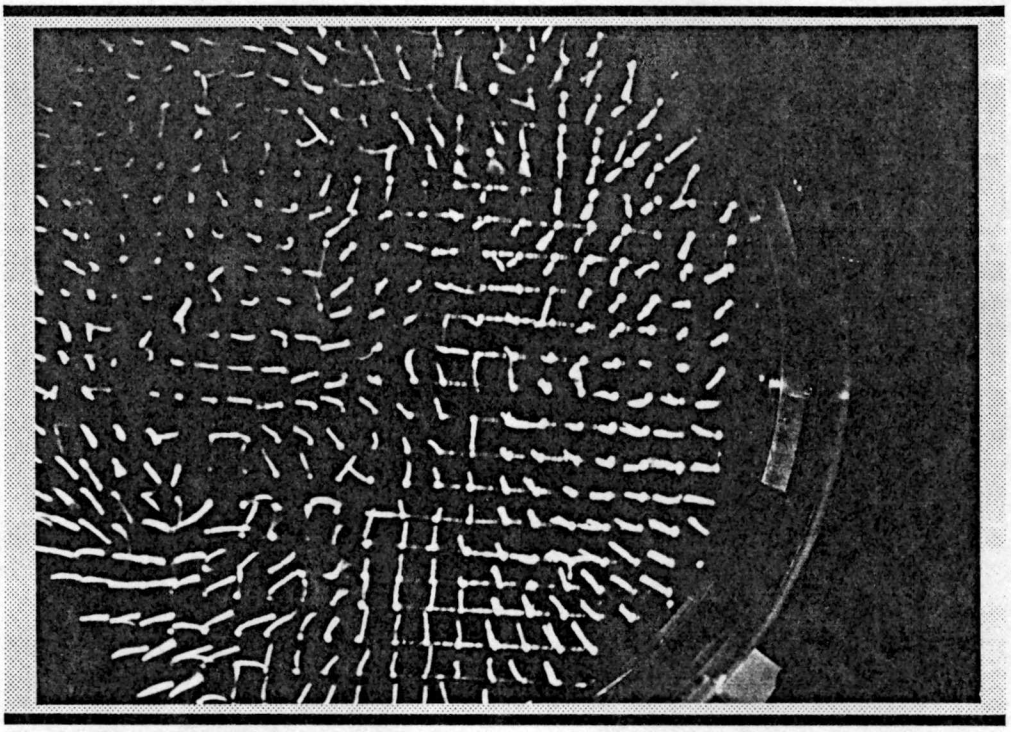


Figure 35: 80% Flow; Keys Aligned

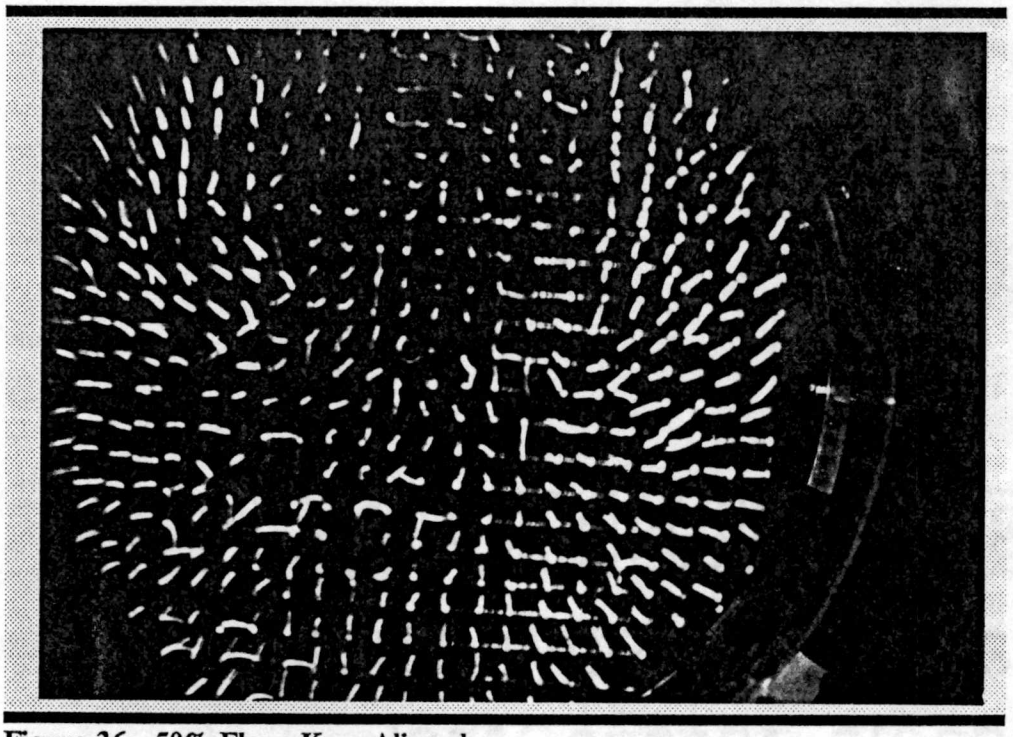


Figure 36: 50% Flow; Keys Aligned

vertically as a unit. No other aspect of the model was changed for these tests.

Three parameters were varied in this set of tests; radial key position, VSD position, and flow rate. As before, two radial key positions, offset and aligned, were modeled. The effect of the vortex suppression device was evaluated in three different positions; the nominal distance below the core support plate, raised one inch, and lowered one inch. Flow rate with the VSD in the nominal position was varied from 50% to 120% in 10% increments for direct comparison with the previous tests. Fewer flow rates, ranging from 60% to 120% in 20% increments, were examined when the VSD was moved to the two off-nominal positions.

It should be noted that the flow field was always visualized between the vortex suppression device and the core support plate. The flow field below the VSD was not observed and vortical flow may develop there. Without a low pressure core which extends to the CSP, vortices in this region should be of little concern.

3.2.1 Observed Flow Fields With Offset Radial Keys

The first series of tests in this set was conducted with the radial keys offset from the cold legs as described in the last section. This key alignment was associated with the strongest vortical flow when the lower plenum was unobstructed. The full range of flows were first observed with the vortex suppression device located at the nominal design elevation. In this configuration, no evidence of vortical flow was observed subjectively or recorded in the photographs at any of the eight flow rates tested.

The effect of the VSD can be seen by comparing Figure 37, which is a reproduction of Figure 23 (120% flow rate without vortex suppression), to Figure 38, which illustrates the flow field for the same conditions as the last photograph with the VSD installed. The flow fields observed for flow rates lower than 120% were virtually identical to that shown in Figure 38.

Similar results were observed when the VSD was lowered one inch below the nominal position. In this configuration, flow rates from 60% to 120% in 20% increments were studied. The flow fields closely resembled those observed with the VSD at the nominal elevation, with perhaps some additional horizontal flow component where the edge of the suppression device closely approaches the plenum wall. This observation may result from repositioning the tuft grid, which is attached to the VSD. No indication of vortical flow was seen at any flow rate. Figures 39 and 40 show the flow fields at 120% and 60% flow rate, respectively.

Raising the vortex suppression device closer to the core support plate, one inch above the nominal elevation, resulted in some noticeable changes, as illustrated in Figures 41 through 44. With the VSD raised, at 120% flow, a weak vortex was clearly visible at about the 200° azimuthal location, with a radial position similar to those observed without the VSD. This flow field, pictured in Figure 41, can be compared directly to the unobstructed flow field in Figure 37. Both flow fields have a similar pattern, but are rotated with respect to each other. The vortical flow in the suppressed case is definitely weaker than in the unsuppressed case. This vortex remains discernable at the lower flow rates, as can be seen in Figures 42 through 44 at 100%, 80% and 60%

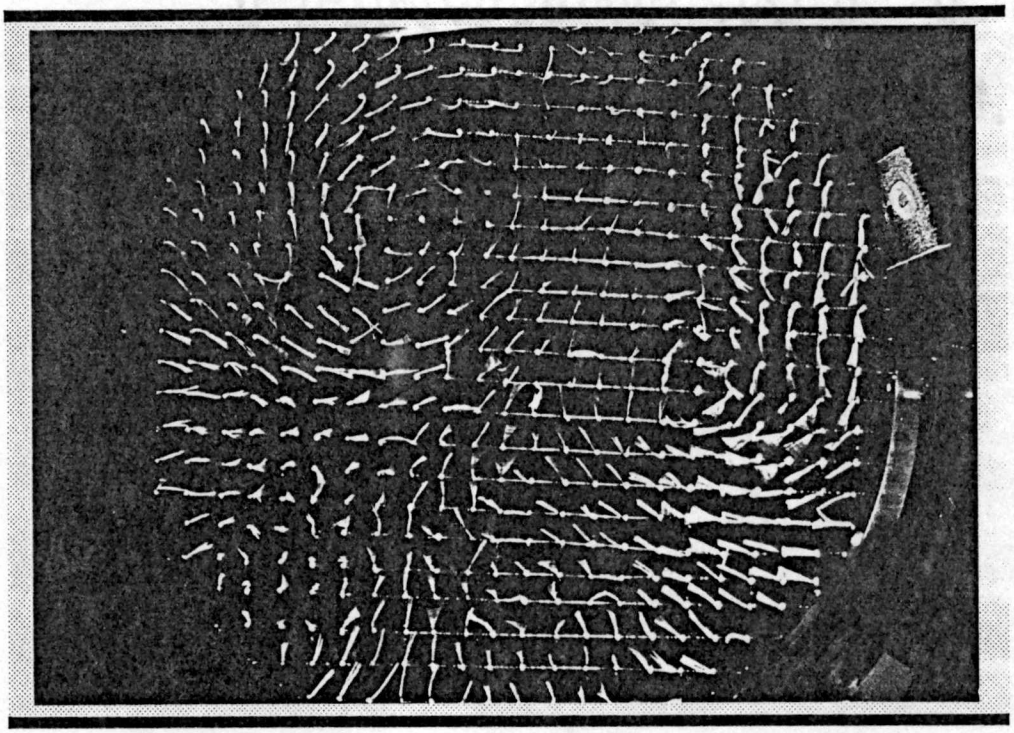


Figure 37: 120% Flow; Keys Offset; No VSD

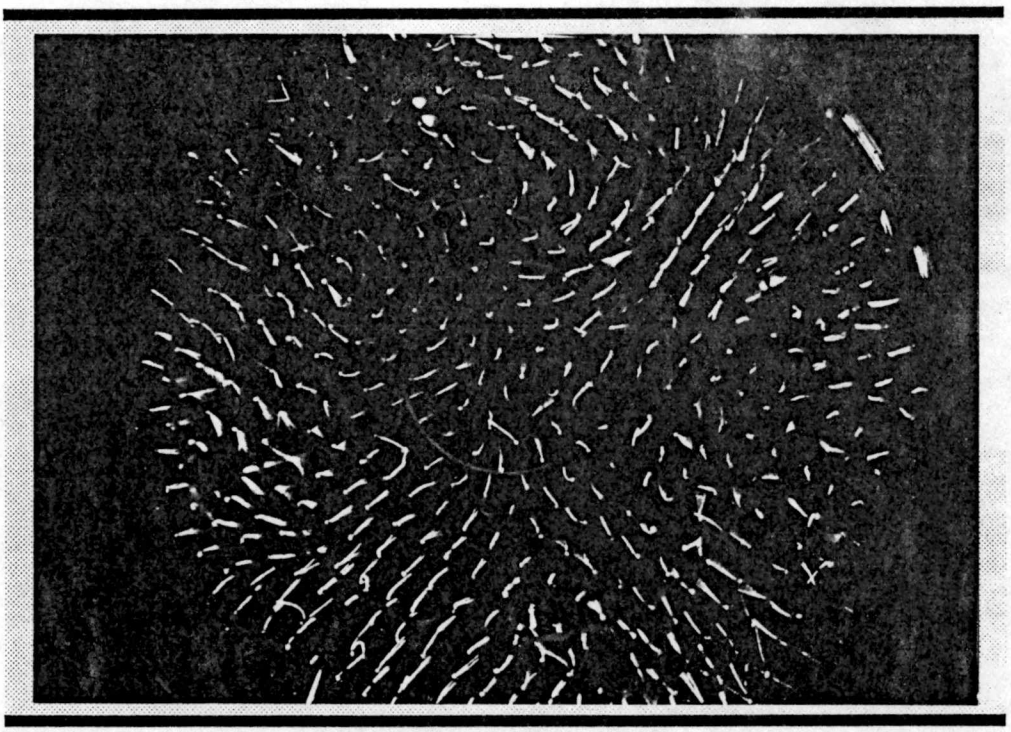


Figure 38: 120% Flow; Keys Offset; VSD Nominal

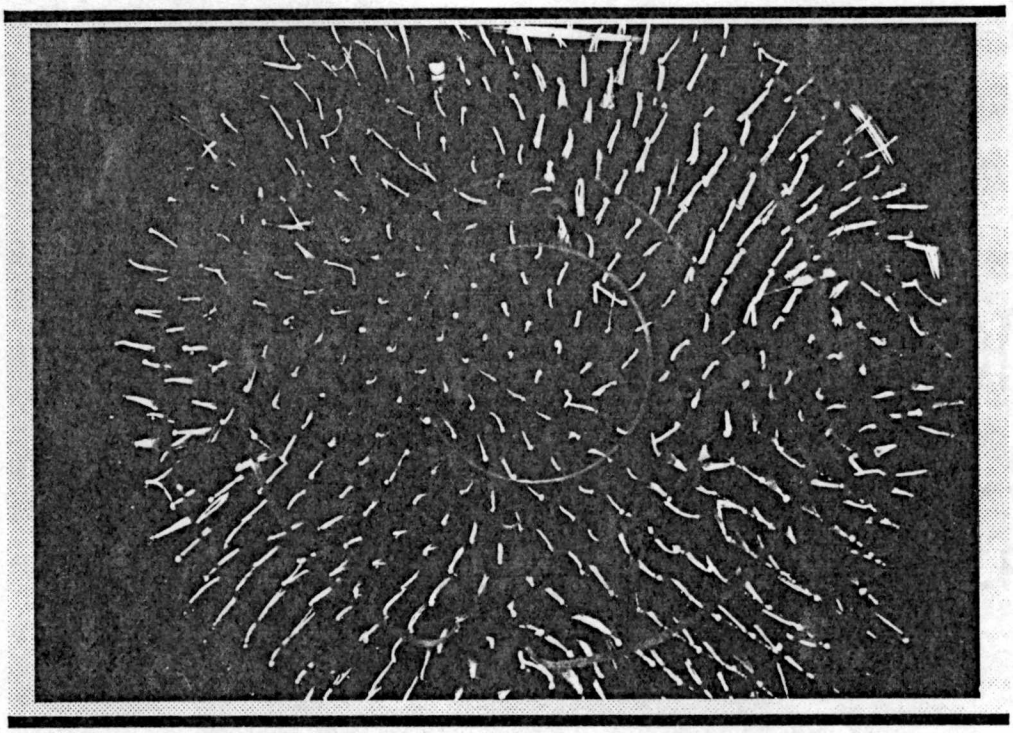


Figure 39: 120% Flow; Keys Offset; VSD Lowered 1"

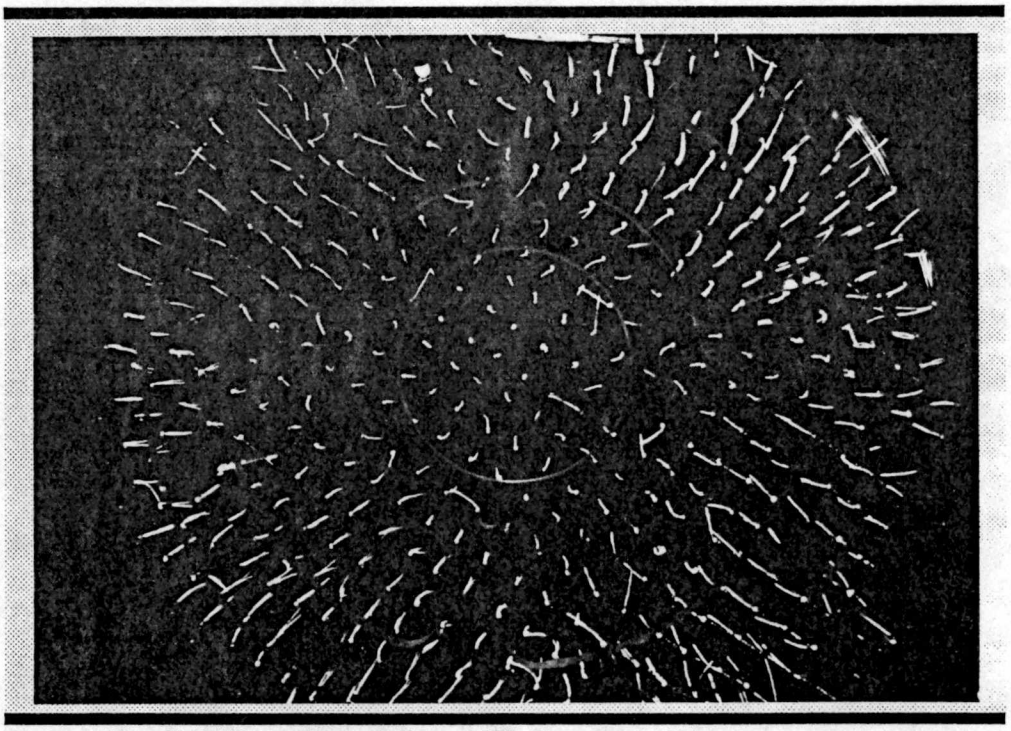


Figure 40: 60% Flow; Keys Offset; VSD Lowered 1"

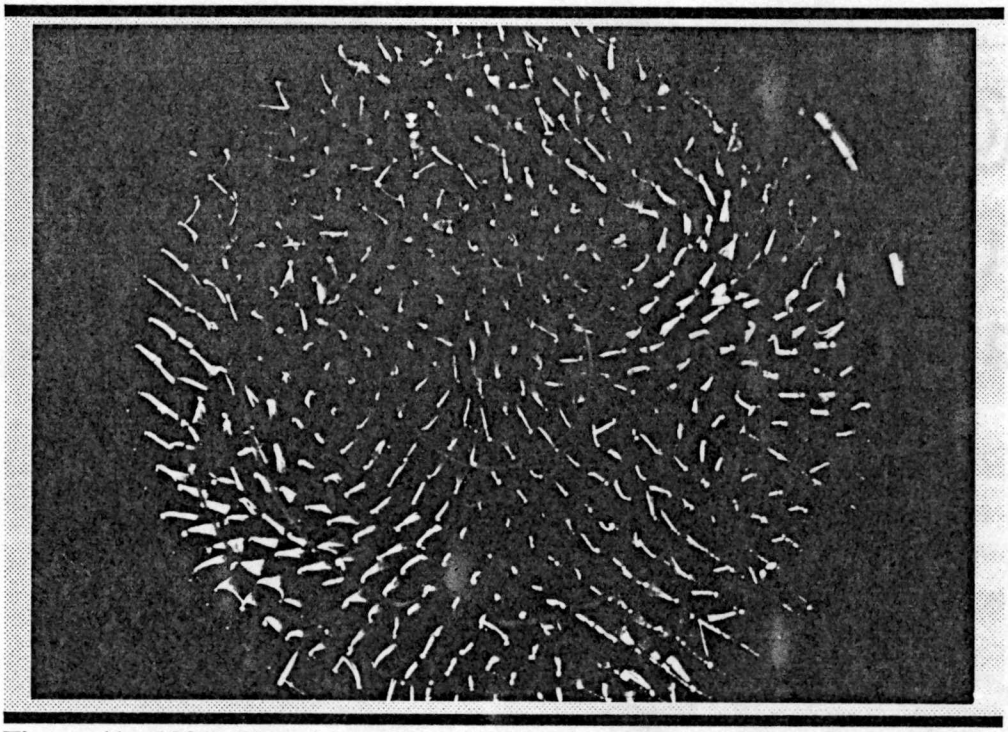


Figure 41: 120% Flow; Keys Offset; VSD Raised 1"

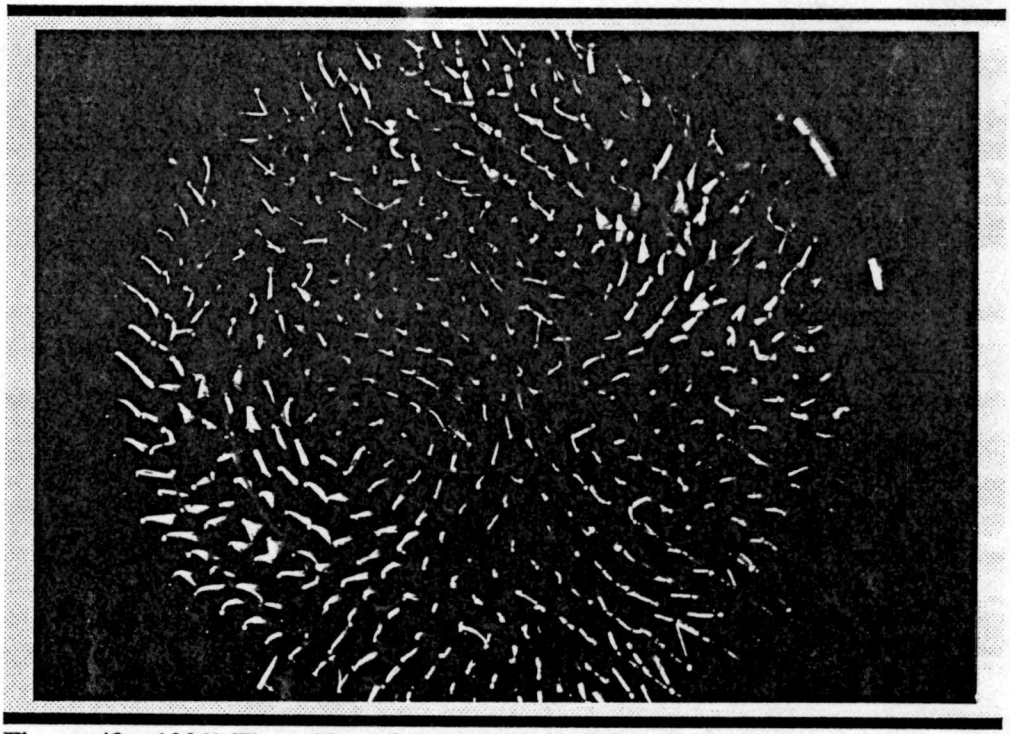


Figure 42: 100% Flow; Keys Offset; VSD Raised 1"

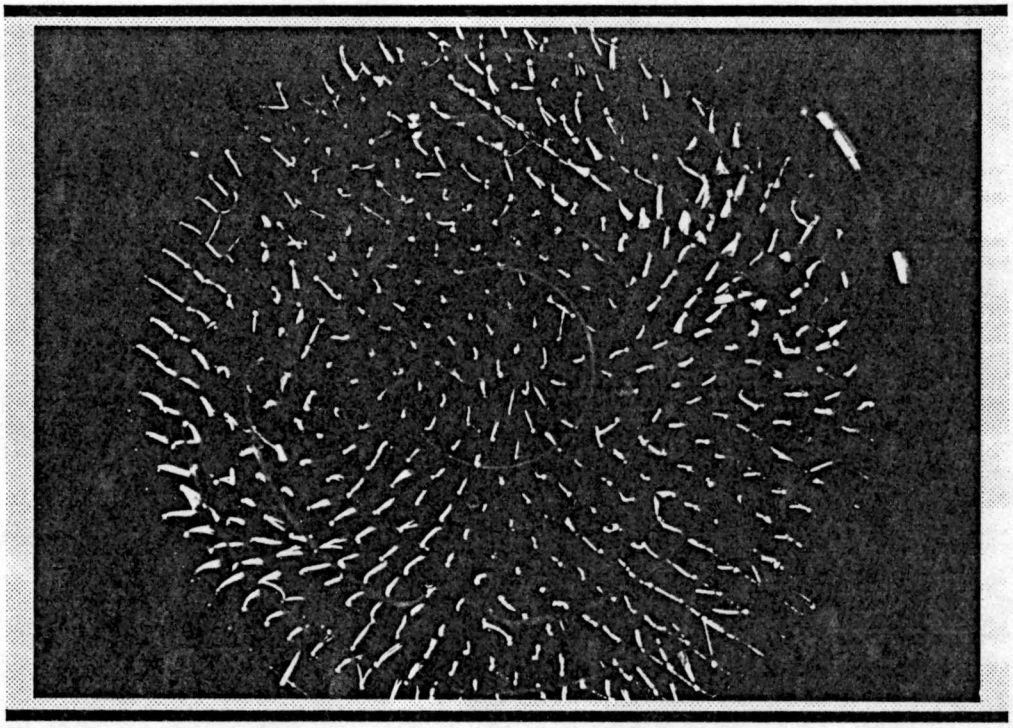


Figure 43: 80% Flow; Keys Offset; VSD Raised 1"

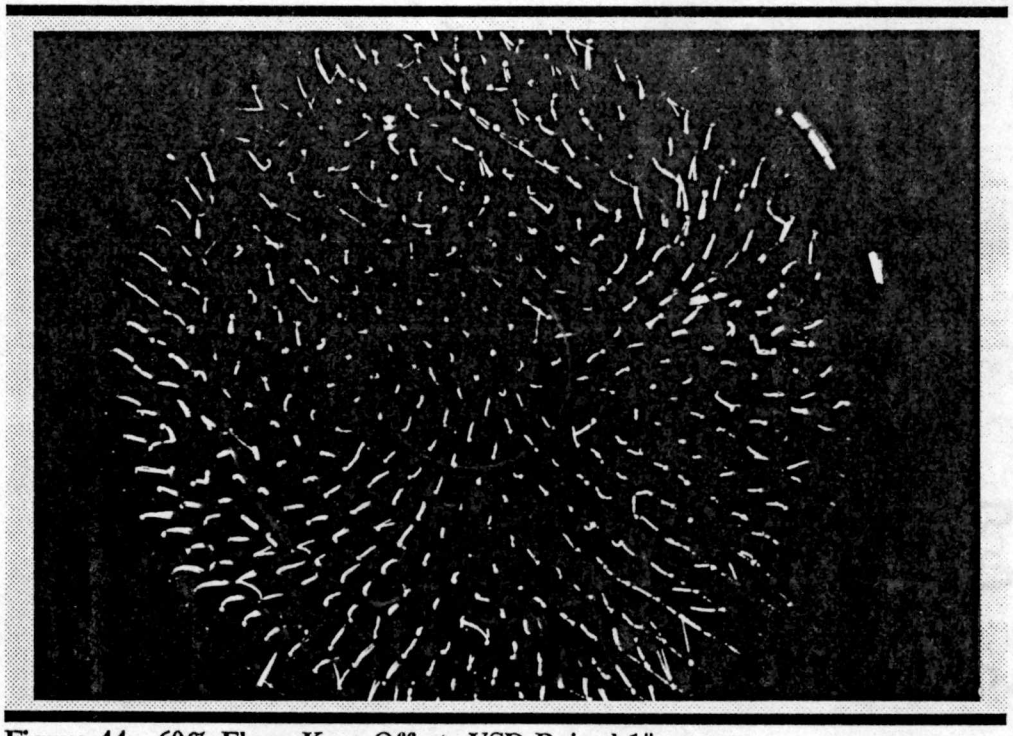


Figure 44: 60% Flow; Keys Offset; VSD Raised 1"

flow rate, respectively.

Comparing the flow field for the three different elevations (for instance, Figures 38, 39, and 41) shows that horizontally opposed "jets," located at about 30° and 210°, appear to occur in all of the cases, a characteristic not shared by the unsuppressed cases. The tendency for these jets to curl into vortices apparently increases as the VSD is raised toward the CSP. This phenomenon may be related to the ability of the jets to contribute angular momentum, dependent on the azimuthal offset and angle of the colliding flows.

3.2.2 Observed Flow Fields With Aligned Radial Keys

The next series of tests were performed with the radial keys aligned directly below the cold leg nozzles at 45, 135, 225, and 315°. It should be noted that the vortex suppression device and the core support plate were also rotated relative to the cold legs in this realignment. The flow fields observed with the VSD at the nominal elevation were similar but not identical to those seen in the last test series. Regions with strong horizontal flow components are still visible but the azimuthal locations are changed, some positions consistent with the 45° rotation of the keys and VSD, others not. Overall, as in the unobstructed tests with this key configuration, the flow field was turbulent and less organized than the offset key configuration.

In any case, no organized vortical flow was observed within the range of flow rates from 50% to 120%. The unobstructed flow field for the aligned key configuration at a flow rate of 120%, previously presented as Figure 33, is reproduced for comparison

in Figure 45. This figure can be compared directly to the most common flow field for the suppressed case, shown in Figure 46. In this configuration and with a flow rate of 120%, some transient curl was observed in the flow field, although it formed only momentarily as turbulent waves rippled across the tuft grid. Figure 47 shows this disorganized flow field. This transient curl was not observed at lower flow rates, where the flow field remained similar to that shown in Figure 46. The flow field at 60% flow rate, shown in Figure 48, demonstrates this.

As before, lowering the VSD to one inch below the nominal position caused little change in the overall flow field. Although some strengthening of the horizontal flow components was observed, the flow vectors stayed basically the same and there were no indications of vortical flow at any of the flow rates tested. The flow fields observed at 120% and 60% flow rate are shown in Figures 49 and 50, respectively.

Raising the VSD to one inch above nominal again caused significant changes. At 120% flow rate, as shown in Figure 51, the flow field appears to be perturbed around the circumference of the VSD, with noticeable curl but no organized vortex. This flow field is very similar to but has a stronger curl than the fields observed in the unobstructed aligned keys cases with flow rates below 70%, as illustrated by Figure 36.

This curl in the flow field persists at 100% flow rate, as shown in Figure 52. Dropping to 80% flow rate as shown in Figure 53 results in a flow field very similar to that observed for low flows at other VSD elevations, with no organized curl at all. The flow field remains free of vortical flow at 60% flow rate, as shown in Figure 54.

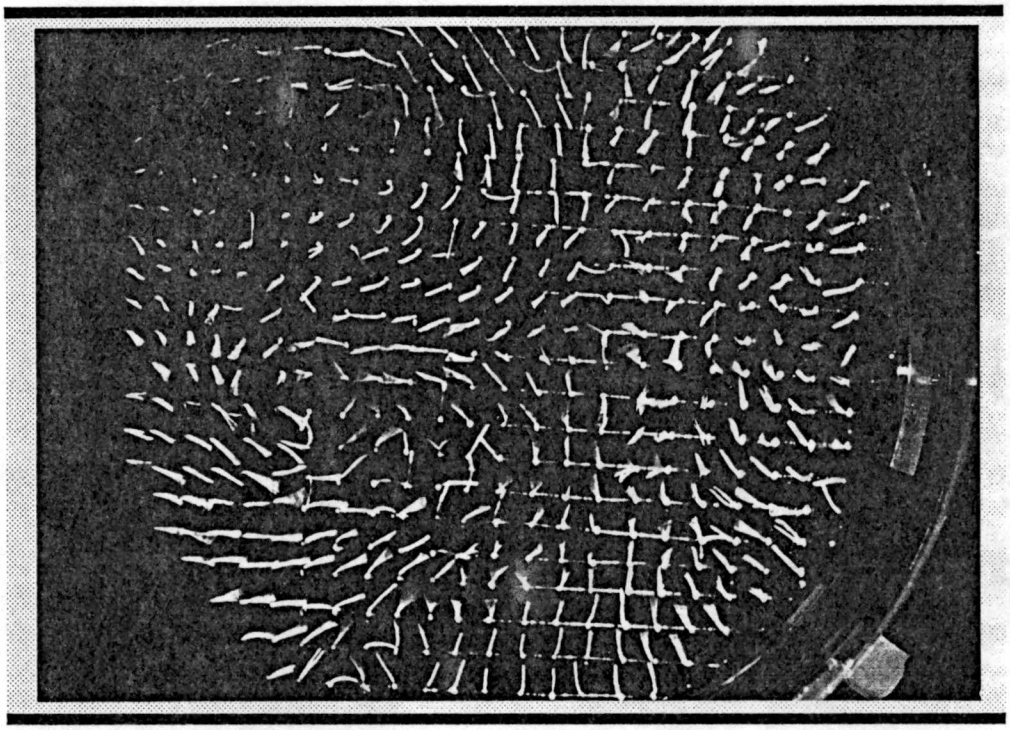


Figure 45: 120% Flow; Keys Aligned; No VSD

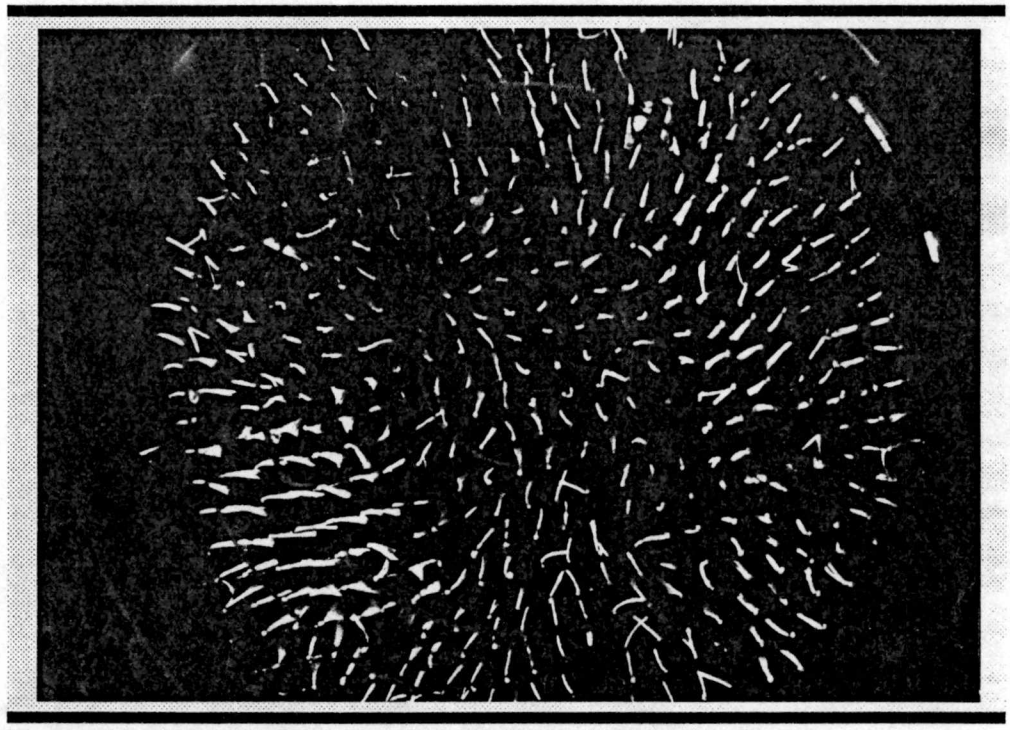


Figure 46: 120% Flow; Keys Aligned; VSD Nominal; No Curl

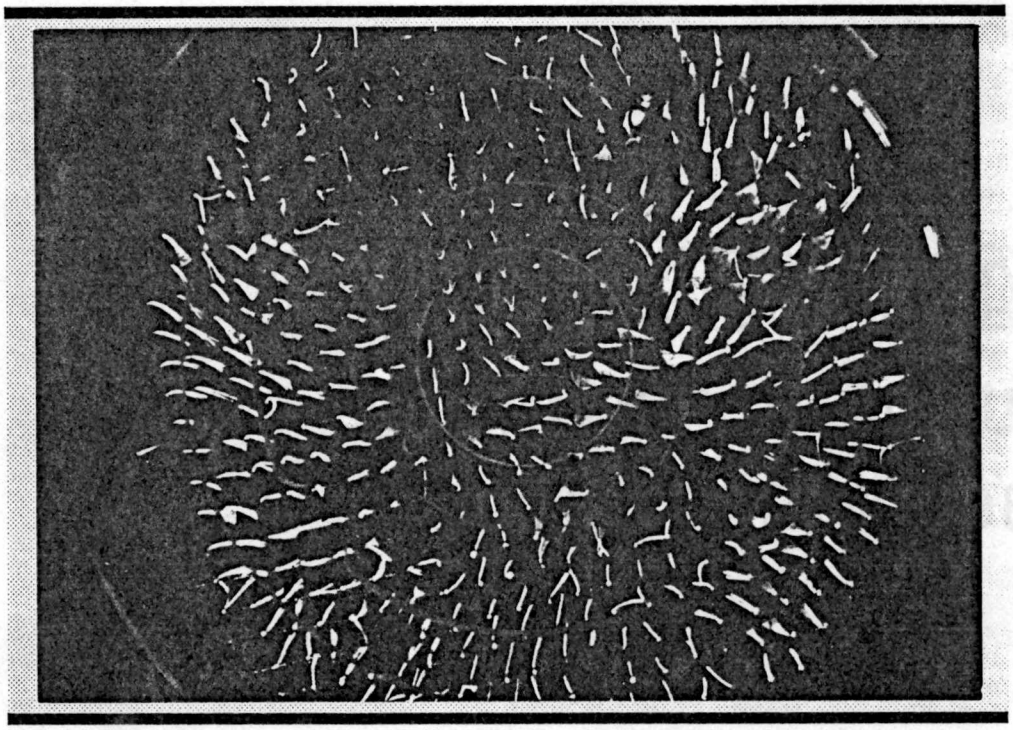


Figure 47: 120% Flow; Keys Aligned; VSD Nominal; Curl

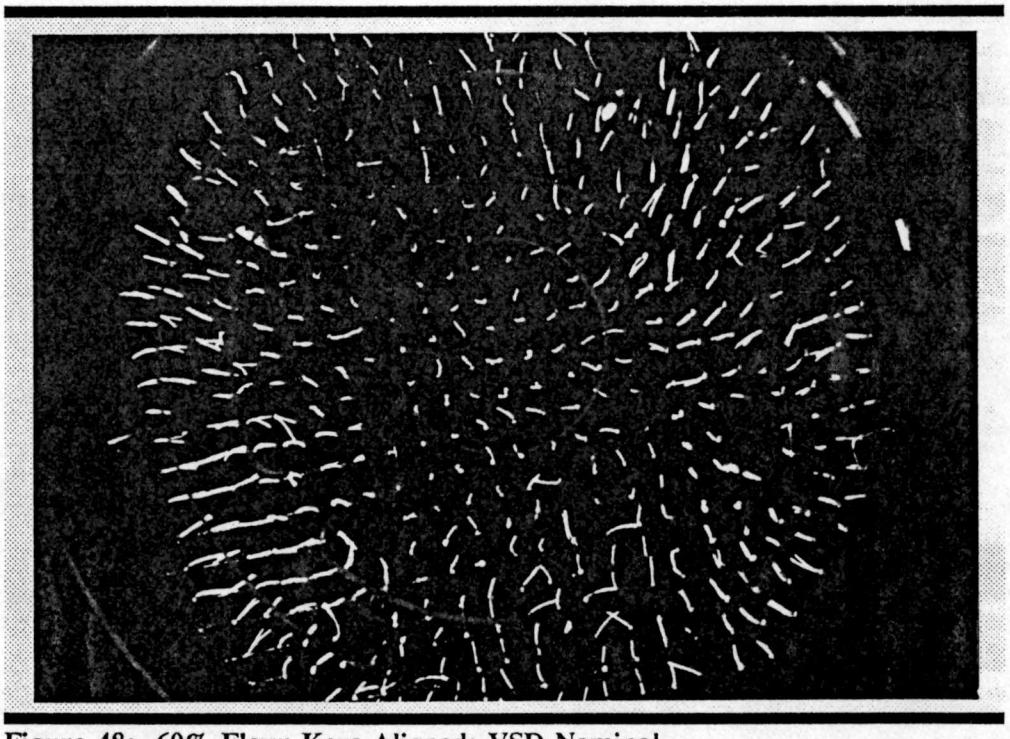


Figure 48: 60% Flow; Keys Aligned; VSD Nominal

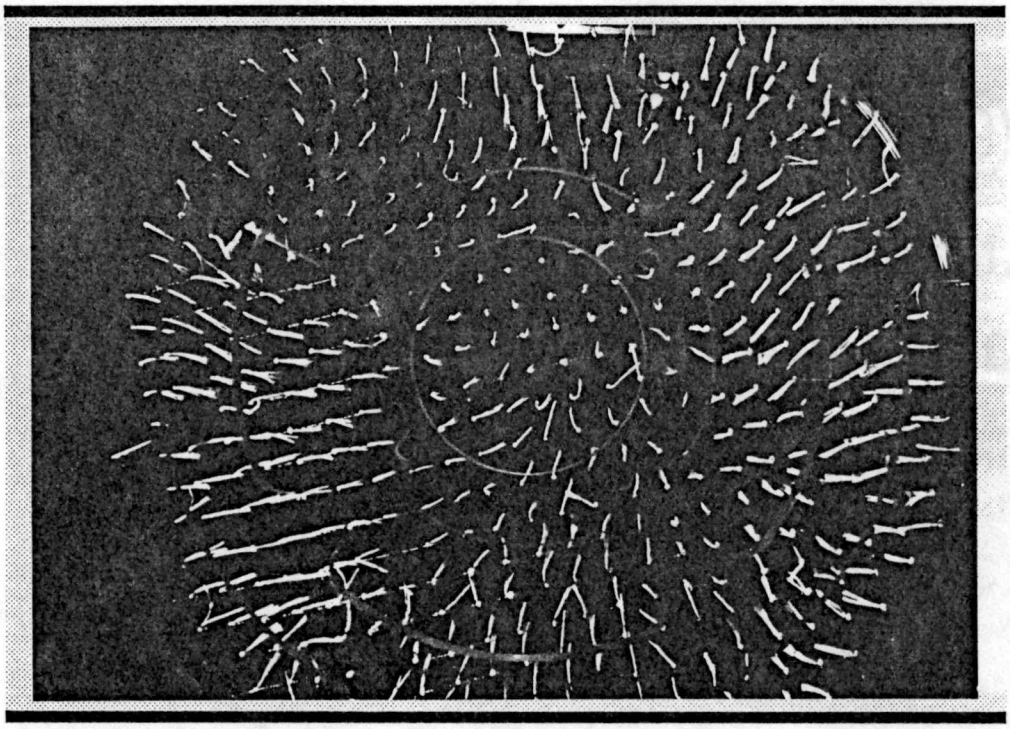


Figure 49: 120% Flow; Keys Aligned; VSD Lowered 1"

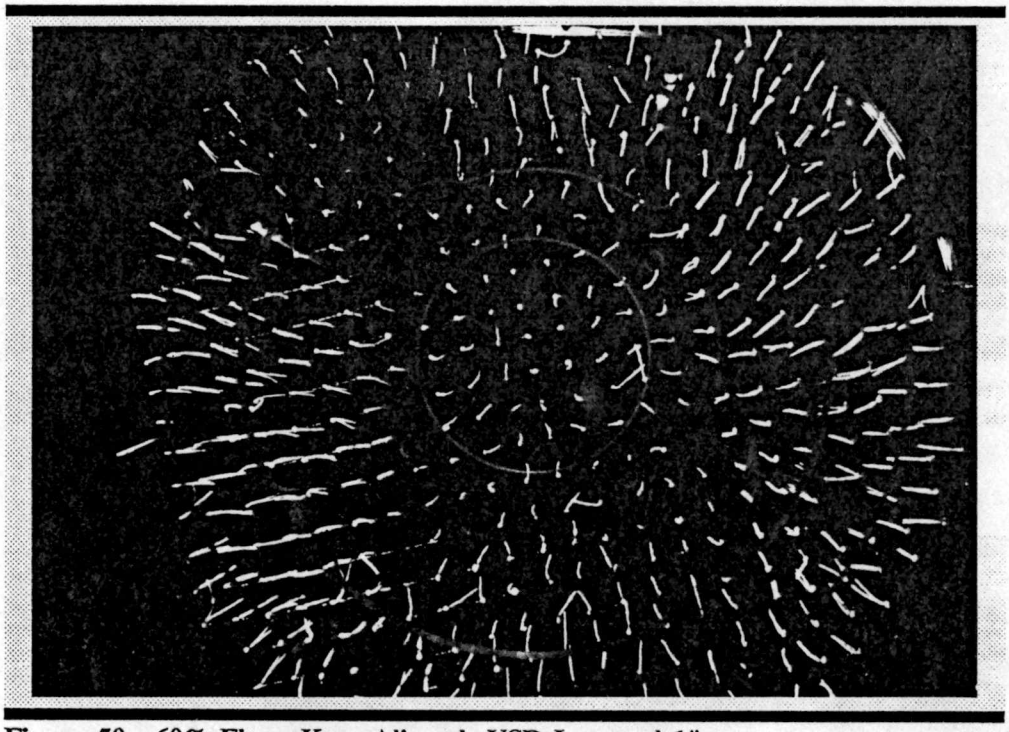


Figure 50: 60% Flow; Keys Aligned; VSD Lowered 1"

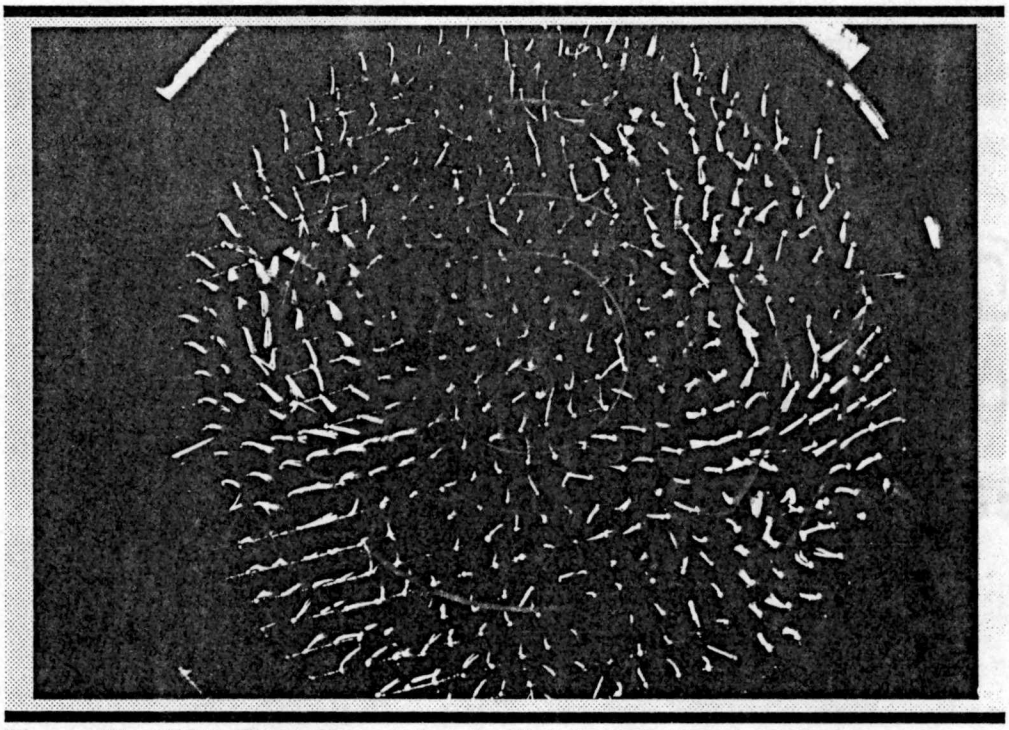


Figure 51: 120% Flow; Keys Aligned; VSD Raised 1"

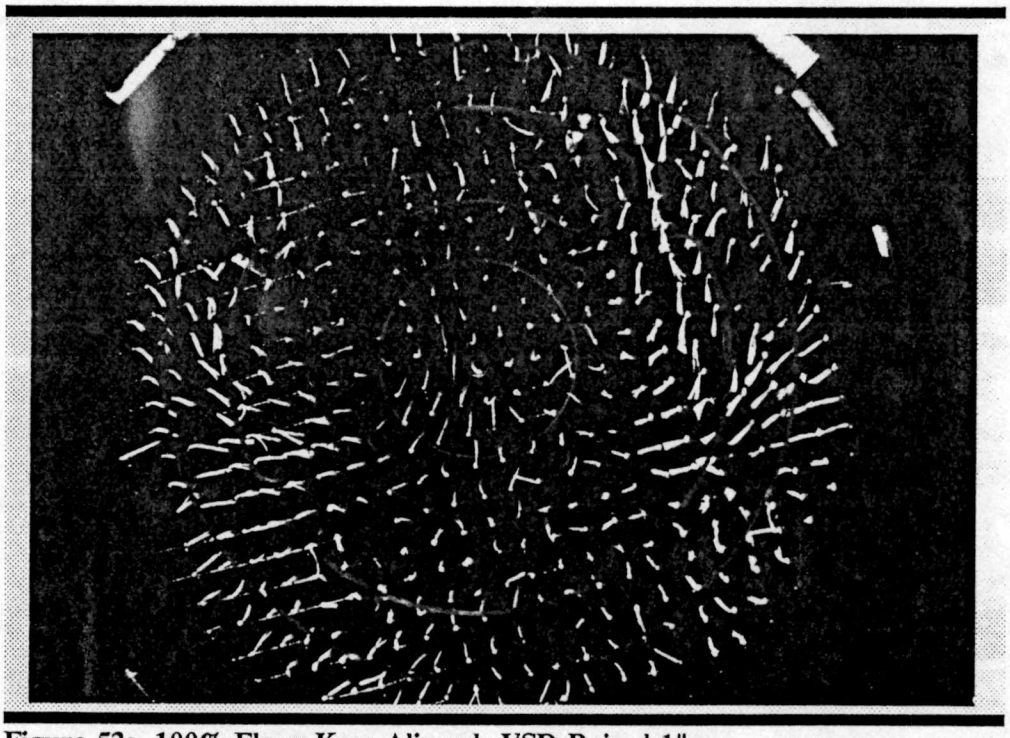


Figure 52: 100% Flow; Keys Aligned; VSD Raised 1"

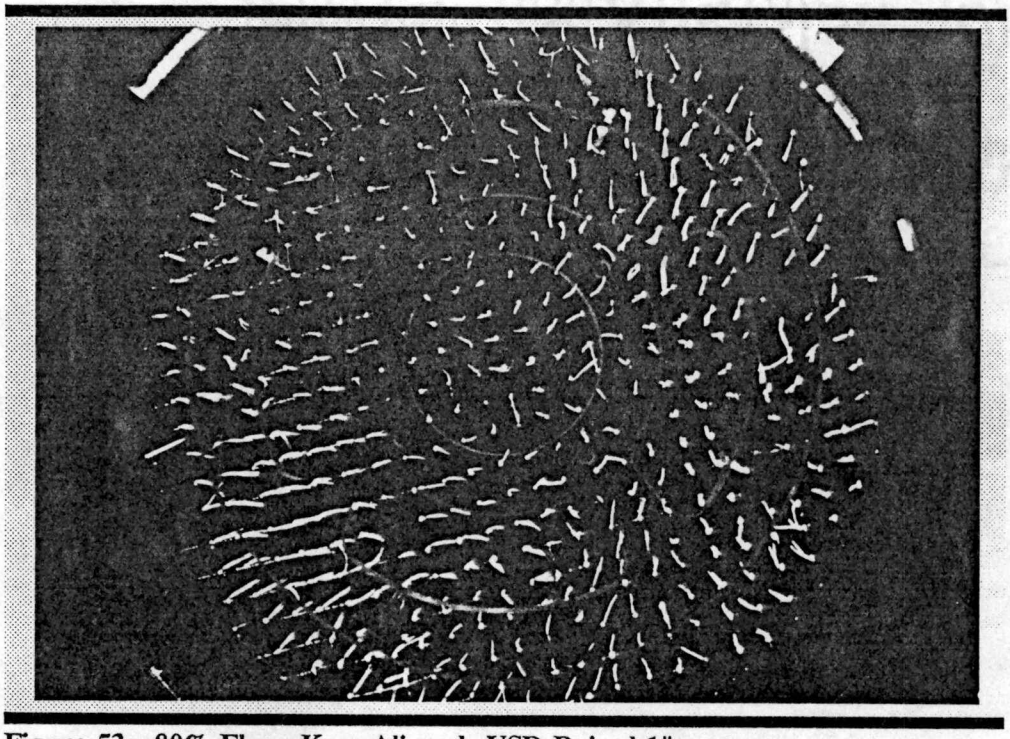


Figure 53: 80% Flow; Keys Aligned; VSD Raised 1"

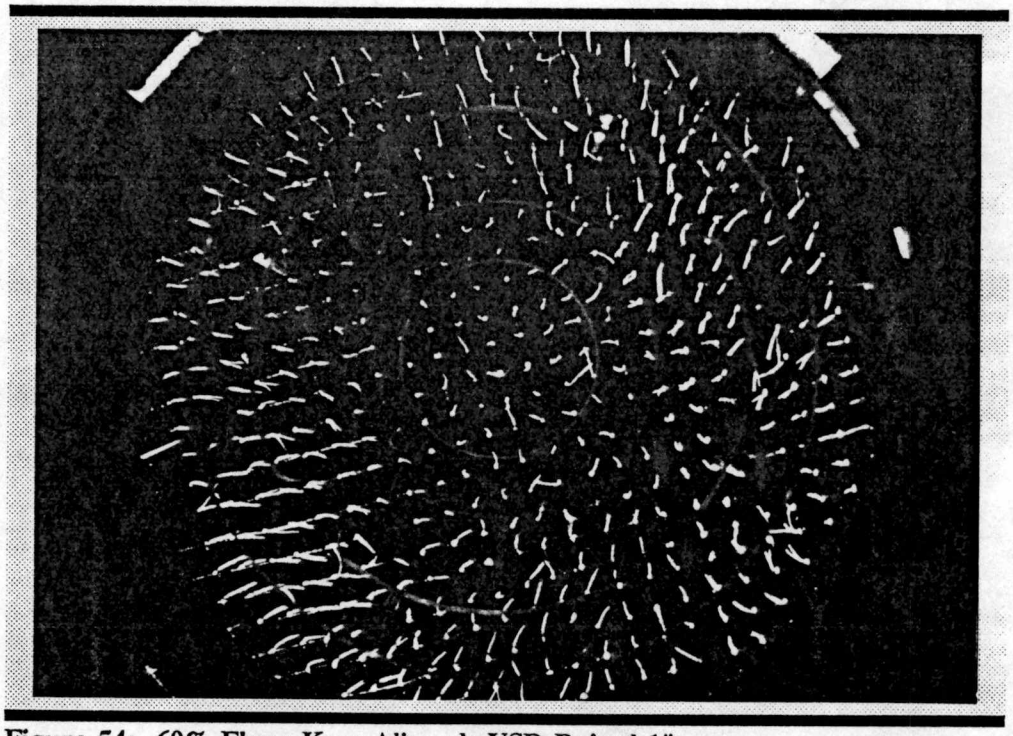


Figure 54: 60% Flow; Keys Aligned; VSD Raised 1"

3.3 Sensitivity of Flow Fields to Loop Flow Imbalance

Since the VSD had proven to be capable of suppressing vortices, at least if it was positioned low enough, there was a need to test the robustness of this suppression. The source of angular momentum to drive the sink-irrotational vortices was hypothesized to be azimuthal variation in the velocities entering the plenum from the downcomer. If this was indeed the case, then imbalances in the flow rate in each cold leg would tend to exacerbate vortical flow. This effect was noted by Westinghouse in the operating reactors which exhibited behavior suggesting vortical flow (Cadek et al., 1988).

A set of tests was performed to evaluate the effect of loop imbalance on the unobstructed and suppressed flow fields observed in earlier tests. To minimize the number of tests, the flow rate was maintained constant at 100% for all tests described in this section, and the VSD was located at the nominal elevation whenever used. Parameters varied included the magnitude of the loop imbalance, the number and pattern of loops affected, the position of the radial keys, and the presence of the suppression device.

3.3.1 Single Loop Imbalance

Four model configurations were studied in this series of tests; with offset or aligned radial keys and with or without the vortex suppression device installed in the lower plenum. In all of these tests, flow was reduced in the loop located at 45°

azimuthally by adding one, two or three additional screens to the loop inlet or by blocking the inlet entirely. The reduced flow rate in this loop varied slightly from test to test but was approximately 85%, 74%, and 65% for one, two, and three additional screens, respectively.

With the VSD removed and the radial keys offset, vortices were observed at all times, regardless of the loop flow rate imbalance. Reducing the flow rate by 15% in the loop resulted in twin vortices at about 100°/220°, as seen in Figure 55. The azimuthal position of the vortices in this configuration with the loop imbalance has changed significantly from the balanced case shown in Figures 23 and 24. In fact, the flow field looks similar to the balanced flow case with aligned radial keys, shown in Figure 33. In either comparison, the vortices observed with the loop imbalance appear weaker than those seen without the imbalance.

Reducing the loop flow rate imbalance to 26% resulted in a fluctuating flow field. A flow field similar to that shown in Figure 55 was observed, but a new pattern of vortices at 150°/300° was also observed. This new flow field was better developed, with stronger vortical flow more comparable to that observed without the flow imbalance. This strengthening is significant since reduction of the flow rate in the unbalanced loop results in an overall drop in model flow which would tend to weaken vortices.

When the loop imbalance was increased to 35%, this new flow field became well established, as pictured in Figure 56. Further reduction in loop flow rate was achieved by completely blocking the loop inlet. In this configuration, the vortices became weak and unstable, although the predominant flow field appeared to be similar to that observed

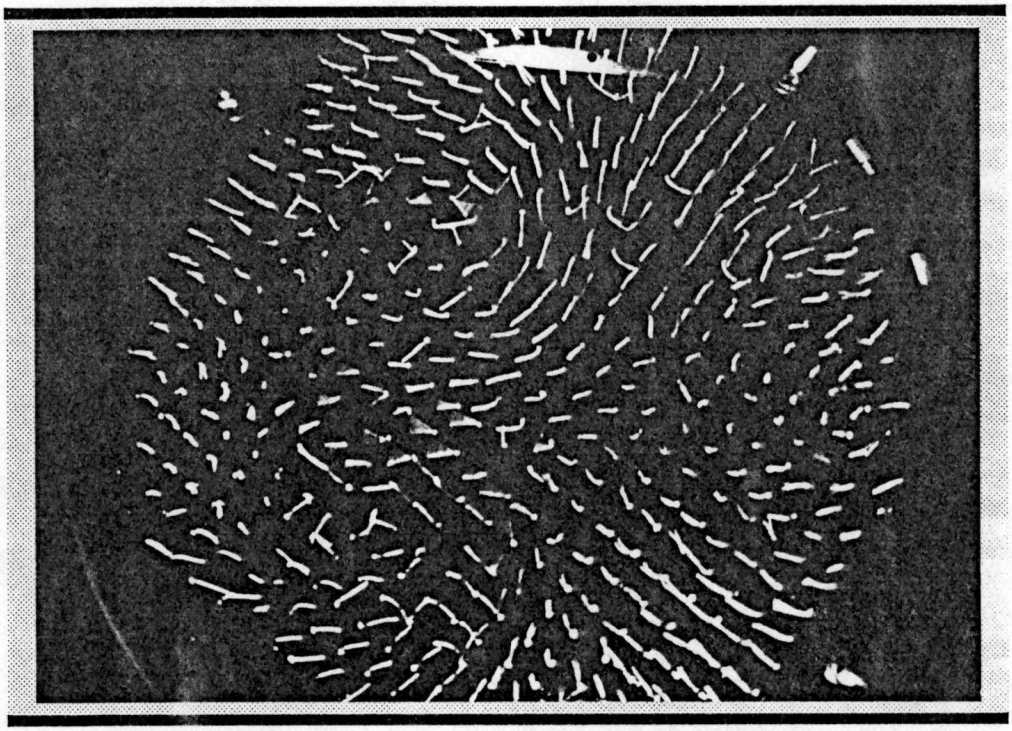


Figure 55: Keys Offset; No VSD; 15% Single Loop Imbalance

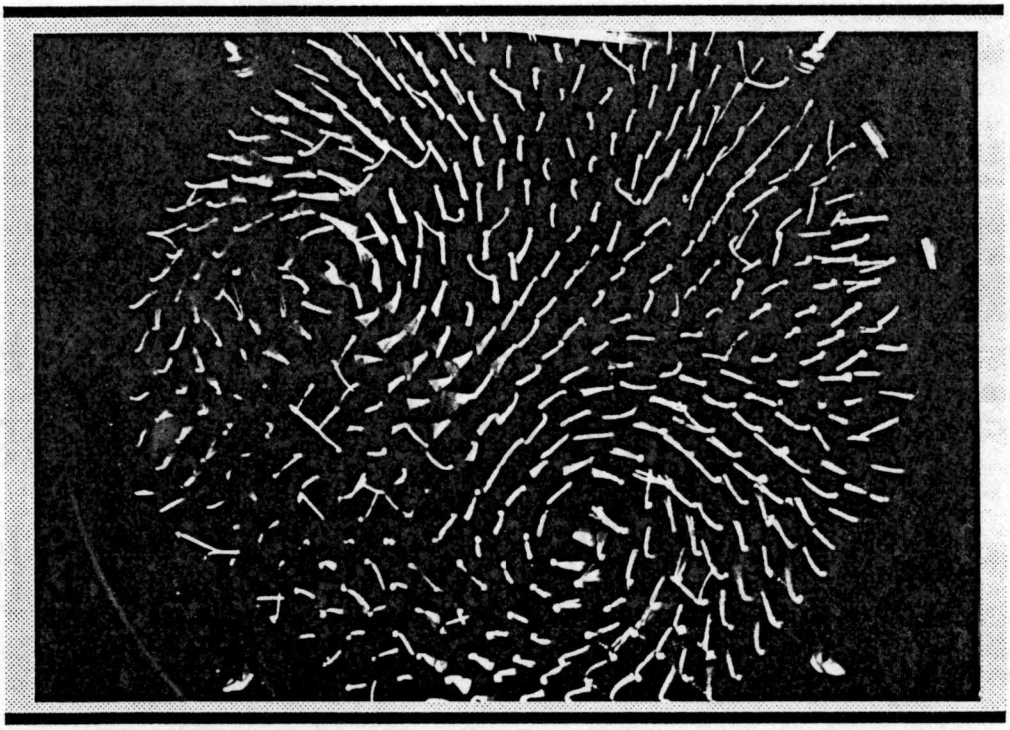


Figure 56: Keys Offset; No VSD; 35% Single Loop Imbalance

with 35% loop imbalance.

Replacing the VSD caused an almost total disruption of vortical flow. With a 15% loop flow rate imbalance, there was absolutely no indication of vortical flow, as shown in Figure 57. As the loop imbalance was increased to 26% and then to 35%, there was some indication of upward spiraling flow very near the edge of the tuft grid at about 300°. This phenomena is pictured in Figure 58. This circulation does not appear to be a vortex and does not bear any clear relationship to the vortices, or even the upward spiraling flow, observed previously. Complete blockage of the loop resulted in a similar flow field, with much less sign of the small circulation pattern.

The next series of tests duplicated the last series except with the radial keys aligned. The observed results are quite similar. Without the VSD in place, vortices were clearly observed, although they were less stable than those observed with offset radial keys. This follows the pattern seen for balanced flows in Section 3.1. With a 15% loop imbalance imposed, the strongest twin vortices were observed at 30°/120°, although these vortices moved about considerably over approximately a 60° azimuthal range. This flow field, which appears surprisingly similar to the flow field for balanced flow with offset radial keys, is shown in Figure 59.

Increasing the loop flow rate imbalance to 26% had little effect on the flow field. Further imbalance caused an abrupt change to a stronger set of vortices at 180°/270°, in a manner similar to that observed in the offset key loop imbalance series. This flow field is shown in Figure 60, although the increased vortex strength was not captured well by the photograph. Complete blockage of the loop resulted in yet another azimuthal

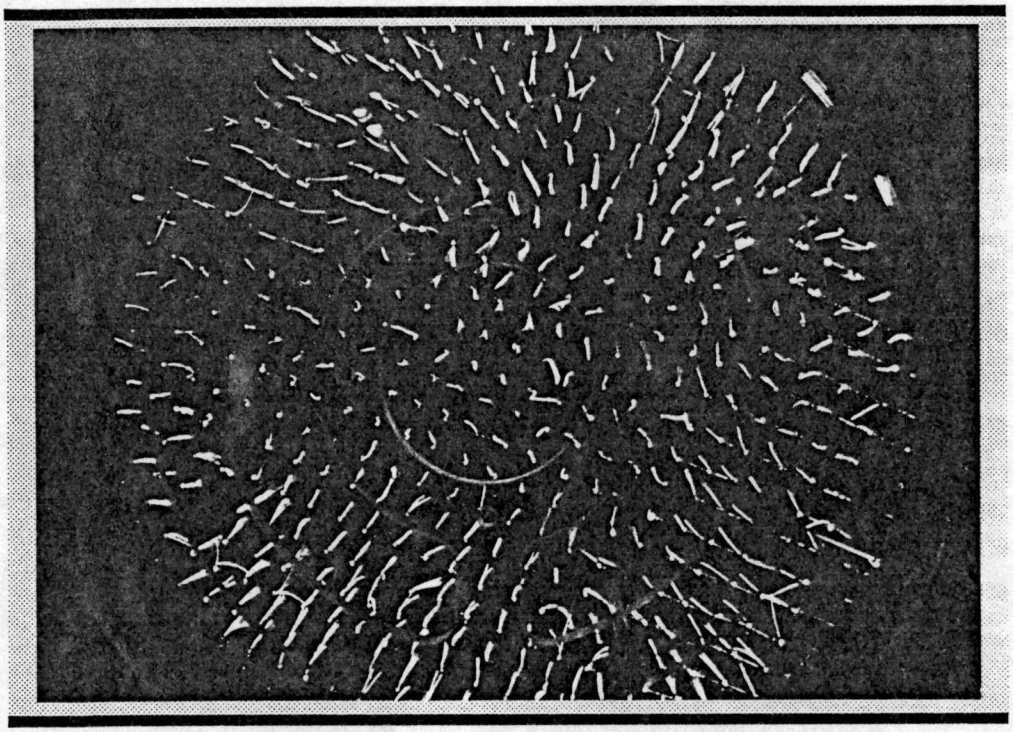


Figure 57: Keys Offset; VSD; 15% Single Loop Imbalance

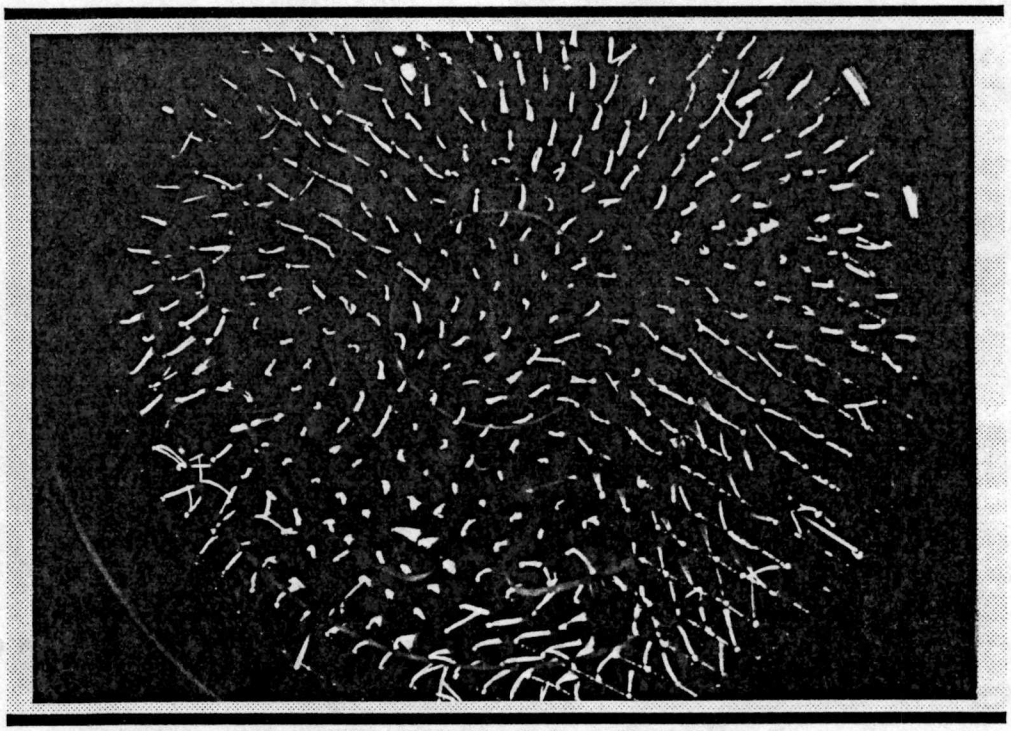


Figure 58: Keys Offset; VSD; 35% Single Loop Imbalance

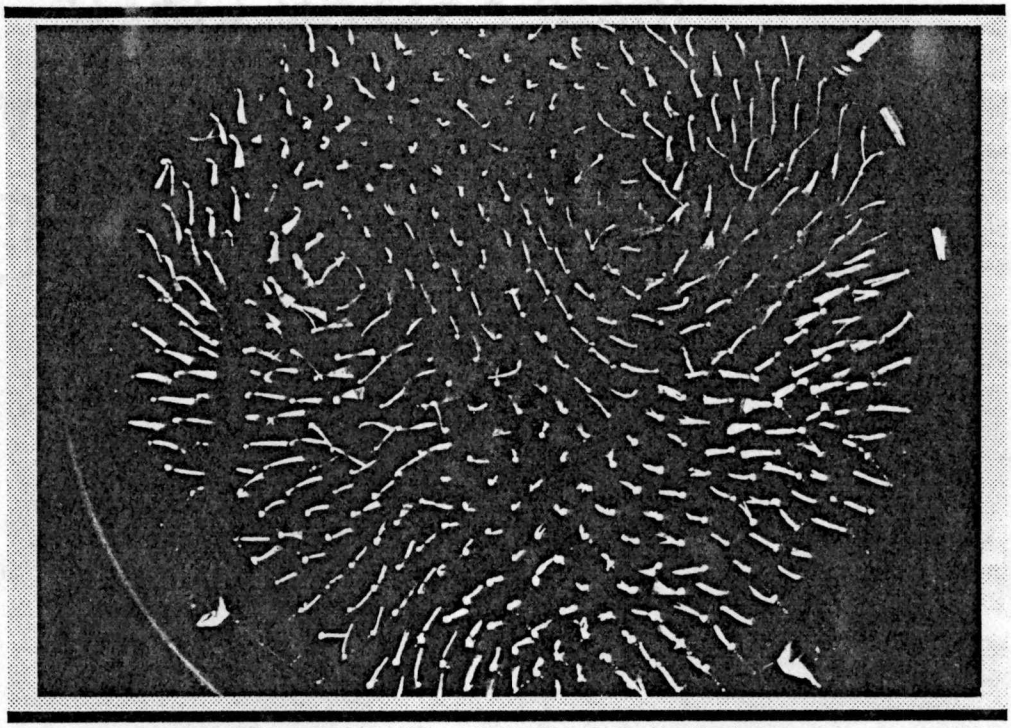


Figure 59: Keys Aligned; No VSD; 15% Single Loop Imbalance

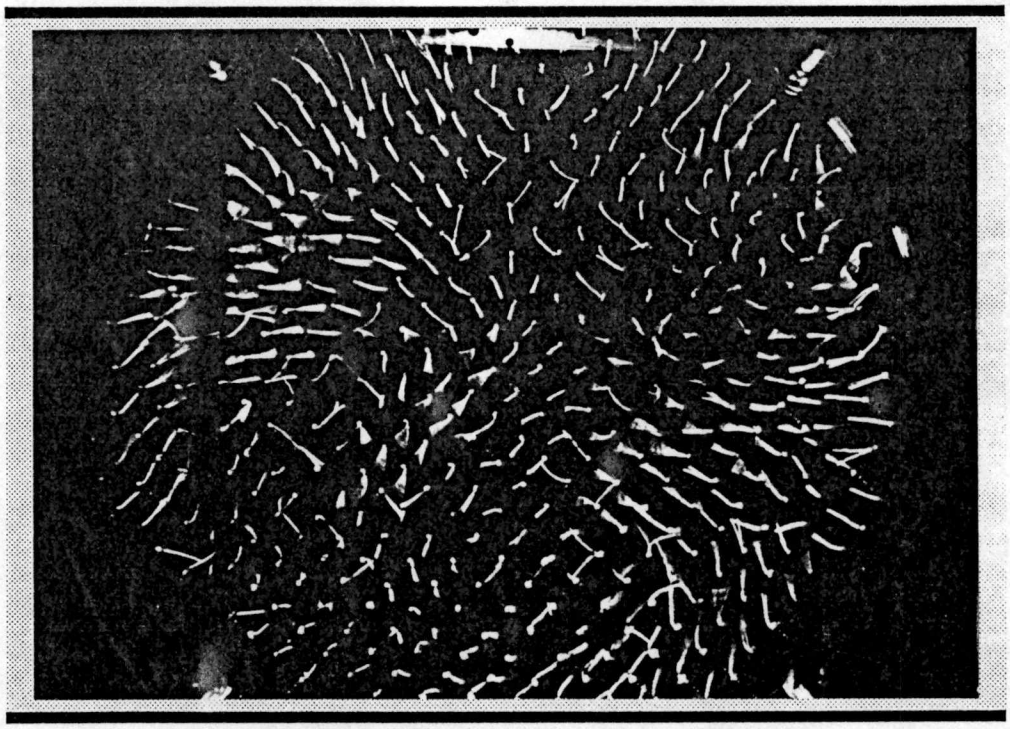


Figure 60: Keys Aligned; No VSD; 35% Single Loop Imbalance

position for the vortices, with circulation centering about 30°/290°. As before, this flow field was highly variable.

Installing the VSD again nullified any significant vortical flow. No organization at all was visible when the loop flow was reduced up to 35%, although a significant horizontal flow component was observed at the tuft grid. This flow field is most clearly represented by the 35% loop imbalance case, shown in Figure 61. The horizontal component is clearly seen in the 150°-230° sector.

Blocking flow to the loop did result in some flow organization, as can be seen in Figure 62. The strong horizontal component seen previously appears to be driving an upward spiraling flow centered about 0°/270°. This flow field is probably the precursor of the vortices observed without the VSD, but the flow does not complete a full rotation and probably cannot support lowered pressure at the circulation center.

3.3.2 Adjacent Loop Imbalances

The next series of tests examined the effect of reducing the flow rate in two adjacent loops. Loops 3 and 4, at 225° and 315° respectively, were arbitrarily chosen. Since reduced flow in two loops is a less likely reactor operation strategy than reduced flow in a single loop (although perhaps possible in adjacent loops in the event of steam generator degradation), the number of variables in this study was reduced. All tests included the vortex suppression device, and only two loop flow rate imbalances, 15% and 100%, were observed. The effect of radial key position was included in the test series.

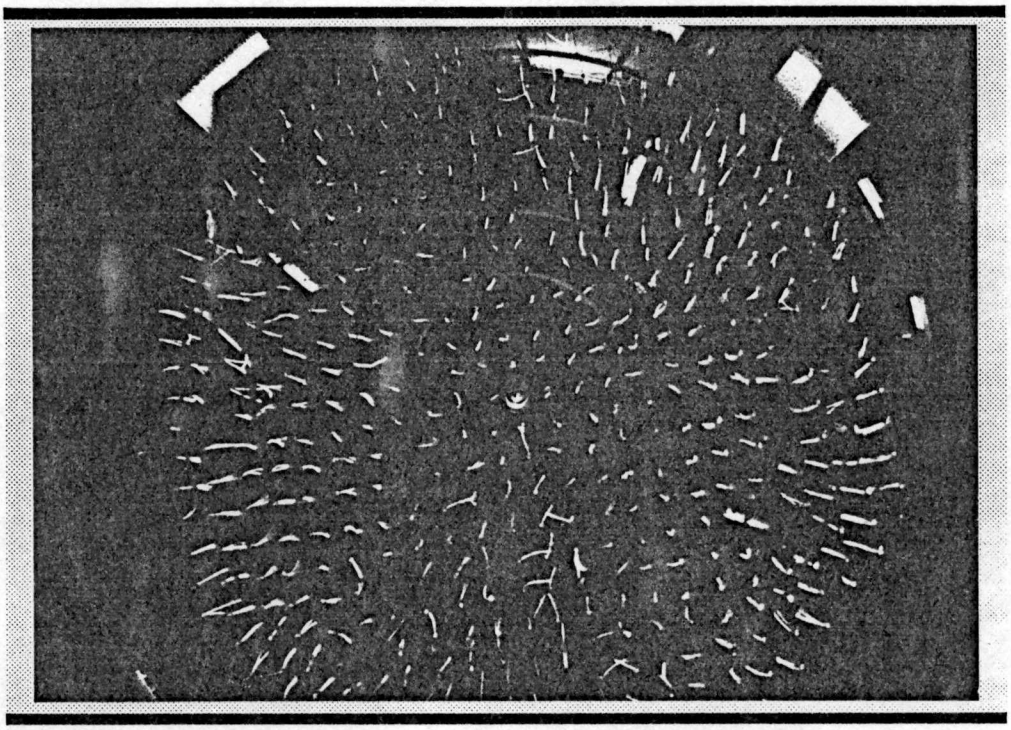


Figure 61: Keys Aligned; VSD; 35% Single Loop Imbalance

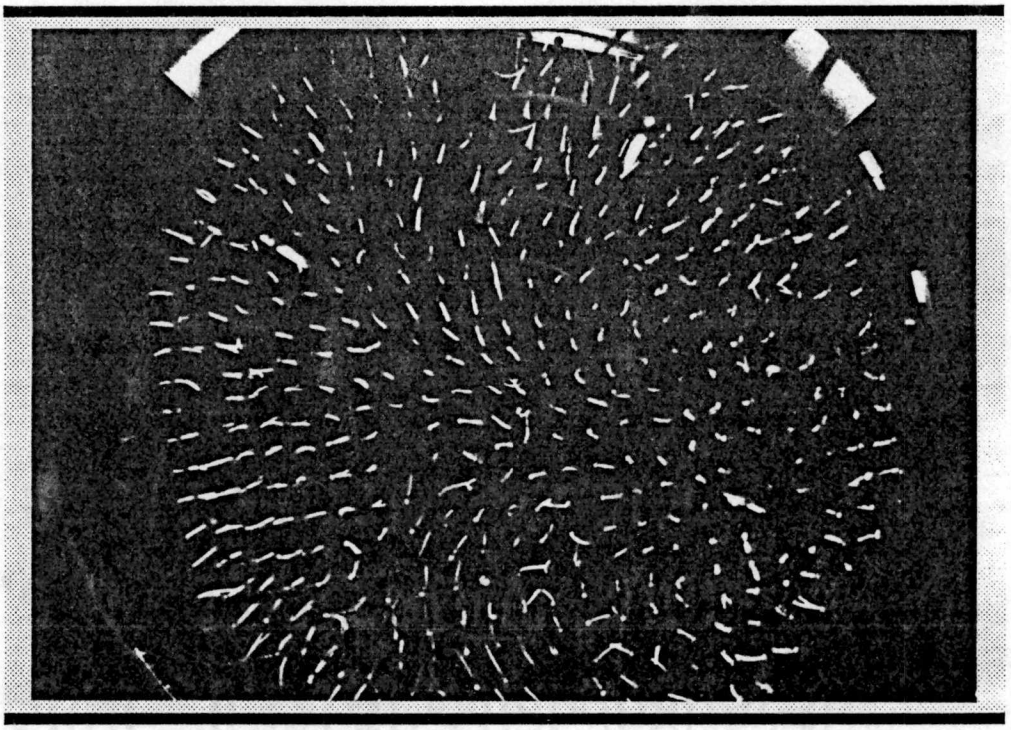


Figure 62: Keys Aligned; VSD; 100% Single Loop Imbalance

With the radial keys offset, some upward spiraling flow was observed, but no complete vortices. The flow fields with 15% and 100% two-loop imbalances are shown in Figures 63 and 64, respectively. In the first figure with a 15% flow reduction, flow spirals around a center at 180°, driven by horizontal flow components at 30°and 210°, but does not form a complete vortex. This flow field was transitory and unstable. The second figure shows the flow field with complete blockage of the two loops. The horizontal component at 30° appears weakened and the circulation has disappeared.

A similar effect was observed when the radial keys were aligned with the cold leg nozzles. With the flow rate in two adjacent loops lowered by 15%, strong horizontal flow components force some circulation at about 160°, but not a full vortex. This flow field is pictured in Figure 65. Complete blockage of the flow in the two loops resulted in absolutely no circulation, as shown in Figure 66.

3.3.3 Opposing Loop Imbalances

The test series performed in Section 3.3.2 was repeated with flow reductions in two opposing loops. Loops 1 and 3, at 45° and 225° respectively, were chosen for these tests. Flow rate reductions of 15% and 100% were imposed on these loops with both offset and aligned radial keys. In all cases studied, no vortical flow or circulation of any type was observed. The flow fields for 15% two-loop imbalances with offset and aligned radial keys are shown in Figures 67 and 68, respectively. Complete blockage of the opposed loops did not cause any significant changes to the flow fields.

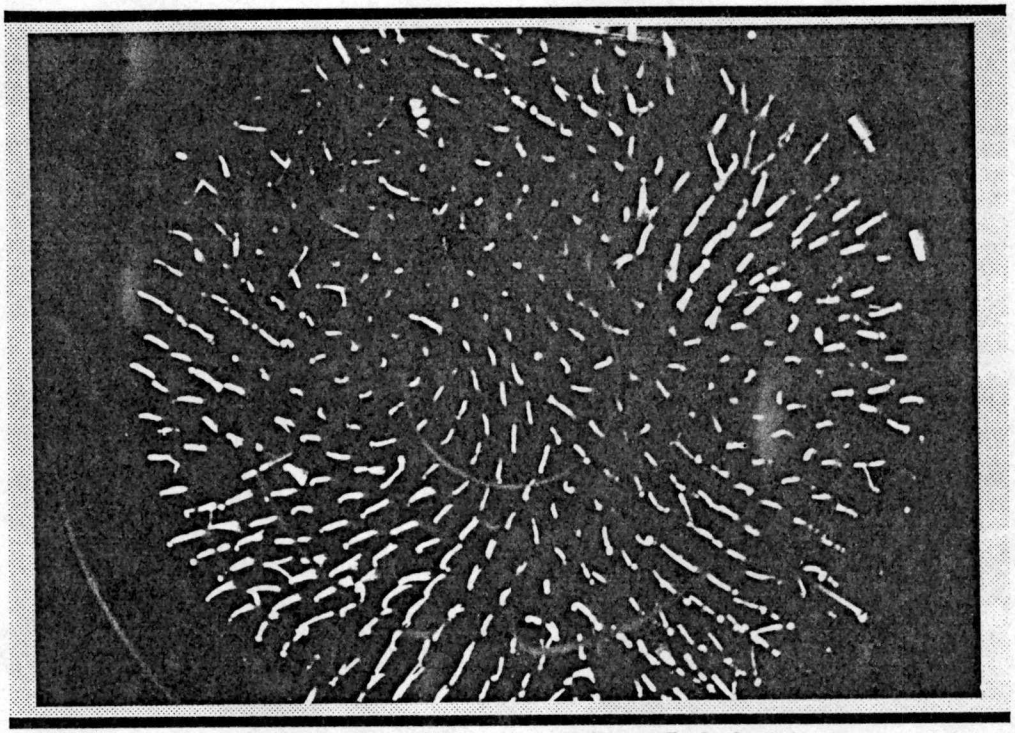


Figure 63: Keys Offset; VSD; 15% Adjacent Loop Imbalance

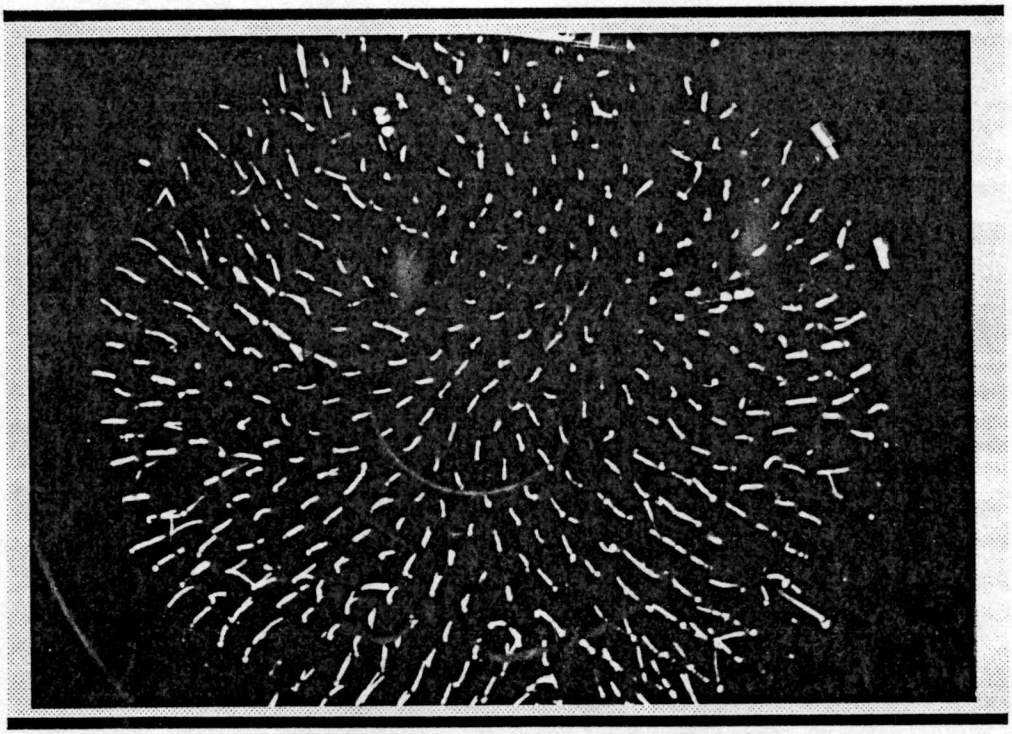


Figure 64: Keys Offset; VSD; 100% Adjacent Loop Imbalance

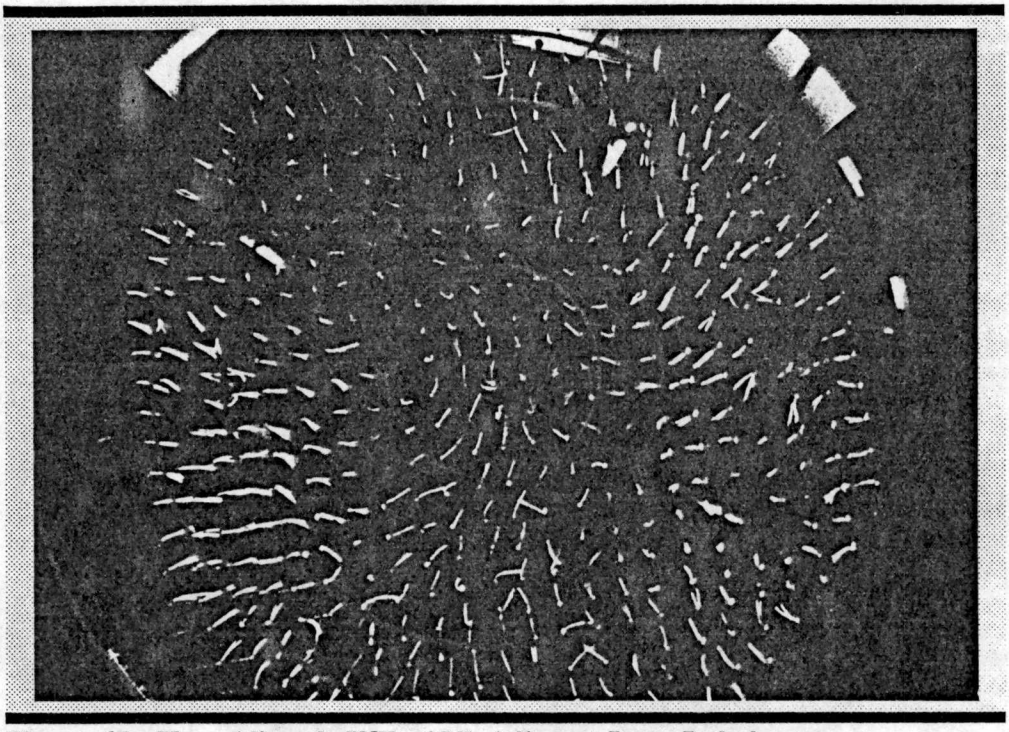


Figure 65: Keys Aligned; VSD; 15% Adjacent Loop Imbalance

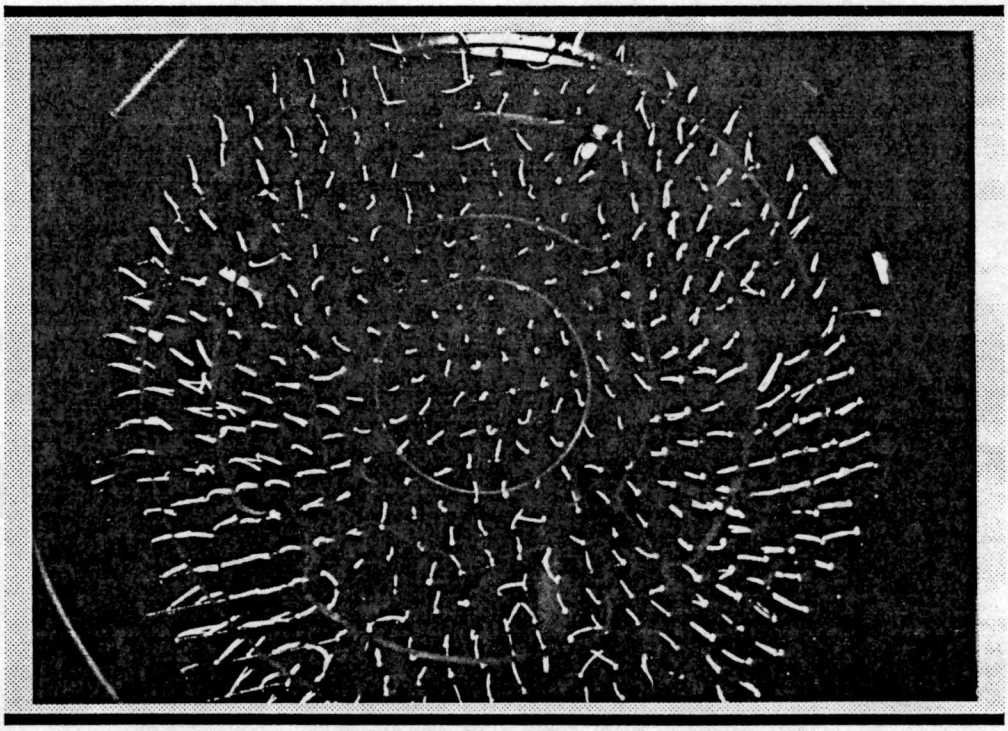


Figure 66: Keys Aligned; VSD; 100% Adjacent Loop Imbalance

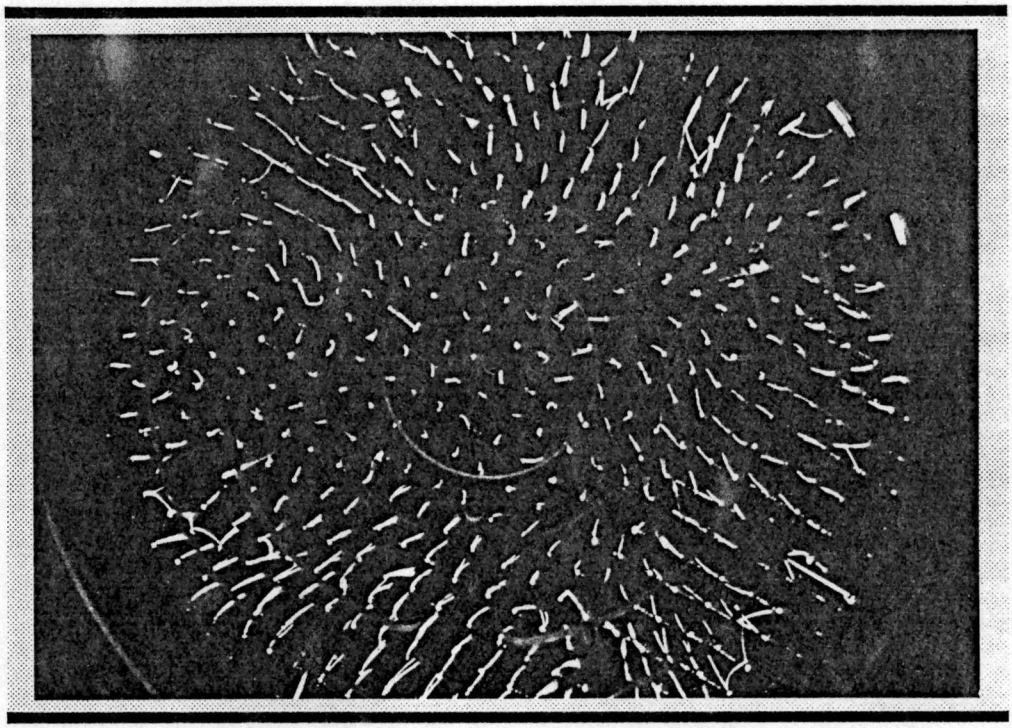


Figure 67: Keys Offset; VSD; 15% Opposing Loop Imbalance

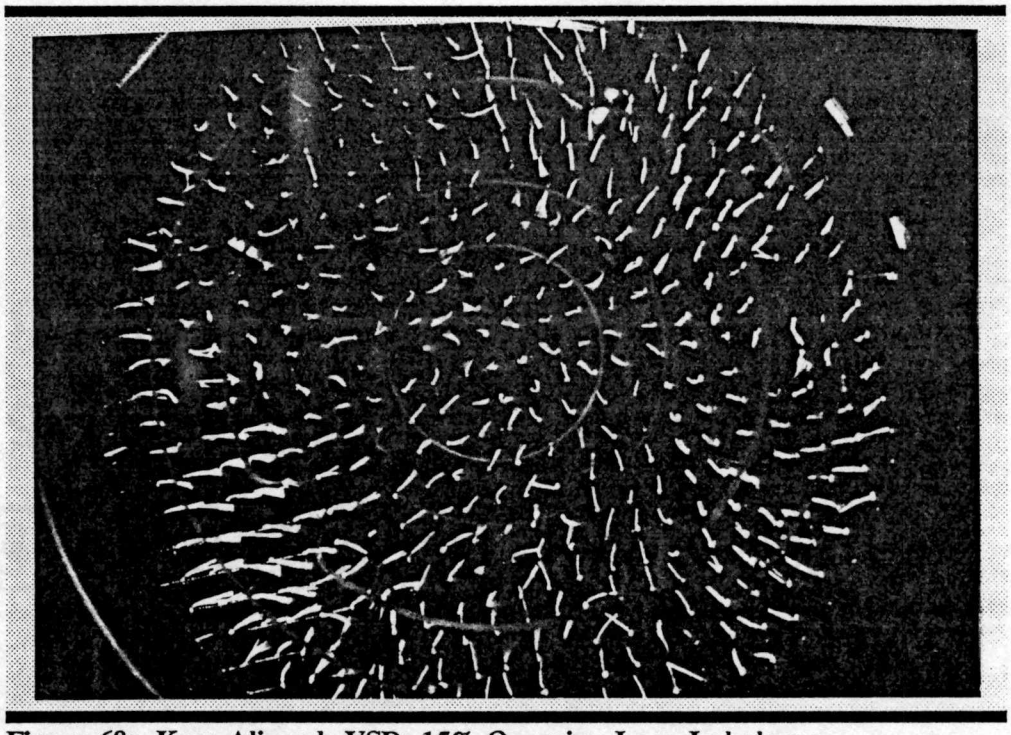


Figure 68: Keys Aligned; VSD; 15% Opposing Loop Imbalance

3.4 Downcomer Azimuthal Velocity Profiles

Concurrent with visualization of the flow fields at 100% of the design flow rate, measurements of the axial downcomer velocity as a function of the azimuthal angle were also taken. Since the observed vortices are thought to be driven, or at least initiated, by shear in the flow leaving the downcomer and entering the lower plenum, some form of relationship between the downcomer azimuthal velocity profile and the vortex positions seemed possible.

These measurements were taken with a pitot tube coupled to a Magnehelic differential pressure gauge. Eight penetrations around the downcomer allowed access to the flow in this region. The penetrations were located every 45° azimuthally, and were centered 7.125 inches above the bottom of the core support plate, an elevation about one-third of the way to the top of the reactor core.

The measurements taken were pressure differences across the dynamic and static taps of the pitot tube. These pressure drops were converted to velocity using the Bernoulli equation:

$$V = \left(\frac{2 g_c \Delta P}{\rho} \right)^{0.5} \qquad (9)$$

where V is the velocity,

ΔP is pressure drop,

ρ is the air density, and

g_c is the gravitational constant.

It should be noted that the pressure differences involved are quite small, on the order of 0.1 inch of water. Because of the small pressure drop and the length of tubing connecting the pitot tube to the gauge, the pressure reading was slow to stabilize, often taking several minutes. The uncertainty in whether the gauge reading had peaked, along with the gauge dial readability, leads to a relatively large error in the pressure drop. This is particularly noticeable at low velocities. For example, an error of 0.005 inch of water on a zero measurement results in a 4.8 ft/s error bar, while the same pressure drop error on a 0.1 inch of water measurement causes an error bar of 0.5 ft/s at 21.3 ft/s.

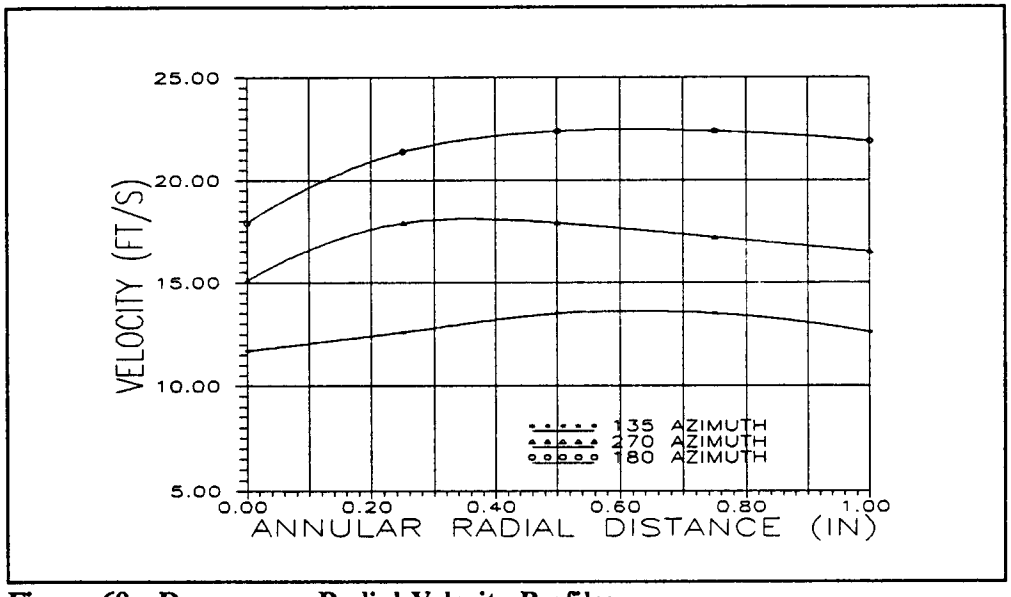


Figure 69: Downcomer Radial Velocity Profiles

Sample measurements were taken during a radial traverse of the downcomer annulus at three azimuthal locations to determine the radial velocity profile in the annulus. The resulting three radial velocity profiles are shown in Figure 69. The variation of velocity as a function of radius is weak, so measurements of downcomer velocity at a single radial position should give a reasonable representation of the average

downcomer velocity at any azimuthal position. For the azimuthal profile measurements, the pitot tube tip was positioned 0.75 inch radially inward from the outer radius of the downcomer annulus, about two-thirds of the 1.1 inch total annular width.

The downcomer azimuthal velocity profiles at 100% flow rate for cases with no vortex suppression and offset radial keys, including the single loop imbalance cases, are shown in Figure 70. The nominal velocity curve shows relatively predictable behavior. The velocities reach a maximum every 90°, between the cold leg nozzles. Visualization in the downcomer shows that flow entering the downcomer from the nozzles distributes isotropically. Upward flow is diverted by the top of the downcomer and is directed downward between the nozzles, resulting in a flow peak. The velocity minimum occurs directly below the nozzles. The reason for the relatively low peak at 90° is not known.

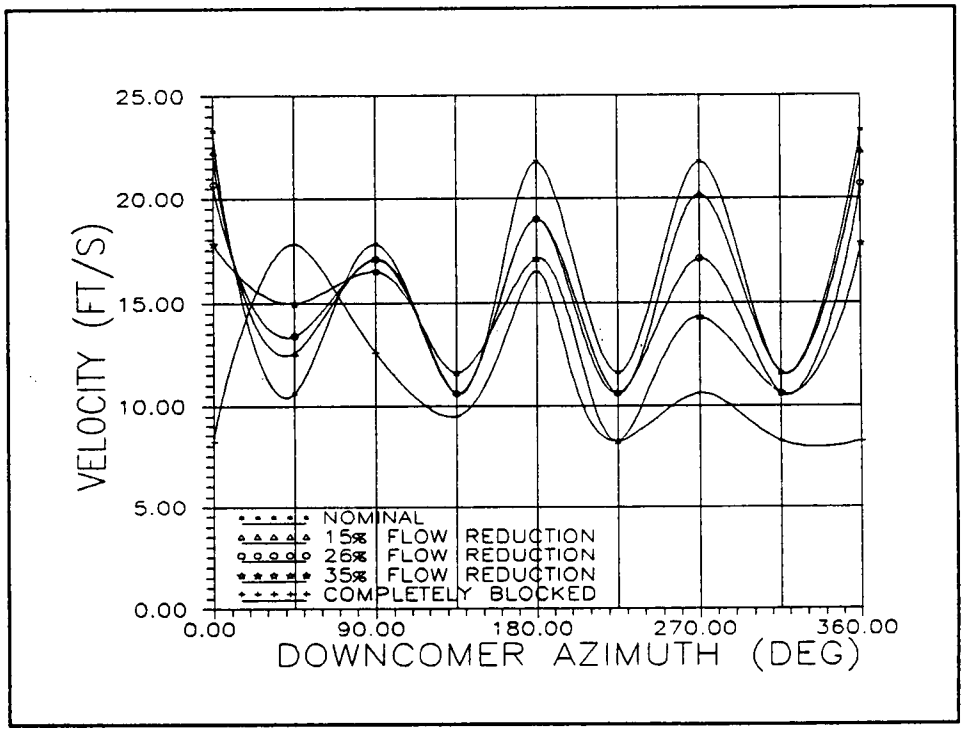


Figure 70: Downcomer Azimuthal Velocity Profile Keys Offset; No VSD; Single Loop Imbalance @ 45°

As the flow rate in the loop located at 45° azimuthally is reduced, the velocity progressively increases at the 45° measurement point. This increase is matched by a velocity decrease elsewhere, although this is most noticeable at 270°. In this configuration with the loop flow balanced, vortices were observed at 100°/340° and 30°/120°. The vortices are centered at azimuths where the velocities are near their midpoints. Observation of the flow fields in Figures 23 and 24 show strong crossflow components around 165° and 295° which are skewed from the peaks in the downcomer measurements. In addition, the direction of these crossflows change in the two figures with no clear analogy to the measurements.

With loop flow reduced by 15%, vortices were observed at 100°/220°, shifting to 150°/300° as flow was reduced further. The associated flow fields, pictured in Figures 55 and 56, show an increase in the horizontal flow component at 45°, with a lessening of the component at 165°. Not expected was the continued strength of the 295° component in the flow fields, when the downcomer velocity measured at 270° was shown to decrease as flow rate imbalance increased in Figure 70.

Other downcomer azimuthal velocity profiles are shown in Figures 71 through 78. Figure 71 shows the nominal and single loop imbalanced velocity profiles for the cases with no vortex suppression and aligned radial keys, while Figures 72 and 73 give the profiles for the cases with the VSD in place and offset or aligned radial keys, respectively. These profiles are all similar to those seen in Figure 70, with small variations that could easily be the result of measurement error.

Figures 74 and 75 show the velocity profiles for two loop imbalance cases with

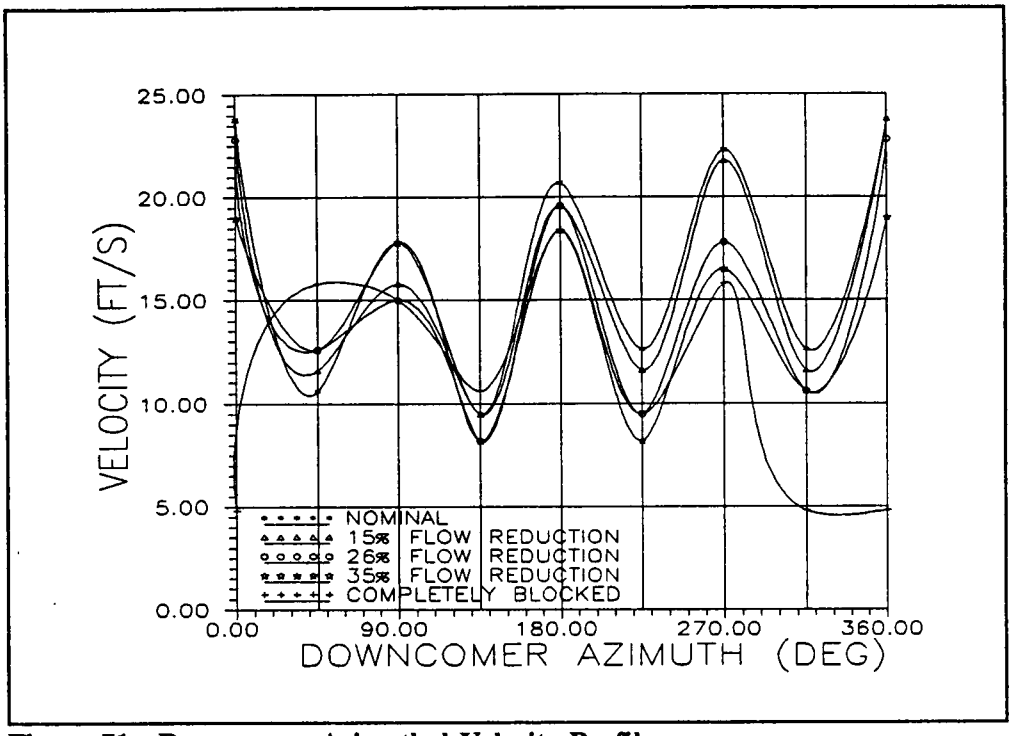


Figure 71: Downcomer Azimuthal Velocity Profile
Keys Aligned; No VSD; Single Loop Imbalance

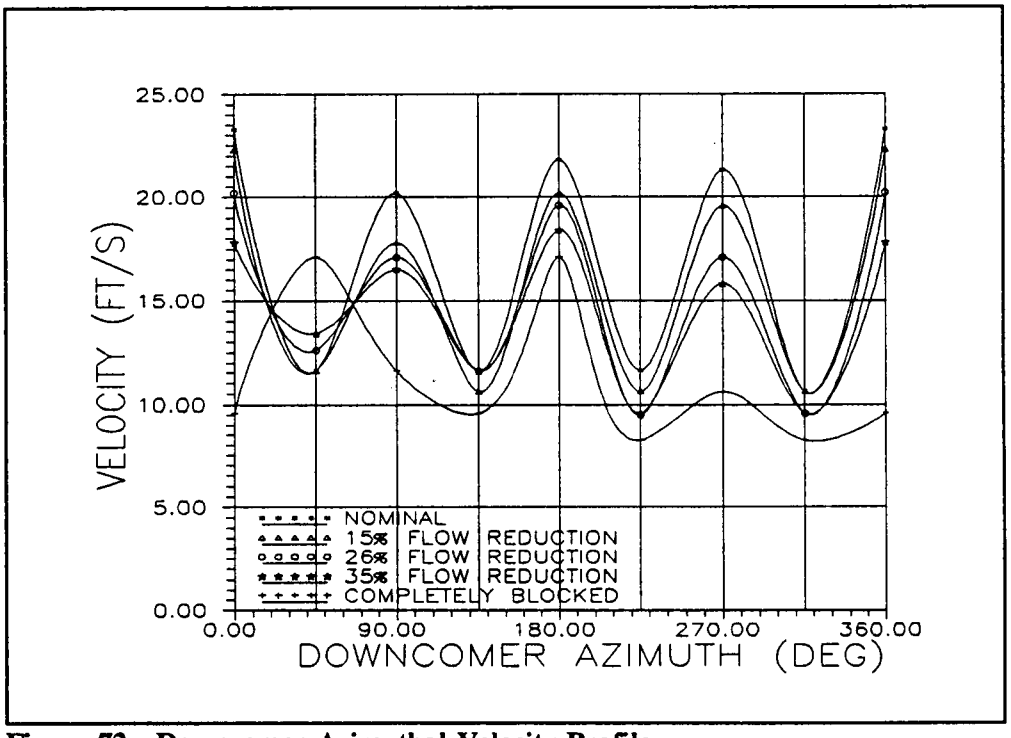


Figure 72: Downcomer Azimuthal Velocity Profile
Keys Offset; VSD; Single Loop Imbalance

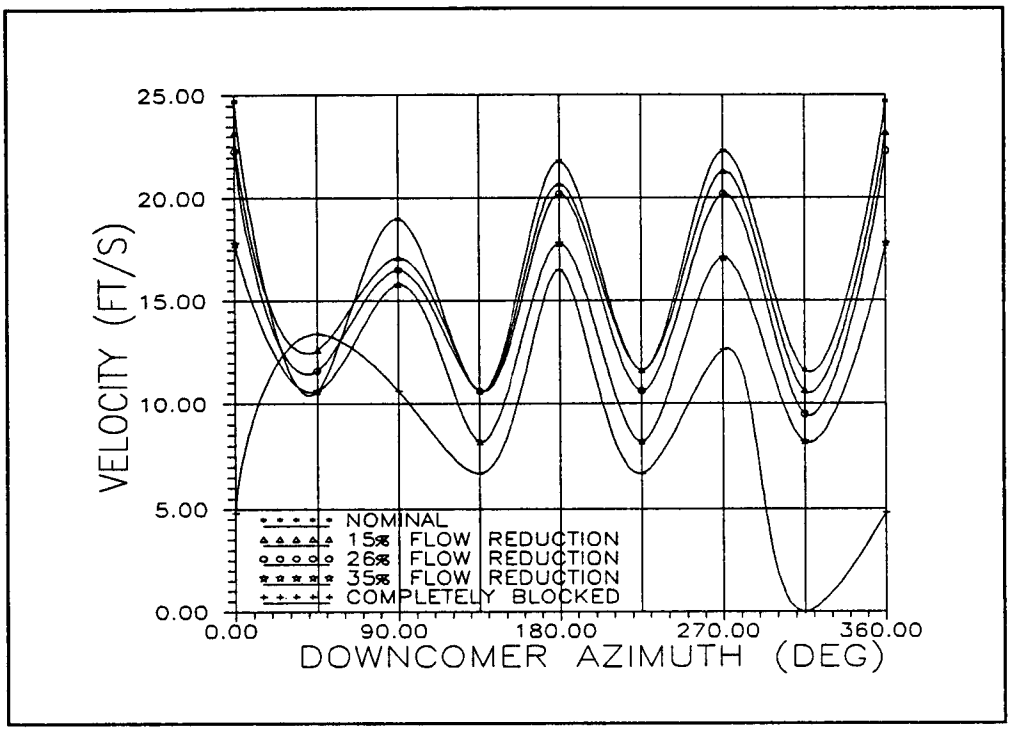


Figure 73: Downcomer Azimuthal Velocity Profile
Keys Aligned; VSD; Single Loop Imbalance

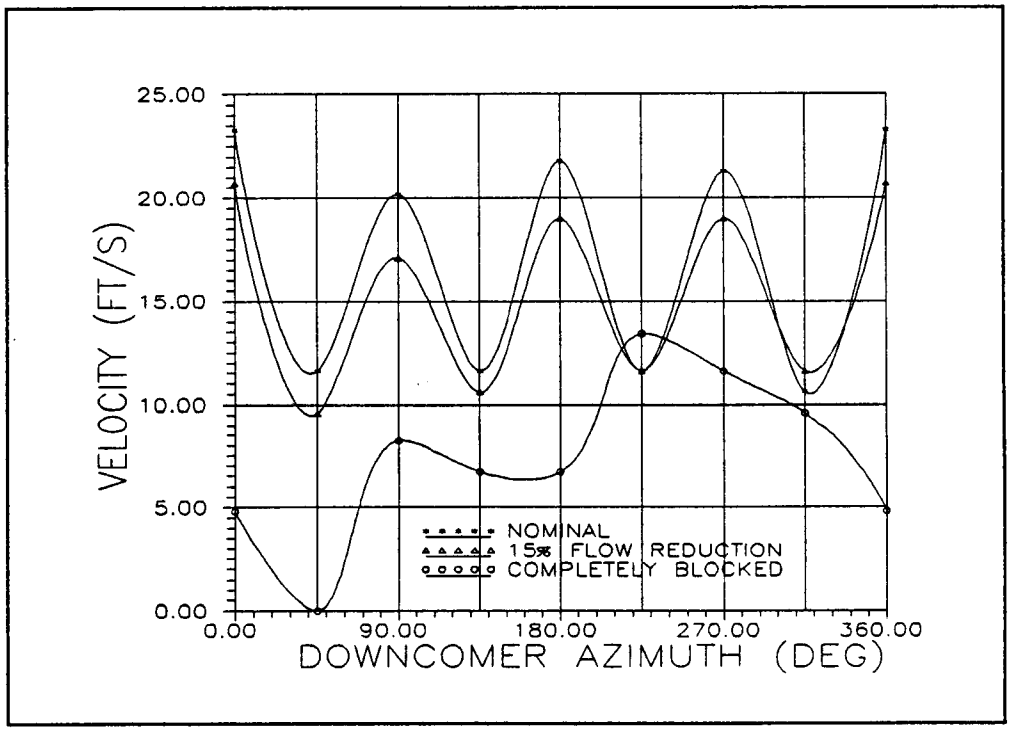


Figure 74: Downcomer Azimuthal Velocity Profile
Keys Offset; VSD; Adjacent Loop Imbalance

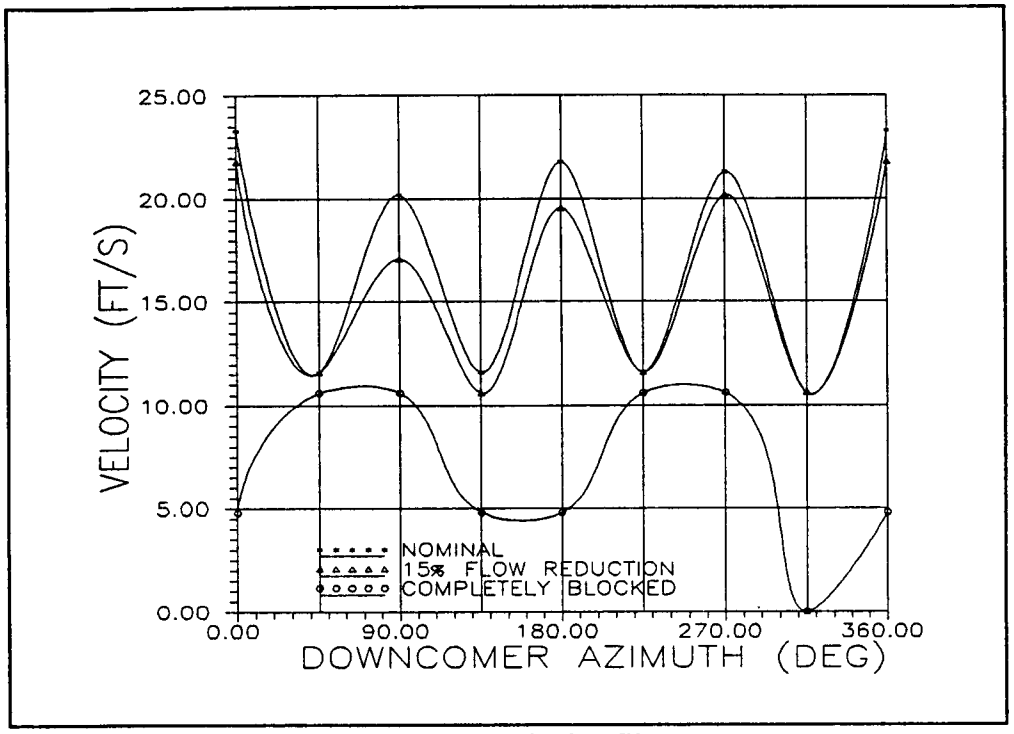


Figure 75: Downcomer Azimuthal Velocity Profile
Keys Offset; VSD; Opposing Loop Imbalance

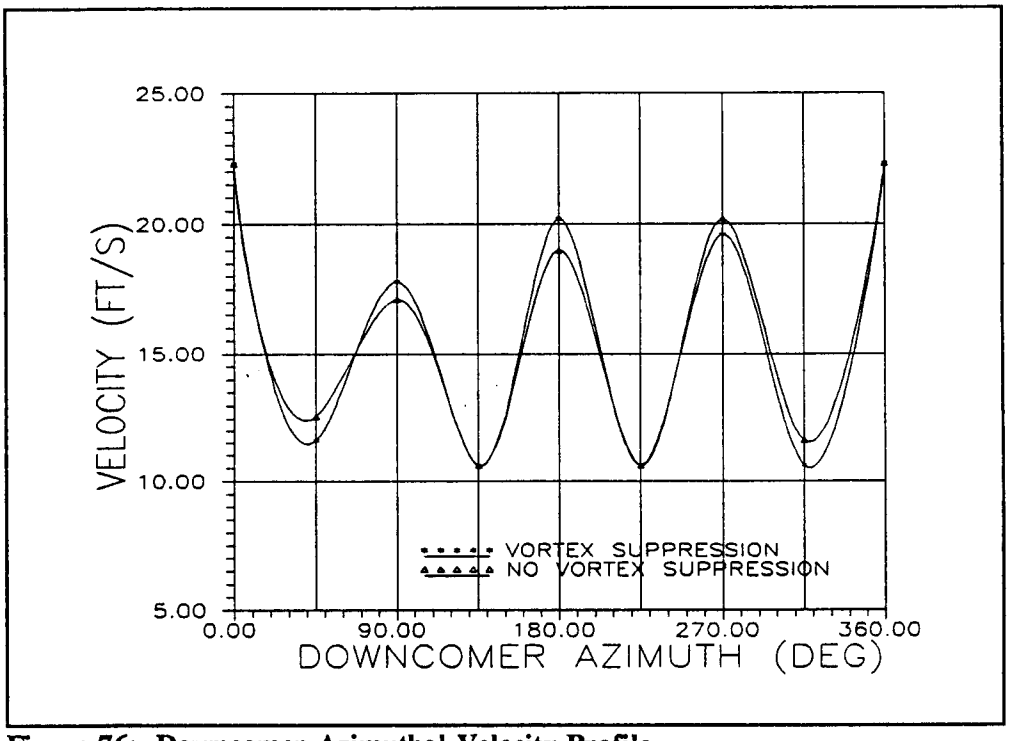


Figure 76: Downcomer Azimuthal Velocity Profile
Comparison: VSD Placement

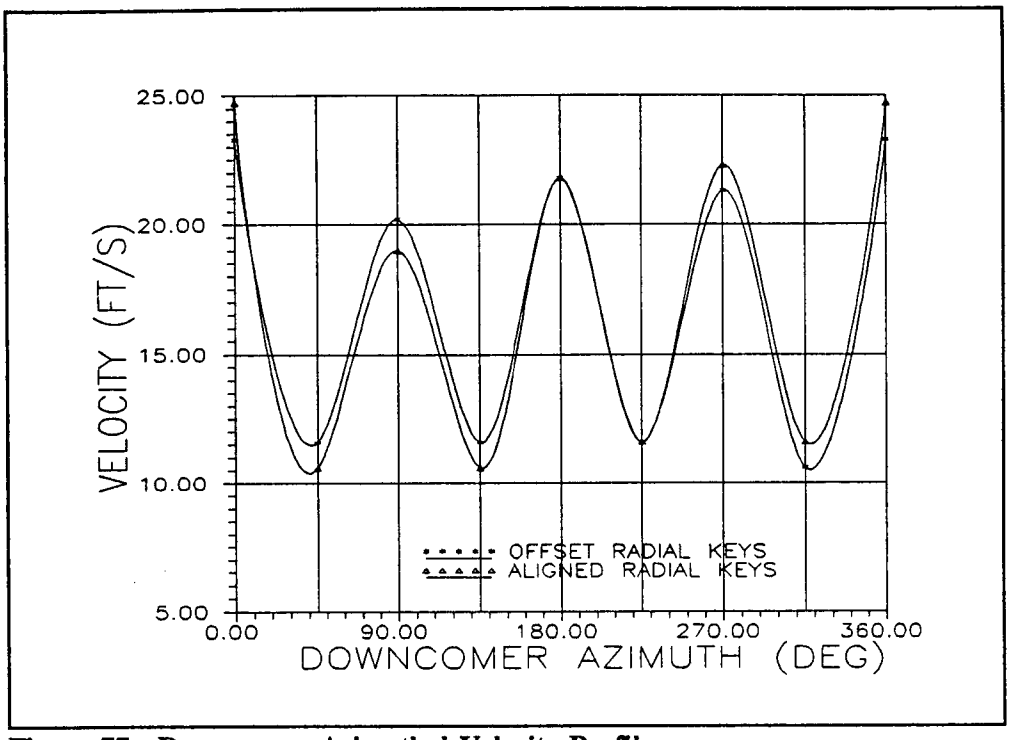


Figure 77: Downcomer Azimuthal Velocity Profile Comparison: Radial Key Alignment

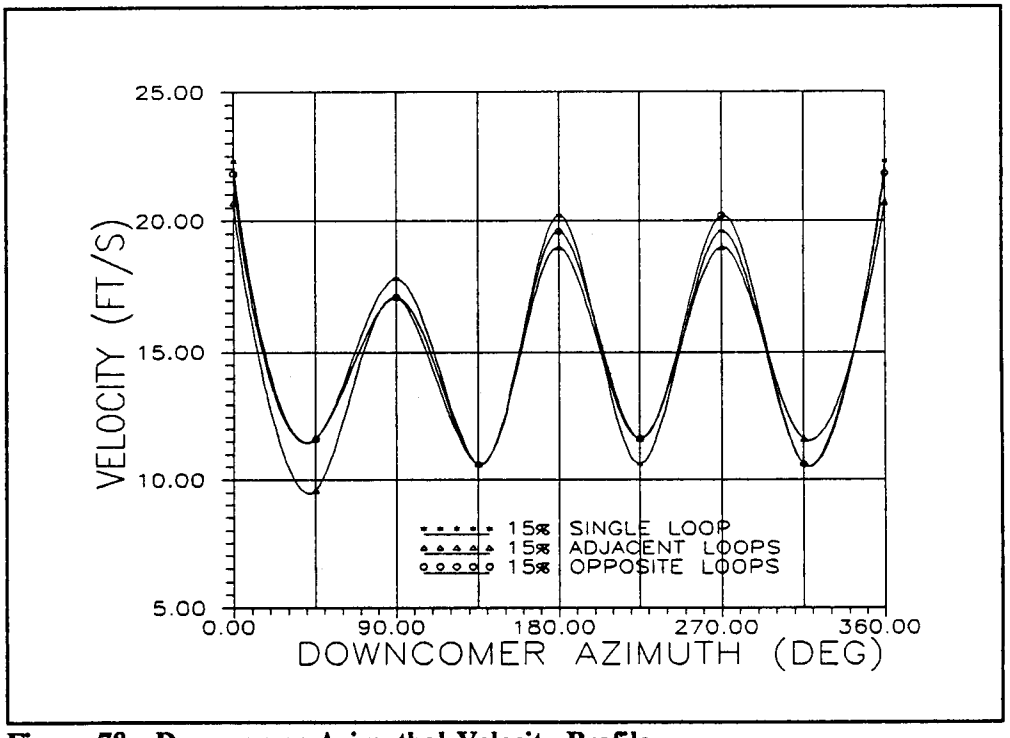


Figure 78: Downcomer Azimuthal Velocity Profile Comparison: Imbalance Configuration

offset radial keys and the VSD in place. The nominal cases are identical in both figures, but the profiles for adjacent loop imbalances are shown in Figure 74, while Figure 75 presents the opposing loop cases. In both figures, the cases with two loops completely blocked show very unorganized profiles, perhaps because of the large measurement errors associated with the low velocities. The profiles for the nominal case and the 15% imbalance cases behave similarly, where the overall drop in velocity for the imbalanced profiles is directly related to the drop in overall flow.

Figures 76 through 78 are comparison figures. The velocity profile changes seen with or without the VSD in place are shown in Figure 76. Although some differences are seen, there is nothing to suggest the drastic change in flow fields that results from inserting the VSD. Figure 77 shows the changes which result from repositioning the radial keys. Again, some differences are observed but there appears to be little relationship to the 45° key position change. Finally, Figure 78 compares the velocity profiles for 15% imbalanced cases with the VSD in place from each combination of loops imbalanced; single, adjacent, and opposed. Here the differences, although relatively small, can be directly related to the changes in upstream phenomena if not to vortical flow.

4.0 CONCLUSIONS AND RECOMMENDATIONS

4.1 Conclusions

Observations of the flow field in this test program have clearly shown that vortices exist in the lower plenum of the "unobstructed" model of the Westinghouse AP600 reactor. These vortices persist even at half the nominal flow rate, which is near the limit of resolution for the visualization technique used. The vortices tend to form in counterrotating pairs of relatively equal intensity and have a fixed radial but variable azimuthal position. The azimuthal position tends to stabilize in one or two predominant patterns which are most stable near the core support plate and become less stable lower in the plenum.

The intensity and predominant azimuthal positions of the vortices are a strong function of the radial support key azimuthal position. The vortices are more organized when the radial keys are positioned in the regions of the highest downcomer velocities, becoming weaker and more transitory when the keys are repositioned into lower downcomer velocity regions. This indicates that the flow field is sensitive to azimuthal variations in the velocity at the downcomer outlet region.

Imposing a flow rate imbalance by reducing flow to one loop also affects the intensity and azimuthal position of the observed vortices. In general, loop imbalances caused the vortices to be less stable in both strength and location, causing them to dart

about, dissipate, and reform. Regardless of the radial key position, significant (> 25%) reduction of the flow rate in a single loop tended to cause an approximately 45° shift in the azimuthal position of the vortices, although exceptions were noted. The maximum strength and radial positioning of the vortices did not change significantly.

Measurements of the downcomer azimuthal velocity profile significantly upstream of the downcomer outlet region show little relationship between downcomer velocity and vortex intensity or position. Some correlation was noted between downcomer velocity and the location of horizontal flow components in the flow fields which appeared to drive vortices, but many exceptions were seen. It is likely that the downcomer velocity measurements taken were too far upstream of the plenum to properly reflect the conditions there.

The theory developed in Section 1.2 suggests that the vortices are driven by the existence of a sink. Once initiated by angular momentum in the fluid, this type of vortex should be able to sustain itself independently of any velocity shear at the downcomer outlet. This could also account for the lack of a relationship between the azimuthal velocity profile and the vortex positions.

Placing the vortex suppression device designed by Westinghouse into the plenum had a drastic effect on the flow field. With the VSD positioned at the design elevation (or lower) and the loop flow balanced, no vortical flow was observed regardless of model flow rate or radial key position. Raising the VSD above the design elevation resulted in the formation of weak vortices which persisted at all flow rates.

With the VSD at the design position, restricting flow between 15% and 100% in

single, two adjacent, and two opposing loops was not sufficient to excite organized vortices. In some cases, most notably the single loop blockage with aligned keys (Figure 62) and the 15% adjacent loop imbalance with offset keys (Figure 63), incomplete circulation was observed which may be caused by upward spiraling flow. This type of flow field is not thought to support a low pressure central core which could affect the reactor flow distribution. It should be noted that visualization of the flow field below the VSD was not performed, so there is some possibility that vortices anchored to the plenum wall and the lower surface of the device may exist.

In conclusion, this experimental program has clearly shown that vortices exist in the model if the lower plenum is unobstructed, and that these vortices are eradicated by placing the VSD in the plenum. These results are expected to typify the response of the actual reactor vessel. The experiments indicate that the best results for vortex suppression with the tested VSD would be achieved by placing the device at an elevation somewhat lower than the referenced design. Also, locating the radial keys in the low velocity region directly below the cold leg nozzles appears to prevent organization of vortices, although it results in greater overall flow turbulence.

4.2 Recommendations for Future Research

Further research would help to quantify the effect of the VSD on the core region flow and clarify the driving mechanism for the vortical flow. The observed incomplete circulation with the VSD in place may have some effect on the flow distribution at the

core support plate. Flow rate or local pressure measurements at the core support plate would identify if this circulation was organized about a low pressure center. The flow rate distribution would also identify any changes in the overall upward flow caused by the VSD.

Understanding the driving force for the vortices may allow more efficient suppression of the vortices without adding structures to the lower plenum. Modifying the downcomer azimuthal flow distribution, the transition region from the downcomer to the plenum, or the bottom face of the CSP could all affect vortex formation. Experiments to evaluate the effect of these changes, as well as more complete characterization of the flow field in the downcomer to plenum transition region, could easily be performed with the existing model. Furthermore, these results could be used to validate existing or future computer models of the downcomer and lower plenum regions.

LIST OF REFERENCES

LIST OF REFERENCES

Bradshaw, P. 1970, *Experimental Fluid Mechanics*, Pergamon Press, Oxford.

Cadek, F.E. et al., 1988, "RCS Flow Anomaly Investigation Report," Westinghouse Electric Corp. Report WCAP-11847.

Garner, D.C. 1991, Westinghouse Electric Corp., Personal Communication.

Holder, D.W. and North R.J., 1963, *Schlieren Methods*, Her Majesty's Stationery Office, London.

Kirchhoff, R.H., 1985, *Potential Flows*, Marcel Dekker Inc., New York.

Lugt, H.J., 1983, *Vortex Flow in Nature and Technology*, John Wiley and Sons.

Meriam Co., 1991, "Installation and Operation Instructions - Meriam LFE Laminar Flow Elements," Model 50MC2-2F, Serial No. 732250-E1.

Olsen, R.M., 1973, *Essentials of Engineering Fluid Mechanics*, Intext Educational Publishers, New York.

Weber, E. and Dittrich, W., 1973, "Hydraulic Studies of the Lower Plenum of a Pressure Water Reactor," NUREG-TR-0009.

Westinghouse, 1989, "Westinghouse Annual Status Report to the USDOE for Technology Programs in Support of Advanced LWRs," DE-AC03-86SF16038.

Westinghouse Drawing RXS-V2-001, rev. 1, 1990, "AP600 Reactor General Assembly" (Proprietary).

Westinghouse Drawing PLOI-V2-001 rev. 1, 1990, "Primary Coolant Loop Layout" (Proprietary).

Westinghouse Drawing M101-V1-003 rev. 1, 1990, "AP600 Lower Internals" (Proprietary).

Wong, H., 1982, "The Taming of the Vortex," *New Scientist*, Vol 94, pp. 566-569.

Yang, W. 1984, "Flow Visualization Techniques, Principles, and Applications," Summer Engineering Conference, University of Michigan - Ann Arbor.

APPENDIX

DIMENSIONED DRAWINGS

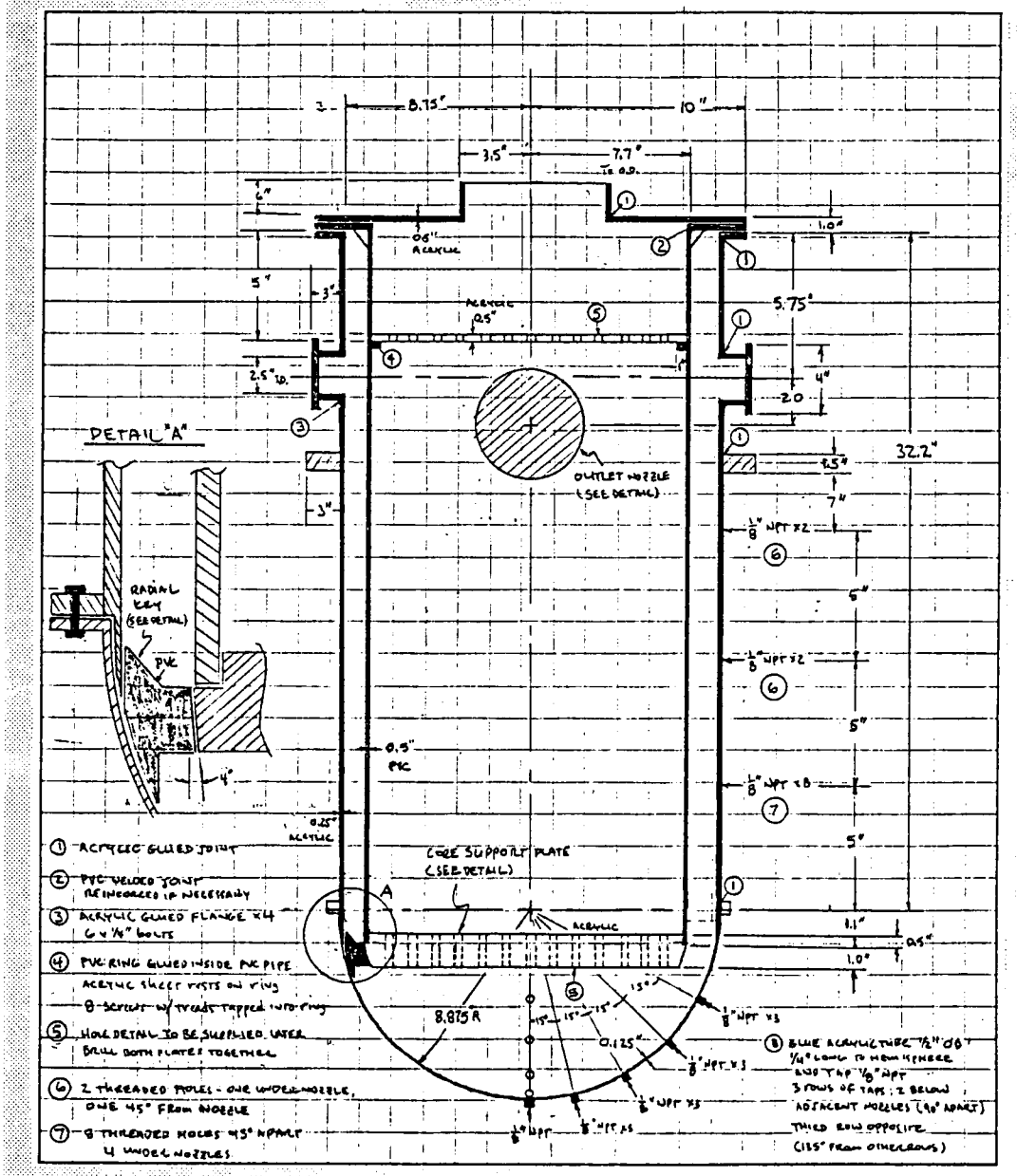


Figure A1: AP600 Reactor Vessel Model Side View

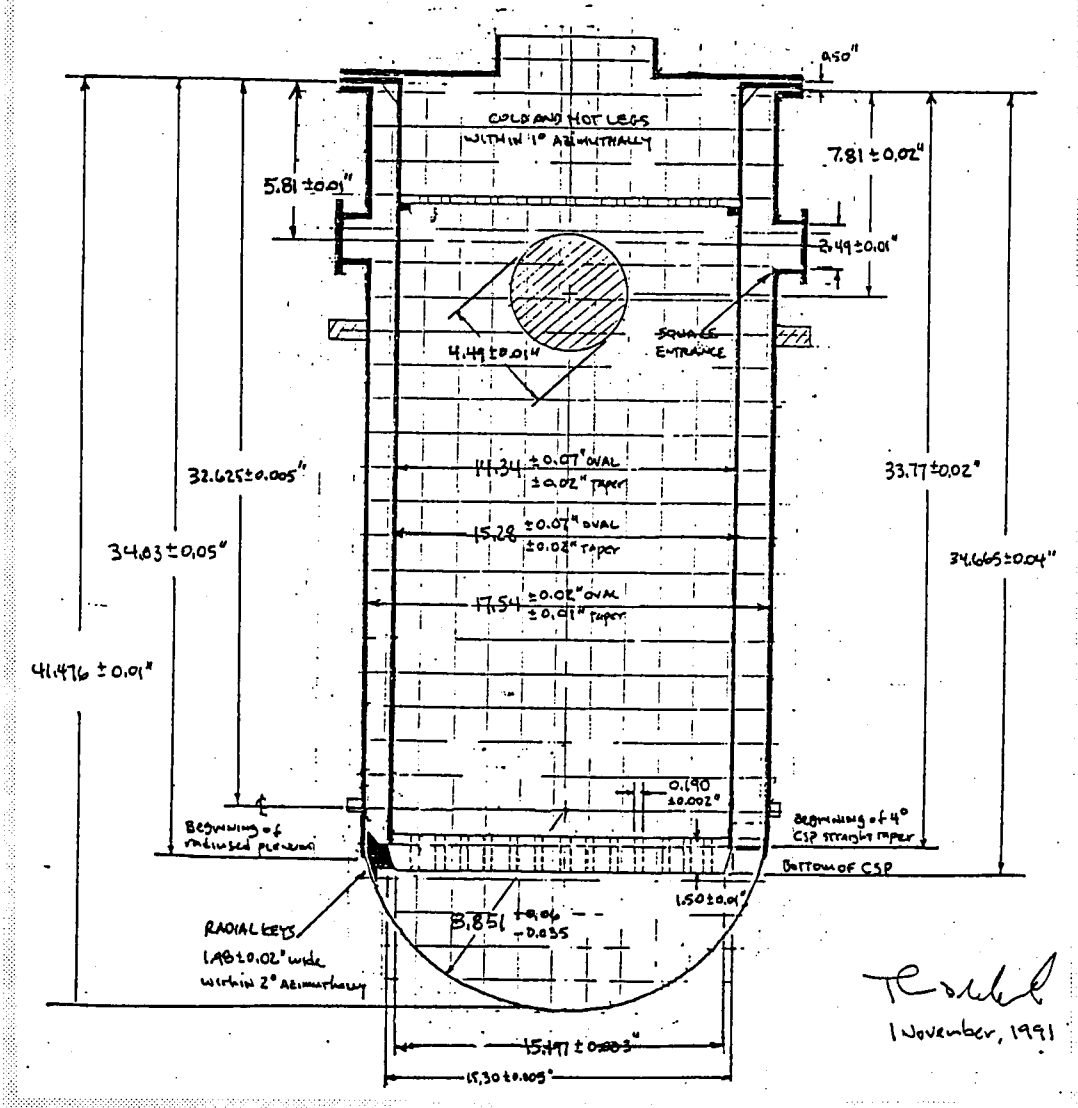


Figure A2: AP600 Model As-Built Dimensions

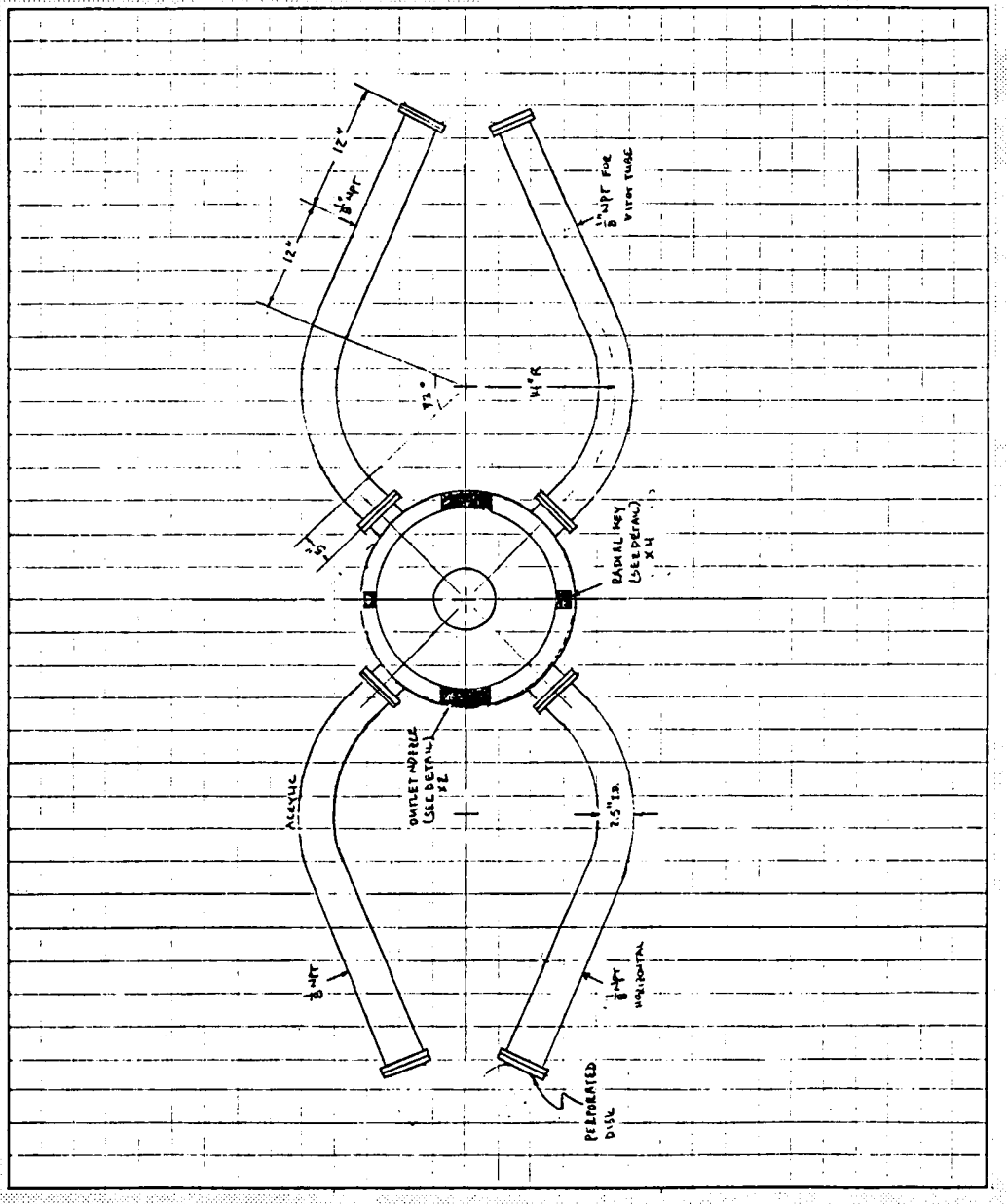


Figure A3: AP600 Model Top View

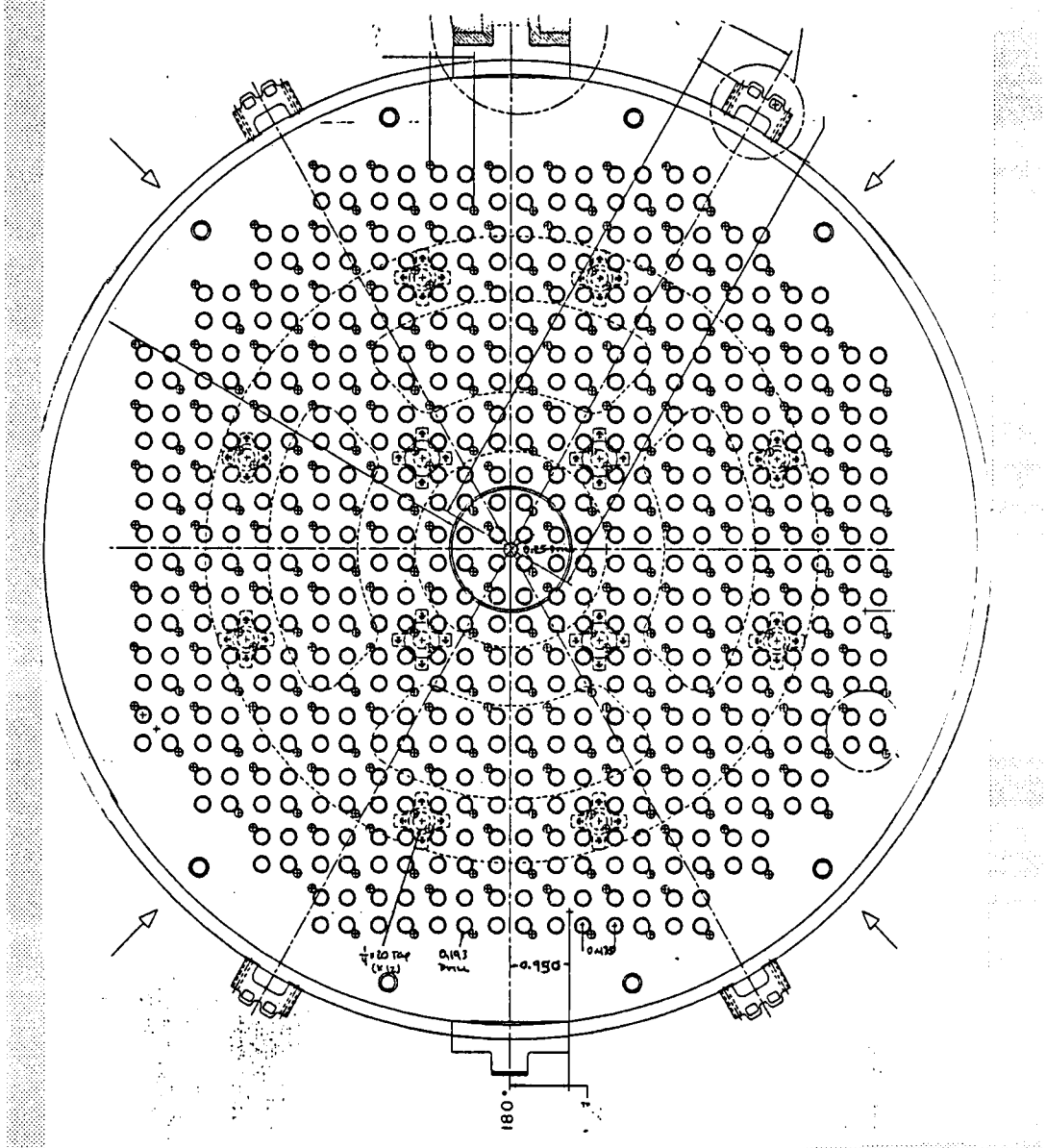


Figure A4: Core Support Plate

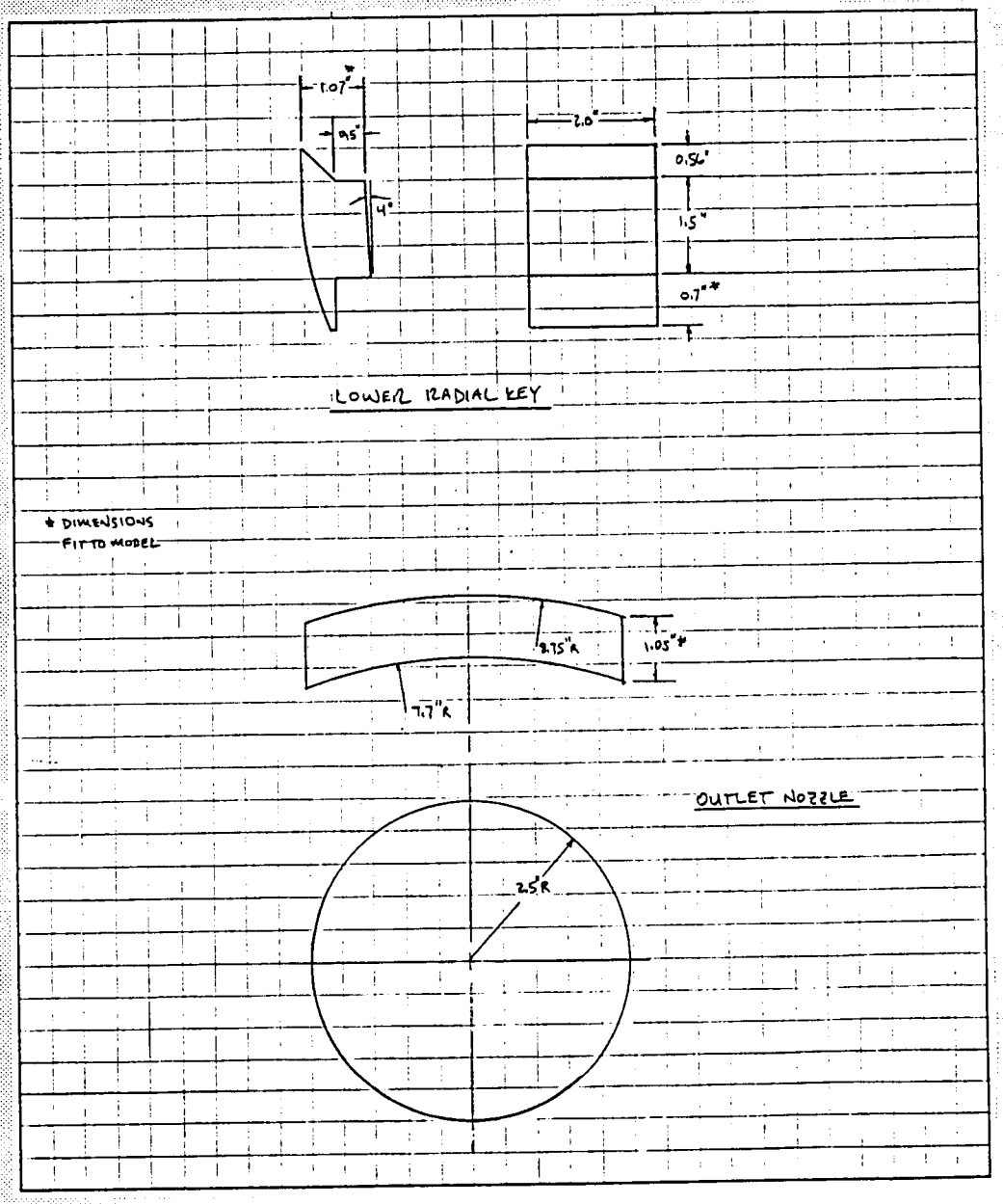


Figure A5: Radial Support Key and Outlet Nozzle

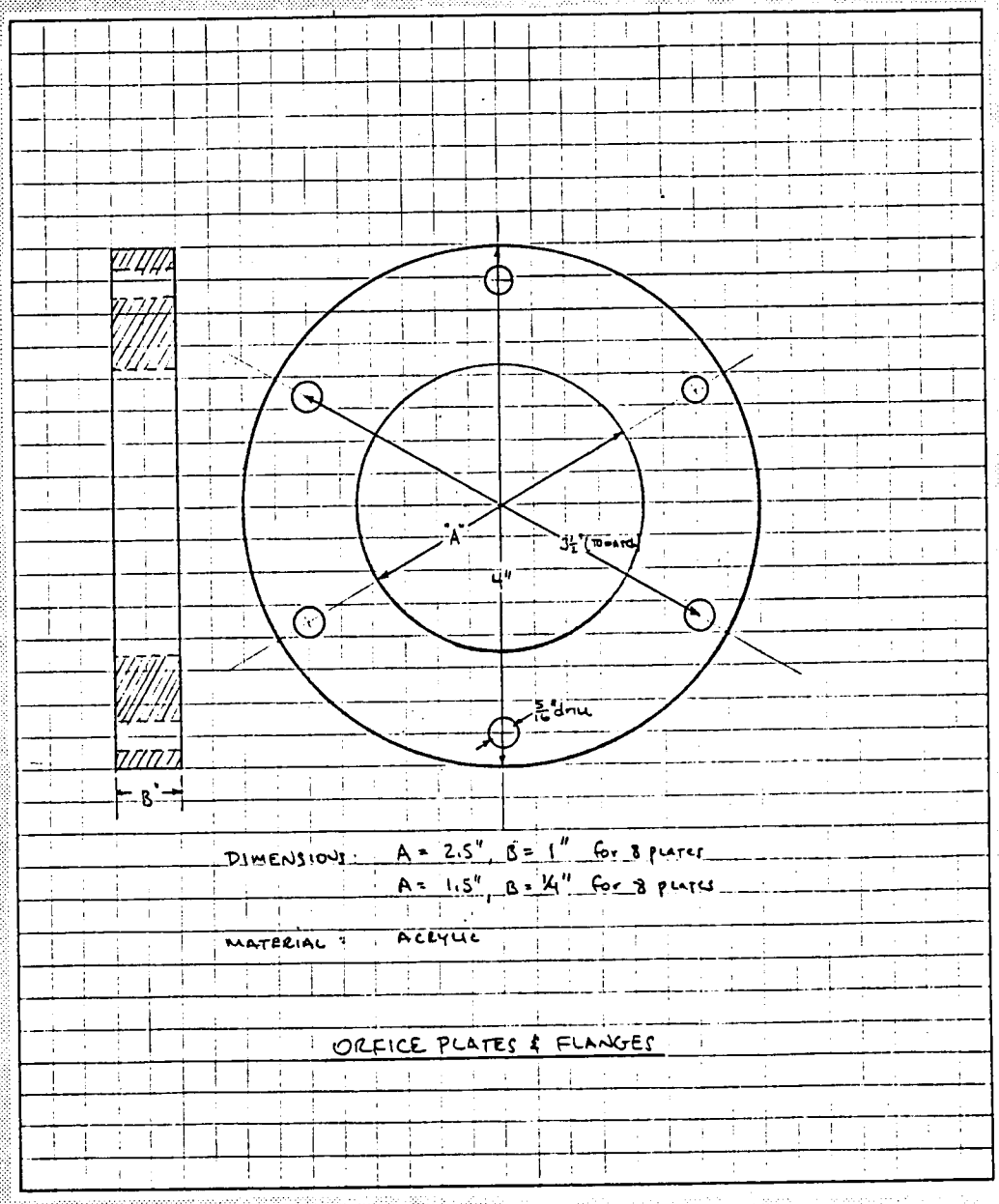


Figure A6: Orifice Plates and Flanges

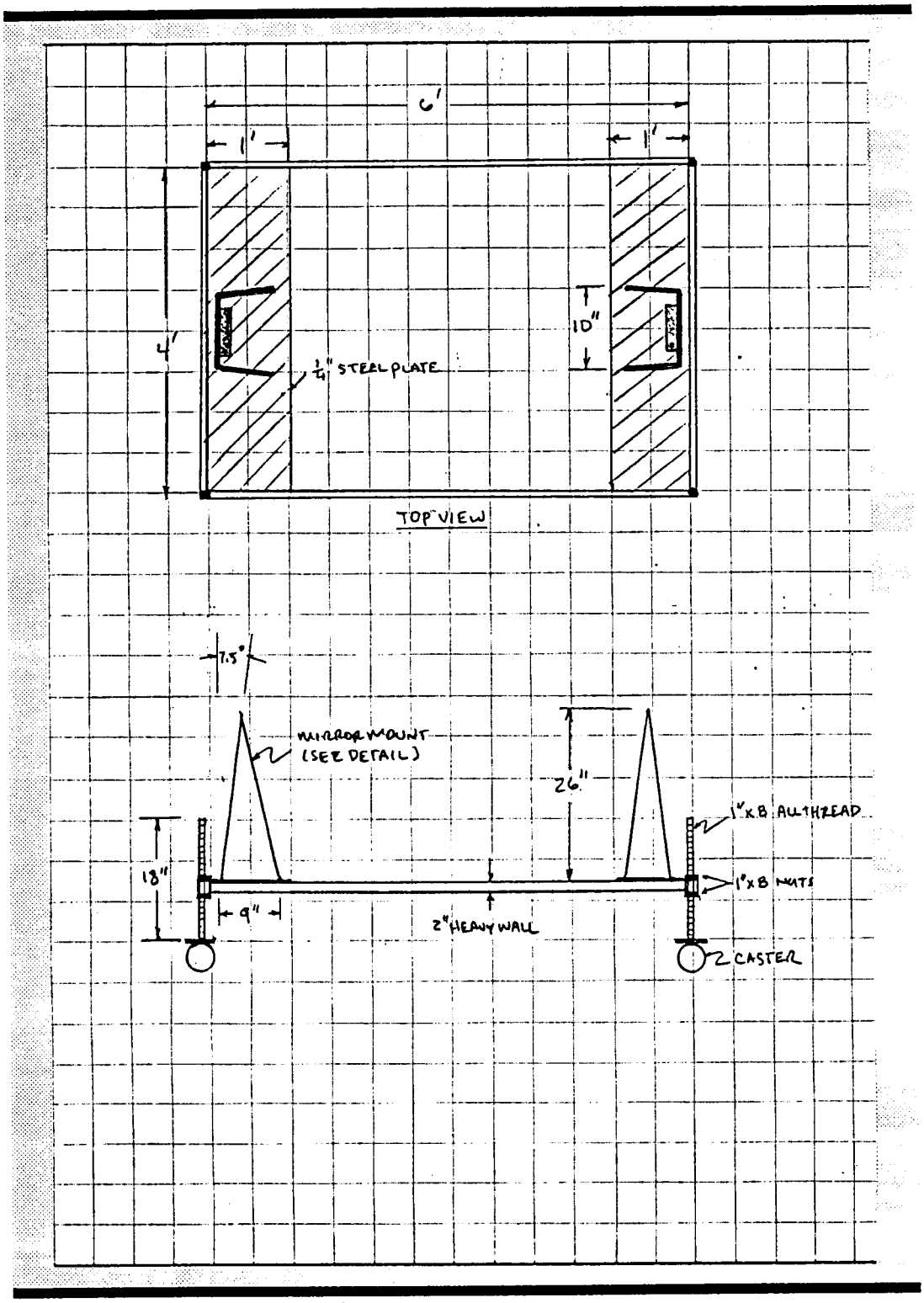


Figure A7: Schlieren Optical System

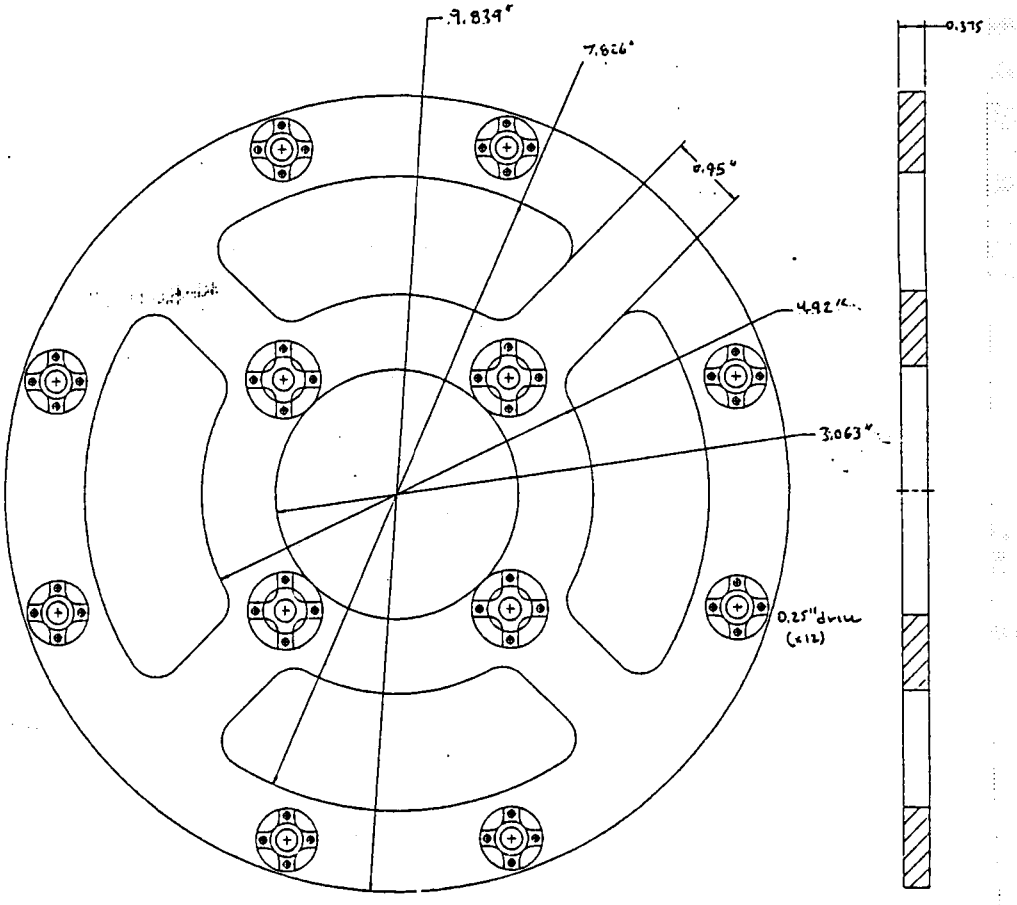


Figure A8: Vortex Suppression Device

VITA

Thomas Dean Radcliff was born in St. Louis, Missouri on July 14, 1958. He attended schools in the St. Charles, Missouri area, graduating from Francis-Howell High School in 1976. The following September he entered the University of Missouri-Rolla, and in 1980 received the degree of Bachelor of Science in Nuclear Engineering.

Mr. Radcliff worked from 1980 to 1983 performing reactor computer simulations for the Babcock and Wilcox company. He then went to the Yankee Atomic Electric company in 1984, where he became the Lead Safety Analyst for the Seabrook nuclear plant. In 1988, he moved to a project engineering position at the Oak Ridge National Laboratory, where he was involved in restart of several research reactors.

In 1990, Mr. Radcliff entered the University of Tennessee-Knoxville, and in May, 1991, received a Master of Science degree in Nuclear Engineering. He remains at the University of Tennessee-Knoxville in pursuit of a Ph.D in Nuclear Engineering.